

Chemical and electrochemical analysis of aqueous redox flow battery electrolytes

Sarah Imhanria

A Thesis in

The Department

of

Chemical and materials Engineering

Presented in Partial Fulfillment of the Requirements

for the Degree of Master of Applied Science at Concordia University,

Montreal, Quebec, Canada.

August 2024

© Sarah Imhanria, 2024

CONCORDIA UNIVERSITY
SCHOOL OF GRADUATE STUDIES

This is to certify that the thesis prepared

By: Sarah Imhanria

Entitled: Chemical and electrochemical analysis of aqueous redox flow battery electrolytes

and submitted in partial fulfillment of the requirements for the degree of

Master of Applied Science

Complies with the regulations of this University and meets the accepted standards with respect to originality and quality.

Signed by the final examining committee:

Dr. Sixu Deng

_____ Chair

Professor Yves Gelin

_____ Examiner

Dr. Marc-antoni Goulet

_____ Supervisor

Dr. Alex De Visscher

Approved by: _____

Chair of Department or Graduate Program Director

30/08/2024

Prof. Mourad Debbabi

Dean of faculty

ABSTRACT

Chemical and electrochemical analysis of aqueous redox flow battery electrolytes

Sarah Imhanria

Redox flow batteries (RFBs) are emerging as a robust solution for large-scale energy storage, crucial for meeting the growing demand for sustainable power sources. While conventional RFBs typically utilize metallic based electrolytes, aqueous organic redox flow batteries (AORFBs) are gaining momentum as a cost-effective and safer alternative. This study delves into the electrochemical characteristics of key redox couples, 1,2-dihydroxyanthraquinone (1,2-DHAQ) and ferrocyanide (FeCN) to assess their potential for AORFB applications. Employing cyclic voltammetry (CV) and rotating disk electrode (RDE) voltammetry, we evaluated their redox reversibility, pH stability, kinetic parameters, and diffusion coefficients. This study reveals that both 1,2-DHAQ and FeCN exhibit quasi-reversible redox behavior, with peak separations (ΔE) of 58 mV and 100 mV, respectively. The half-wave potentials ($E_{1/2}$) versus an Ag/AgCl reference of 0.864 V for 1,2-DHAQ and 0.253 V for FeCN indicate their suitability as negolyte and posolyte, respectively. In addition, 1,2-DHAQ's redox behavior is influenced by pH due to proton-coupled electron transfer (PCET) mechanisms, while FeCN's redox potential remains stable across pH variations due to its coordination with cyanide ligands. Kinetic analyses showed that 1,2-DHAQ has a charge transfer coefficient (α) of 0.23 and a rate constant (k^0) of 1.05×10^{-3} cm/s, compared to FeCN's α of 0.7 and k^0 of 1.2×10^{-3} cm/s. Diffusion coefficients, determined via the Randles-Sevcik equation, were 1.78×10^{-6} cm²/s for 1,2-DHAQ and 2.17×10^{-6} cm²/s for FeCN.

1,2-DHAQ electrolytes were cycled in both symmetric and full cell configurations and found to decrease in capacity over time. To understand the source of this capacity fade, aliquots of cycled electrolyte were analysed via CV and UV-Vis spectroscopy to track the concentration of 1,2-DHAQ over time. Although capacity fade was always associated with a decrease in 1,2-DHAQ concentration, the amounts were not consistently in quantitative agreement, suggesting that more work needs to be done to identify and quantify degradation mechanisms. Lastly, a combination of CV and open-circuit voltage (OCV) measurements were used to estimate the state of charge (SOC) of electrolytes. This method was found to be effective for quasi-reversible systems like 1,2-DHAQ and FeCN but less accurate for irreversible systems like the V^{4+}/V^{5+} redox couple. The study also validated the use of a pseudo-reference electrode, which simplifies experimental setup and reduces contamination risks, thus enhancing the reliability of SOC measurements.

ACKNOWLEDGEMENTS

How time flies! It feels like just yesterday that I began my master's program, and now it is almost coming to an end. Reflecting on the journey, it has indeed been a path marked by laborious effort and challenges. Nevertheless, the joy of reaching this milestone has become a cherished memory. Over the past two years, I have been left with a dream, a fighting spirit, and most importantly, the support and encouragement from many individuals along the way.

Looking back, I can confidently say that I have benefited greatly, even beyond my wildest imagination. This experience will undoubtedly inspire me throughout my life. In the future, I will always maintain a positive and optimistic spirit, never be discouraged, and with a grateful heart, face my fears at every step of my life's journey.

I am grateful to God Almighty for His grace throughout this journey. He has been faithful to His promises in Hebrews 13:5, Jeremiah 29:11, and 1 Peter 5:7. I would not have made it this far without Him.

I owe a deep debt of gratitude to my supervisor, Dr. Marc-Antoni Goulet. Thank you for accepting me as your student and for the funding you provided. You helped me find my footing as I started this process and guided me through the completion of my thesis with great care and effort. Over the past years of working in your group, I have faced many challenges ranging from academic to health and psychological issues. During these times, you were patient and guided me with your extensive professional knowledge, which I know will benefit me for the rest of my life. Your advice and generosity have deeply impacted me, sparking my keen interest in higher education. Thank you for being kind, approachable, and non-discriminative. You are a role model worthy of emulation.

A very special thanks to Meysam Maleki, Lisa Duguet, Orcun Dincer, and Elia Gaillard, who closely assisted me throughout this program. I will always remember and appreciate your help. I am also grateful to my other teammates Farzad Mizaie, Rozhin Saebi, Cristina Pomilio, Dharik Purohit, and Adil Mehboob. Thank you all for your guidance, support, encouragement, and valuable suggestions.

To my sister, Harriet Laryea, I am glad to have met you here. You have been incredibly supportive throughout this journey. Thank you for loving and looking out for me. You have inspired and motivated me to become a better person all around.

I would also like to thank the Department of Chemical and Materials Engineering for granting me the privilege to be here for my master's program. Thank you for your support and for providing me with funding.

My family deserves my endless gratitude. They have been my solid strength, always by my side to encourage and pray for me. Thank you for your unconditional love, understanding, and tolerance.

To my dearest husband, Erhunwunsee Famous, I deeply appreciate your companionship and sacrifices. Thank you for being my lover, teacher, financial strength, driving force, and best friend. This journey would not have been possible without you. Your support keeps me going.

Finally, I sincerely want to thank the experts and professors who took time out of their busy schedules to review my thesis

TABLE OF CONTENTS

LISTS OF ACRONYMS	viii
LIST OF TABLES	x
LIST OF FIGURES	xi
CHAPTER 1: INTRODUCTION	1
1.1. Background	1
1.2. Redox flow batteries for energy storage	1
1.3. Inside a redox flow battery: Structure and operation	2
1.4. Challenges facing organic RFBs	3
1.5. Thesis Objectives	3
CHAPTER 2: THEORY	4
2.1. Types of redox flow battery cells	4
2.1.1. Asymmetric Cells/Full cell	4
2.1.2. Symmetric Cells.....	4
2.2. Components of a redox flow battery	5
2.2.1. Electrodes and electrode properties	5
2.2.2. Membranes and separators.....	5
2.3. Cycling/operation.....	5
2.4. Performance Metrics	6
2.4.1. Capacity	6
2.4.2. Voltage efficiency (VE).....	7
2.4.3. Capacity retention/fade	7
2.5. Capacity fade in flow batteries.....	8
2.5.1. Apparent capacity fade	8
2.5.2. Real capacity fade.....	8
2.6. Electrolytes.....	9
2.6.1. Aqueous metal-based electrolytes.....	9
2.6.2. Aqueous Organic Redox Flow Chemistries	10
2.6.3. Nonaqueous Organometallic Redox Flow Chemistry.....	10
2.6.4. Nonaqueous Organic Redox Flow Chemistry	10
2.7. Chemical Properties of redox flow battery electrolytes	11
2.7.1. Wide Potential Window	11
2.7.2. High Solubility	12
2.7.3. High Ionic Conductivity	12

2.7.4. Fast reaction kinetics	12
2.7.5. Low viscosity.....	12
2.7.6. Robust Chemical Stability	12
2.7.7. Synthetic cost.....	13
2.7.8. Safety.....	13
2.8. Degradation mechanisms	13
2.8.1. Precipitation.....	13
2.8.2. Chemical decomposition	13
2.9. Characterization of electrolyte degradation	15
2.9.1. Cell Cycling.....	15
2.9.2. Cyclic Voltammetry.....	16
2.9.3. Rotating disc electrode (RDE) voltammetry.....	17
2.9.4. Ultraviolet and visible light (UV-Vis) spectroscopy	19
CHAPTER 3: LITERATURE REVIEW	21
3.1. Aqueous electrolytes of interest	21
3.1.1. Inorganic.....	21
3.1.2. Metal ligand complexes.....	22
3.1.3. Organic electrolytes	23
3.2. Electrolyte Characterization.....	25
3.2.1. Cyclic voltametric study	25
3.2.2. Ultraviolet-visible (UV-Vis) spectroscopy/spectrophotometry	26
3.2.3. Mass spectrometry	27
3.2.4. Nuclear magnetic resonance (NMR) spectroscopy.....	28
3.2.5. Fourier-transform infrared (FTIR) spectroscopy	28
3.3. Different SOC evaluation techniques.....	28
3.3.1. Coulomb counting	28
3.3.2. Open circuit voltage (OCV).....	29
3.3.3. Spectroscopy and photometry.....	30
CHAPTER 4: PRELIMINARY ELECTROLYTE CHARACTERIZATION	32
4.1. Experimental Methods	32
4.1.1. Reagents.....	32
4.1.2 Electrochemical measurements.....	32
4.2. Results	32
4.2.1. CVs for Redox Potential.....	32
4.2.2. Pourbaix Diagram.....	34
4.2.3. Kinetics.....	36

4.2.4. Diffusion coefficient.....	38
4.3. Discussion	39
CHAPTER 5: CHARACTERIZATION OF ELECTROLYTE DEGRADATION.....	42
5.1 Experimental methods.....	42
5.2 Results.....	42
5.2.1 Crossover data	42
5.2.2. Symmetric cycling with of 1,2-DHAQ in 2 M KOH concentration.	44
5.2.3. Full cell cycling with 1.2 M KOH concentration.....	45
5.3. Discussion	48
CHAPTER 6: STATE OF CHARGE MEASUREMENTS	50
6.1. Experimental	50
6.1.1. Materials	50
6.1.2. Preparation of samples.....	50
6.2. Results	50
6.2.1. Theoretical Prediction.....	50
6.2.2 Quasi-reversible systems	51
6.2.4 Irreversible system.....	55
6.2.5. A Pseudo-Reference Electrode	56
6.3. Discussion	57
CHAPTER 7: CONCLUSIONS AND FUTURE WORK	59
7.1 Summary of results.....	59
7.2 Overall conclusion.....	60
7.3 Future recommendations	61
REFERENCES	63

LISTS OF ACRONYMS

Alpha-CD: Alpha cyclodextrine
AORFB: Aqueous organic redox flow battery
AQDS: Anthraquinone disulfonic acid
BQDS: 4,5-dihydroxy-1,3-benzenedisulfonic acid disodium salt monohydrate
CV: Cyclic voltammetry
CE: Coulombic efficiency
CEM: Cation exchange membrane
CLS: Capacity limiting side
CPL: 3-carbamoyl-2,2,5,5-tetramethylpyrrolidine-1-oxyl
DABP: 3,3'-dimethylaminemethylene-4,4'-biphenol
DAEAQ: N, N'-(9,10-anthraquinone-2,6-diyl)-di- β -alanine
DART-MS: Direct Analysis in Real Time-Mass spectrometry
DHAQ: Dihydroxyanthraquinone
DHDMBS: 1,4-dihydroxy-2,6-dimethylbenzoquinone-3-sulfonic acid
DMPZ: 5,10-dihydro-5,10-dimethyl phenazine
EDTA: Ethylenediaminetetraacetic acid
EDDS: Ethylenediamine-N, N'-disuccinic acid
NTA: Nitrilotriacetic acid
DTPA: diethylenetriaminepentaacetic acid
EE: Energy efficiency
Epa (Epc): Anodic (cathodic) peak (in CV)
EV⁺: Ethyl viologen radical
Fc: Ferrocene
GC: Glassy carbon
GC-MS: Gas chromatography–mass spectrometry
HER (OER): Hydrogen (oxygen) evolution reaction

ICB: Iron-chromium battery
ICP-MS: Inductively coupled plasma mass spectrometry
IEM: Ion exchange membrane
IVB: Iron-vanadium battery
K-L: Koutecký-Levich equation
LC-MS: Liquid chromatography–mass spectrometry
MALDI-TOF: matrix-assisted laser desorption/ionization time-of-flight mass spectrometry
MV: Methyl viologen
NCLS: Non-capacity limiting side
NMR: Nuclear magnetic resonance
3-NT: 3-nitrotoluene
OCV: Open circuit voltage
PCET: Proton-coupled electron transfer
PTIO: 2-phenyl-4,4,5,5-tetramethylimidazoline-1-oxyl-3-oxide
RDE: Rotary disk electrode
RFB: Redox flow battery
SHE: Standard hydrogen electrode
SOC: State of charge
SWO: Silicotungstic acid
TEMPO: 2,2,6,6-tetramethylpiperidin-1-yl (oxyl)
TEMPOL: 4-OH-TEMPO
TRYP-SO₃H: Sulfonated tryptanthrin
VE: Voltage efficiency
VRFB: Vanadium redox flow battery
UV-Vis: Ultraviolet and Visible light spectroscopy

LIST OF TABLES

Table 6. 1: Deviation of 1,2-DHAQ from theory	53
Table 6. 2: Deviation of FeCN electrolyte from theory	54
Table 6. 3: Deviation of vanadium electrolyte from theory	56
Table 6. 4: Deviation of FeCN with the use of a pseudo reference electrode from theory	57

LIST OF FIGURES

Figure 1. 1 The levelized prediction of renewable energies by 2050.3 b) The intermittent nature of renewable energy.....	1
Figure 1. 2 a) schematic representation of a redox flow battery. b) exploded view of a single cell.	2
Figure 2. 1 a) Symmetric cell b) Asymmetric cell.	4
Figure 2. 2 Pourbaix diagram of Vanadium at different pHs.	11
Figure 2. 3 a) cyclic voltammetry analysis demonstrating the controlled variation of working electrode voltage between two vertex potentials over time. b) Resulting current measurements plotted against the controlled voltage.	16
Figure 2. 4 a) Linear voltammograms obtained at different Rotating Disk Electrode (RDE) rotation rates. b) Levich plot illustrating the linear relationship between the limiting current and the square root of the rotation rate.....	17
Figure 2. 5 a) Linear Voltammogram. b) Koutecky-Levich Plot showcasing the reciprocal kinetic current at different electrode overpotentials.	18
Figure 2. 6 a) A schematic UV-Vis spectrometer set-up. b) A typical absorbance spectrum.	19
Figure 3. 1 a) Schematic of the Michael reaction on BQDS during charging. b) Mechanism of Michael reaction on BQDS showing nucleophilic addition of water. c) Quinone methide formation: reaction of methyl groups with the basic media. d) Mechanism of protonation.	25
Figure 3. 2 a) A typical CV showing degradation of electrolyte overtime'	26
Figure 3. 3 Ultraviolet–visible (UV-Vis) absorption spectra of 1.0 mmol/L [(NPr) ₂ PV] ·4Cl anolyte at different charge states.....	27
Figure 4. 1 CV of 10mM 1,2-DHAQ measured at a glassy carbon electrode in 1M KOH; scan rate 100 mV s ⁻¹ ; room temperature.....	33
Figure 4. 2 : CV of 5mM FeCN in 1M KOH measured at a glassy carbon electrode; scan rate 100 mV s ⁻¹ ; room temperature.	34
Figure 4. 3 a) Combined CVs of 5mM 1,2-DHAQ in pH buffers measured at a glassy carbon electrode; scan rate 100 mV s ⁻¹ ; room temperature; b) Pourbaix diagram (E ⁰ vs pH).....	35
Figure 4. 4 a) Combined CVs of 50mM FeCN in pH buffers measured at a glassy carbon electrode; scan rate 100 mV s ⁻¹ ; room temperature; b) Pourbaix diagram (E ⁰ vs pH).....	35
Figure 4. 5 a) RDE voltammetry curves of 1,2-DHAQ (10 mM) in 1 M KOH solution on a glassy carbon electrode at 6 rotation rates ranging from 400 to 2500 rpm. (b) Koutecky-Levich plots derived from RDE data at 7 different 1,2-DHAQ reduction overpotentials.	37
Figure 4. 6 a) RDE voltammetry curves of FeCN (10 mM) in 1 M KOH solution on a glassy carbon electrode at 6 rotation rates ranging from 400 to 2500 rpm. (b) Koutecky-Levich plots derived from RDE data at 7 different FeCN reduction overpotentials. (c and d) Fitted c and d) Fitted curve of Butler-Volmer equation for FeCN using the kinetic current density (i _k) obtained from the zero-intercept of Koutecky -Levich plots in (b) at six different reduction overpotentials	38
Figure 4. 7 a) CVs of 1,2-DHAQ (10 mM) in 1 M KOH solution on a glassy carbon electrode at different scan rates; b) Plot of the reduction peak current density versus square root of the scan rates for 1,2-DHAQ.	39
Figure 4. 8 a) CVs of FeCN (50 mM) in 1 M KOH solution on a glassy carbon electrode at different scan rates; b) Plot of the reduction peak current density versus square root of the scan rates for FeCN...	39
Figure 5. 1a) UV-Vis calibration spectra at different concentrations of 1,2-DHAQ in 1.2M KOH, b) A standard calibration curve determining the absorbance of 1,2-DHAQ at different concentrations ...	43

Figure 5. 2 : a) UV-Vis absorption spectra of 1,2-DHAQ in 1.2M KOH over time, b) Concentration of 1,2-DHAQ electrolyte obtained by the flow through redox battery over time.....	44
Figure 5. 3: Symmetric cell cycling of 0.1M 1,2-DHAQ in 2M KOH at cut off voltage of +/- 400mV with a limiting current density of 5mA/cm ² . a) Cycling performance. b) CV degradation profiles. c) UV-Vis calibration curve at different concentration with absorbance wavelength of 567.767nm, d) UV-Vis degradation profile	45
Figure 5. 4: Full cell normal cycling of 0.1M 1,2-DHAQ in 1.2M KOH a) Cycling performance. b) CV degradation profiles, c) UV-Vis degradation profile	46
Figure 5. 5: Full cell aggressive cycling of 0.1M 1,2-DHAQ in 1.2M KOH a) Cycling performance. b) CV degradation profiles, c) UV-Vis degradation profile.....	48
Figure 6. 1 Theoretical relationship between equilibrium potential and mole fraction of reduced and oxidized species for a 1-electron reaction.	51
Figure 6. 2: 1,2- DHAQ a) Combined CVs at different SOCs. b) Combined OCVs at different SOCs. c) Comparison of experimental 'E-E1/2' vs mole fraction of reduced 1,2-DHAQ with theoretical curve.	52
Figure 6. 3: FeCN a) Combined CVs at different SOCs. b) Combined OCVs at different SOCs. c) Comparison of experimental 'E-E1/2' vs mole fraction of reduced 1,2-DHAQ with theoretical curve	54
Figure 6. 4: Vanadium a) Combined CVs at different SOCs. b) Combined OCVs at different SOCs. c) Comparison of experimental 'E-E1/2' vs mole fraction of V ⁴⁺ with theoretical curve	56
Figure 6. 5: FeCN with a pseudo reference electrode a) Combined CVs at different SOCs, c) Comparison of experimental 'E-E1/2' vs mole fraction of reduced FeCN with theoretical curve	57

CHAPTER 1: INTRODUCTION

1.1. Background

The world's energy consumption is increasing daily due to the growing world population and booming industrial development, particularly in densely populated countries such as India and China. Energy production still relies mainly on fossil fuels that urgently require a substitute, given their finite resources and negative environmental impact.[1] To reduce the burning of fossil fuels, renewable energy installations relying on solar and wind is being increasingly developed. Renewables are predicted to become the primary energy source by 2050, with an average annual percentage growth rate of 3.6% (Fig 1.1a).[2] Solar and wind energies are responsible for 70% of total renewable production. However, the intermittent nature (Fig 1.1b) of both sources demands the development of safe, environmentally friendly, and low-cost energy storage systems to bridge the gap between generation and consumption.

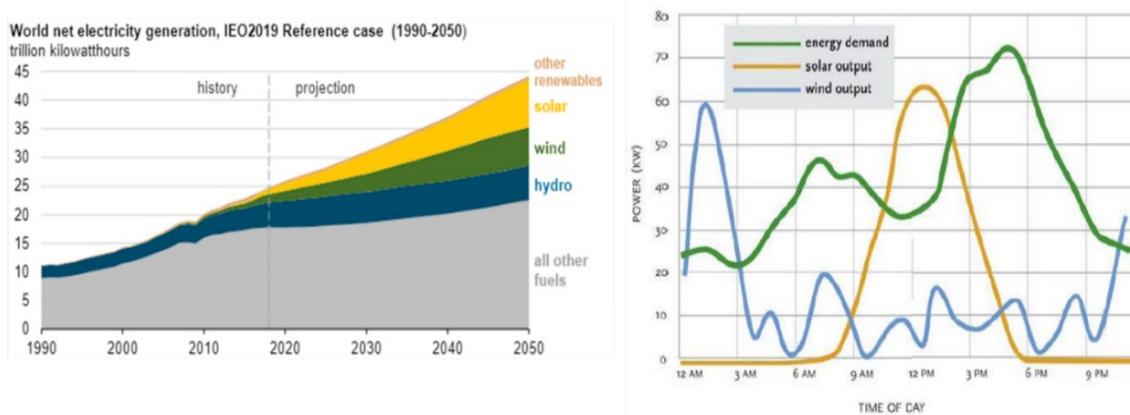


Figure 1. 1 The levelized prediction of renewable energies by 2050.³ b) The intermittent nature of renewable energy.²

1.2. Redox flow batteries for energy storage

While various storage technologies such as capacitors, flywheels, and enclosed batteries exist for short-duration grid services such as grid power quality and frequency regulation, achieving long-duration discharge necessary for the regulation of wind or solar sources primarily relies on pumped hydroelectric energy storage.[3] Unfortunately, pumped hydroelectric storage presents challenges, notably a substantial spatial footprint and geographical constraints arising from the necessity of two large reservoirs at significantly different elevations.

Redox flow batteries (RFBs) are considered a promising technology for large-scale energy storage of renewable sources such as wind and solar.[4] RFBs have decoupled energy and power, which allows for easy scaling of system size and integration with various applications. Additionally, RFBs allow for active electrolyte replacement or enhancement by the addition or replenishment of electrolyte tanks.

A major aspect of RFBs is the redox-active electrolyte materials. Over the last decades, various redox couples have been explored focusing on inorganic metal, halogen ions, organometallic and organic materials.[5] The first inorganic redox species can be dated back to the 1940s, and after several decades of progress, many other systems have been explored.[6] The most common of these is the all-vanadium system pioneered by Skyllas-Kazacos which has attained commercial application.[7]

1.3. Inside a redox flow battery: Structure and operation

Redox Flow Batteries (RFBs) are a type of battery that store energy in liquid electrolytes. Unlike other battery types such as Li-ion batteries or solid-state batteries, where the reactions occur within solid electrodes, RFBs operate at the solid–liquid interface. The active species in RFBs engage in reduction and oxidation reactions while being dissolved in liquid electrolytes. The diagram in Figure 1.2 illustrates a generic RFB setup, comprising a cell enclosed by a blue dashed rectangle, a flow system encompassing electrolyte tanks, pumps, and pipes, and electrical controls denoted in black.

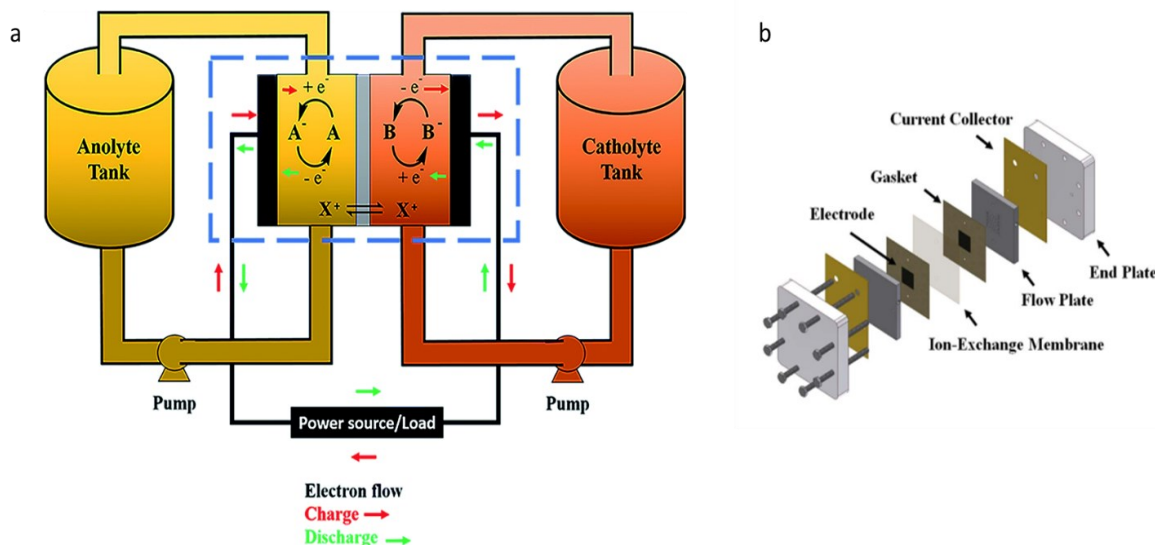


Figure 1. 2 a) schematic representation of a redox flow battery. b) exploded view of a single cell.¹¹

In RFBs, active species (A and B) are dissolved in a liquid and are separated by an ion-exchange membrane (IEM) indicated in grey. The two half-cells are linked by conductive electrodes in black, which remain chemically inert. When the battery is being charged, A is oxidized to A⁺ and loses one electron. This electron is then driven to the other half cell where it reacts with B, reducing it to B⁻. The charged species in this system are A⁺ and B⁻. The state-of-charge (SOC) for the battery is defined as the percentage of species in a charged state in respect to the discharged species, B and A. To maintain charge neutrality, cations pass through the membrane. The solution in the cell is continuously renewed because of the flow of the electrolyte, which is maintained by pumps connected to an external tank that acts as an electrolyte reservoir.

When the battery is being discharged, the inverse process occurs spontaneously, resulting in a potential difference equal to the difference between both reduction potentials. This potential value is directly related to the energy quantity that a battery can store.

In addition to the typical cell endplates and current collector, certain distinctive features specific to RFB systems are noteworthy. The flow plates establish the flow pattern in direct contact with the electrodes. Within the schematic representation, the electrodes are enclosed within a gasket, providing a stable foundation for their integration into the cell structure. Finally, the Ion-Exchange Membrane (IEM), positioned between the two half-cells, serves as the separator for the two electrolytes. Its primary role is to mitigate the crossover of active species between the half-cells while facilitating the exchange of ions to maintain charge balance on both sides.

1.4. Challenges facing organic RFBs

As with many technologies, flow battery systems for commercial applications need to achieve certain performance, cost and durability requirements. Although many flow battery chemistries, such as the all-vanadium redox battery, have demonstrated sufficient performance, their cost remains too high or their durability too low to become widely adopted for grid storage. In general, the cost of materials and components must be minimized to align with economically attractive benchmarks, as emphasized in existing literature.[8] The U.S. Department of Energy has proposed a capital cost target ranging from \$100 to \$120 per kilowatt-hour (kWh) for emerging energy storage systems. This target serves as an “allowable” upper limit on capital investment, ensuring that the cost of stored energy per kWh is commensurate with the cost of electricity throughout the operational lifespan of the system.[9] These ambitious targets are predicated on the relatively low cost of electricity in North America. Techno-economic analyses indicate that aqueous organic redox flow batteries (AORFBs) exhibit potential to meet these targets with further refinement. It is recommended to explore a parameter space characterized by high cell voltage (1-1.5 V), low molecular weight (150 g/ (mol e)), and high solubility (1-2 M) to uphold cost-effectiveness in aqueous systems. Addressing these issues is crucial for positioning RFB systems as financially competitive and sustainable solutions in the energy storage landscape.

Regarding system durability, many of the novel electrolytes being developed still require substantial improvements in their stability.[10] Improving the stability of cells and extending chemical lifetimes are crucial aspects that essentially lead to a reduction in overall system costs. Numerous studies have been dedicated to pushing the boundaries of electrolyte stability, with the latest investigations adopting a more comprehensive approach to understanding how various factors, including ambient atmosphere and cycling protocols, influence cell stability. The accumulation of knowledge in this area will facilitate the development of novel materials or cycling protocols, ultimately contributing to the extension of the operational lifetimes of organic redox flow batteries.

1.5. Thesis Objectives

Research on the degradation of aqueous organic electrolytes, particularly in the context of AORFBs using anthraquinone derivatives like 1,2-DHAQ, is still in its infancy. Understanding the mechanisms and factors contributing to the degradation of these electrolytes is paramount for enhancing the long-term performance of AORFBs.

This thesis centers on the characterization of aqueous organic electrolytes, with particular focus on anthraquinone derivatives, as well as aqueous organometallic complexes such as potassium ferrocyanide. The primary objectives are as follows:

1. Characterization of common electrolyte parameters such as diffusion coefficients, kinetic constants (k^0), and pH.
2. Correlating capacity fade with ex situ concentration measurements and other changes in electrolyte properties.
3. Demonstration and assessment of a SOC measurement technique for flow battery electrolytes

CHAPTER 2: THEORY

2.1. Types of redox flow battery cells

2.1.1. Asymmetric Cells/Full cell

Redox flow batteries are typically composed of two different electrolytes separated by a specialized membrane used to keep these electrolytes apart while maintaining ionic conductivity. This typical configuration is known as a ‘full cell’ and may also be referred to as asymmetric cell. When used as commercial power sources, the two electrolytes will usually have closely matched charge capacities to minimize the system size. During flow battery research and development however, it is common practice to limit the volume of the electrolyte of interest, while the other half-cell has an excess of material. This configuration is adopted to understand the importance of the limiting electrolyte on the overall stability of the full cell. Full cells are most often used to gauge full cell performance metrics, including voltage and coulombic efficiency, impedance, power density, and capacity fade. Full cells are also useful for measuring reactant crossover through the membrane, and the effect of cross contamination of electrolytes.

2.1.2. Symmetric Cells

A symmetric cell refers to a flow cell where the same electrolyte is utilized in both half-cells. The electrolyte undergoes cycling between the same two oxidation states in both half-cells, with one half-cell charging while the other discharges. Consequently, the average cell voltage is 0 V. This cell configuration is therefore not useful as a power source, but is most often used to assess the intrinsic molecular stability of the electrolyte material without crossover effects. Fig. 2.1a and b depicts a schematic of a symmetric and asymmetric flow cell respectively. For the remainder of this thesis, flow batteries and cell cycling tests will refer to full cell tests by default, whereas symmetric cell tests will be called out specifically when they are implemented.

In some cases, the term "symmetric cell" has also been used in the literature to describe a hybrid of symmetric and asymmetric cells, employing a redox material with more than two oxidation states. While the same material is used in both half-cells, each half-cell cycles between different oxidation states. Due to the variation in solubility and standard reduction potential between the two half-cells, a non-zero cell voltage is achieved, in contrast to the previous definition of symmetric cells.[11]

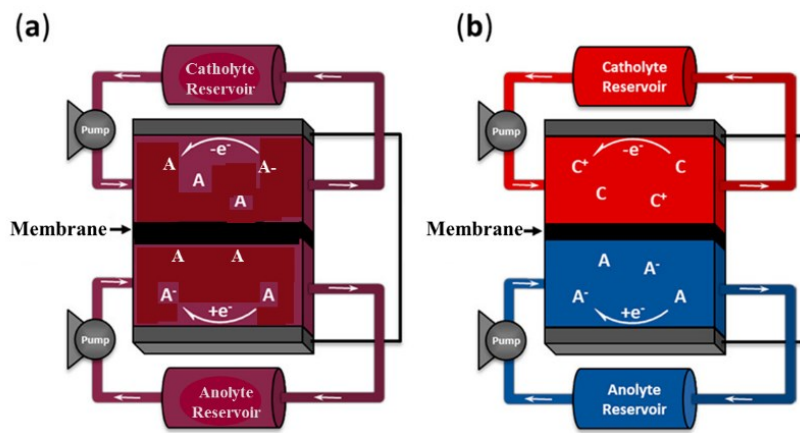


Figure 2. 1 a) Symmetric cell b) Asymmetric cell. Adapted from Hu et al.¹²

2.2. Components of a redox flow battery

The composition of both electrolytes of a full cell is referred to as the ‘cell chemistry’ and is typically the defining feature and starting point in flow battery development. The electrolytes are typically chosen to maximize the solubility, ionic conductivity, stability (both chemical and electrochemical), and the open-circuit voltage (OCV) of the cell on one hand, while minimizing the viscosity, toxicity, and cost of the electrolyte. Once the cell chemistry is determined, the other flow battery components, such as the membrane, electrodes, flow plates and gaskets are typically selected accordingly.

2.2.1. Electrodes and electrode properties

Fibrous carbon paper or felt electrodes are commonly used in Redox Flow Batteries (RFBs) due to their high fluid permeability, specific surface area, electrochemical activity, conductivity, and cost-effectiveness. Carbon electrodes are also preferred for aqueous systems due to their robust chemical resistance and substantial overpotential for water-splitting reactions. RFB systems with carbon paper electrodes, which are 100 to 300 μm thick, have become increasingly popular over the past decade due to their ability to reduce ohmic and mass-transport losses. The thin carbon paper electrodes promote electrolyte convection, facilitated by an adjacent flow field. Graphite felt electrodes, typically around 3 mm thick, have traditionally been prominent in VRFB literature. Electrolyte convection in graphite felt electrodes is primarily achieved by directing electrolyte flow within the felt plane. Recent research developments in the last two years have heightened interest in woven carbon cloth electrodes for AORFS due to their enhanced electrolyte transport properties. The subsequent sections provide a detailed exploration of the effects of electrode pre-treatment, microstructure, and precursor material on flow cell performance.

2.2.2. Membranes and separators

Membranes/separators play a crucial role in Redox Flow Batteries (RFBs) by facilitating the movement of ions between the two half-cells while keeping the redox active species separated. Additionally, RFB membranes should prevent excessive solvent crossover between the two half-cells. These membranes are generally categorized into two technologies: ion-exchange membranes (IEMs) and microporous separators. A majority of aqueous RFBs utilize IEMs, which are made from a specific type of polymer electrolyte containing fixed charges that enable selectivity to conduct the corresponding counterions in solution. VRFBs typically employ cation exchange membranes (CEMs) like Nafion, which leverage the high mobility of acidic protons in solution. While Nafion CEMs exhibit high conductivity, they are not perfectly selective against small, charged vanadium cations. Moreover, Nafion CEMs are produced from costly fluorinated polymers, constituting a significant portion of cell material costs.

2.3. Cycling/operation

Cell cycling, a crucial method for characterizing flow batteries electrochemically in situ, involves using a potentiostat to control the cell's charging and discharging processes. The circulation of electrolyte within the cell is managed by a pump, ensuring proper wetting of the electrodes and removing trapped gas bubbles before initiating charge-discharge cycling. During this stage, the OCV of the cell can be measured. By applying a positive current or potential above the OCV, both sides of the cell are charged, leading to the oxidation of the electrolyte on the positive side (posolyte) and reduction on the negative side (negolyte). The reverse reaction occurs during discharge.

Galvanostatic (constant current) and potentiostatic (constant potential) modes are commonly used in cell cycling to assess flow battery performance. Galvanostatic cycling is often used to control the duration of the charge and discharge steps and to observe the onset of primary and secondary reactions that appear as voltage plateaus in the measured potential. In contrast, potentiostatic cycling maintains a constant potential between the electrodes of the battery to prevent undesirable side reactions from occurring and to determine when the majority of the capacity has been reached for the primary reactions under study. The amount of capacity or SOC accessed is controlled by the current limit condition set by the operator. In both cases, parameters such as coulombic efficiency (CE), voltage efficiency (VE), and energy efficiency (EE) can be calculated for each cycle.

On the other hand, potential hold involves maintaining a constant voltage across the battery for a specific duration, allowing researchers to observe the battery's response under steady-state conditions. This technique is useful for studying the battery's behavior at a fixed potential, providing information on its stability and performance over time. Potential hold experiments can help identify any changes in the battery's behavior or characteristics under constant voltage conditions, aiding in the assessment of its electrochemical processes and long-term reliability. These techniques offer valuable insights into various overvoltage contributions, aiding in the understanding of electrochemical processes in flow batteries.

2.4. Performance Metrics

It is crucial to assess the performance of RFBs with reliability and precision by using well established methods and metrics. These are discussed below.

2.4.1. Capacity

The capacity of a redox flow battery is a fundamental measure of its energy storage capability and operational efficiency, representing the amount of energy that the battery can store and deliver during its operation. Typically quantified by the total discharge capacity the battery can provide, this metric is directly tied to the volume of electrolyte stored in the system and the concentration of active species within it.

The equation for evaluating the capacity of a redox flow battery can be expressed as:

$$Q = nFCV$$

Where:

- Q is the capacity of the battery,
- n is the number of electrons involved in the redox reactions,
- F is Faraday's constant (96485C/mol),
- C is the concentration of active species in the electrolyte, and
- V is the volume of the electrolyte.

This equation considers the number of electrons transferred in the redox reactions, the concentration of active species, and the volume of the electrolyte to determine the overall capacity of the redox flow battery. Capacity utilization, which compares the actual capacity to the theoretical capacity based on the amount of electroactive species present, plays a significant role in system cost. Lower utilization may lead to increased costs due to the need for larger quantities of electroactive species and higher storage volumes. Factors such as current density and inherent cell losses affect capacity utilization, with utilization typically decreasing at higher current

densities. The relationship between capacity utilization and current density is illustrated in Figure 4, where longer charge and discharge times correspond to higher capacity utilization at lower current densities.

2.4.2. Voltage efficiency (VE)

The voltage efficiency (VE) is a measure of the ratio between cell voltage during discharge and charge processes at a specific time or desired SOC.

$$VE = \frac{\text{Average discharge voltage}}{\text{Average charge voltage}} \times 100$$

The measurement is usually taken with a constant current density. VE is always less than 100% due to various sources of overvoltage, including kinetic, ohmic, and mass transport losses which generally increase with current density.

Meanwhile, the coulombic efficiency (CE) is the proportion of electrical charge that is withdrawn during discharge compared to the total current passed during charging.

$$CE = \frac{\text{Discharge capacity}}{\text{Charge capacity}} \times 100$$

Typically, the CE is less than 100% due to undesirable electrolyte decomposition, the simultaneous production of hydrogen, oxygen or other side reactions, and the crossover of redox-active electrolytes

It is important to consider the energy efficiency (EE), which is calculated by dividing the discharged energy by the charged energy during a constant current charging-discharging process. EE is directly related to both Coulombic efficiency (CE) and Voltage efficiency (VE), and it can be calculated as the product of these two parameters.[12]

$$EE = CE \times VE$$

The use of reliable separators, such as Nafion membranes, is crucial in achieving high EE in aqueous RFBs, thanks to their high ionic conductivity and chemical stability.

2.4.3. Capacity retention/fade

The capacity retention rate is a metric to measure the stability of a RFB system. The average capacity retention rate per hour or day, represented by the symbol Cr, is calculated using the formula:

$$Cr = \left(\frac{Q_n}{Q_1} \right)^{\left(\frac{1}{t} \right)}$$

Where, Q_n is defined as the discharge capacity of the nth cycle, Q₁ is the discharge capacity of the first cycle, and t is the time in hours or days.

Similarly, we can also define the average capacity fade as:

$$\text{Av CF} = \frac{Q_i - Q_f}{Q_i} \times 100$$

Where, Q_i is defined as the initial capacity and Q_f as the final capacity. This capacity fade is often divided by a relevant quantity, such as the time or the number of cycles, to express a capacity fade rate. It provides a relative measure of the battery's degradation and loss of capacity throughout its operational lifespan.

2.5. Capacity fade in flow batteries

During charging and discharging, flow battery electrolytes undergo oxidation and reduction reactions consecutively, in turn storing and releasing electrical energy. However, over time, the flow battery capacity may not reach the same level which was stored in the original electrolytes. This fade in capacity can be due to various mechanisms discussed in this section and can be generally classified under two types: apparent (reversible) or real (irreversible) capacity fade.

2.5.1. Apparent capacity fade

Apparent capacity fade is associated with a reduction in the measured capacity of the battery that is not related to a reduction in the actual concentration or number of moles of the limiting reactant. Common causes of apparent capacity fade include increased cell resistance, electrolyte imbalances and side reactions.

When strictly galvanostatic (constant current) cycling is used, charge and discharge capacities depend on the voltage cutoff criteria. If the cell resistance increases over time however, these voltage cutoffs will be reached earlier, leading to a lower capacity. Although the amount of redox active material in the electrolytes has not changed, the cell cannot reach the original capacity due to increased resistance of its other components. The primary way to avoid this type of capacity fade is to impose a constant voltage at each cutoff, forcing the cell to stay at the cutoff voltage until all redox active species have reacted.

Even when voltage holds are imposed however, the amount of capacity accessed may differ from the original amount due to slight variations in the equilibrium voltage difference between the two electrolytes. In other words, the voltage reference points may shift over time due to changes or imbalances in the electrolyte concentrations. Electrolyte imbalance refers to the case where the non-capacity limiting side (NCLS) starts to become limiting due to its average SOC drifting over time. This may occur due to crossover or self-discharge of the electrolytes. Although some of this may be minimized by using symmetric cells, this solution is not applicable to batteries for energy storage which require a full cell configuration. Lastly, side reactions may also change the average SOC of the electrolytes over time, leading to the same concentration effects on the equilibrium voltage reference points. Although apparent capacity fade results in a loss of energy efficiency, it is generally reversible by simply rebalancing electrolytes or intentionally generating side reactions (such as hydrogen or oxygen evolution) to shift the state of charge back to its starting point.

2.5.2. Real capacity fade

This refers to the permanent loss of capacity over the lifetime of the battery. This can be caused by a variety of factors, including crossover and precipitation of active species, the irreversible degradation of the active species, loss of electrolyte via leakage.

In RFBs, crossover refers to the migration of redox-active species through the ion-conducting membrane, leading to issues such as self-discharge, irreversible reactions, reduced Coulombic

efficiency, and capacity decay. Strategies like the Donnan effect and size exclusion, coupled with careful membrane selection, can mitigate crossover to some extent, but achieving perfect selectivity remains challenging. Crossover poses a significant challenge for various types of inorganic RFBs, including those based on iron, manganese, vanadium, polysulfide, and iodide. The acceptable level of crossover and associated CE losses depend on whether the crossover species can be recovered or are permanently destroyed. For instance, while a CE of 97% might be acceptable if the active species can be recovered, practical applications often require a much higher CE of over 99.99% when crossover species are destroyed irreversibly. As crossover rates can vary significantly at different SOCs, assessing crossover at these various SOCs during long-term cycling can provide valuable insights. Water and supporting ions may also migrate across the membrane, leading to volume imbalances and pH fluctuations. Fortunately, the rate of crossover can be generally improved by enhanced ionic membranes selectivity, and functionalization of redox active species.

Precipitation can occur for both organic and inorganic redox active species in electrolytes, leading to a loss of measurable capacity. Although these species can sometimes be redissolved into the electrolyte, the precipitate often blocks flow channels and porous electrodes leading to cell or system failure overall.

Decomposition or chemical breakdown of the of redox-active species in aqueous organic electrolytes on the other hand, is the most common capacity fade mechanism in organic-based RFBs utilizing substances like quinones, viologens, aza-aromatics, nitroxide radicals, and ferrocene. This degradation mechanism encompasses four main types: nucleophilic addition or substitution, disproportionation, dimerization or polymerization, and tautomerization. In RFBs significantly affected by self-decomposition, assessing time-dependent capacity decay (% per day) over a specified period is crucial since self-decomposition is time-sensitive. It is important to note that self-decomposition accelerates with the concentration of active materials present; thus, comparisons should consider both active material concentration and state of charge.

Lastly, electrolyte leakage from cell compartment can also lead to permanent capacity fade. This can be managed by proper mechanical engineering system.

2.6. Electrolytes

Due to advancements in research on RFBs, a diverse collection of redox flow formulations has been developed. These formulations are typically grouped into four categories according to their electrolyte composition, specifically considering solvents (water or organic solvents) and redox-active materials (metal compounds or organic species): aqueous metal-based, non-aqueous metal-based (referred to as organometallic), aqueous organic, and non-aqueous organic formulations.

2.6.1. Aqueous metal-based electrolytes

With advancements in RFB research, a diverse range of chemistries has been developed, categorized based on electrolyte composition into aqueous metal-based, nonaqueous metal-based, aqueous organic, and nonaqueous organic formulations. Aqueous metal-based RFBs are the most established systems, with the iron-chromium flow battery (ICB) being an early successful prototype utilizing $\text{Fe}^{2+}/\text{Fe}^{3+}$ and $\text{Cr}^{3+}/\text{Cr}^{2+}$ redox reactions with a standard potential of 1.18V. Despite its pioneering status, ICB faced challenges like hydrogen evolution and sluggish kinetics of the $\text{Cr}^{3+}/\text{Cr}^{2+}$ couple. The all-vanadium redox flow battery (VRB) is a prominent system utilizing four oxidation states of vanadium with reactions involving $\text{VO}^{2+}/\text{VO}_2^+$ and $\text{V}^{3+}/\text{V}^{4+}$,

resulting in a standard cell voltage of 1.26V. VRBs encounter issues like active material crossover, gas evolution, and high costs of components. Variants of VRBs, such as iron-vanadium (IVB) and vanadium-polyhalide, have been developed to address challenges. IVBs combine features of ICB and VRB systems, offering improved kinetics and reduced corrosiveness but with a lower theoretical voltage of 1.02V, impacting energy density. Strategies like increasing active material concentrations and operating at high states of charge can help mitigate this limitation.

2.6.2. Aqueous Organic Redox Flow Chemistries

Aqueous organic redox flow chemistries are categorized by the active materials they employ and the pH at which they operate. For example, quinone-based flow chemistry uses quinone derivatives capable of two-electron transfer processes, well-known for their redox activity in RFBs. Enhancements like introducing sulfonic and hydroxyl groups into quinone structures have been studied to improve solubility and subsequently increase the energy densities of RFB systems.

Another approach involves TEMPO-based reactants, utilizing the stable radical TEMPO (2,2,6,6-Tetramethylpiperidin-1-yl) oxyl, which undergoes single-electron reversible transfer processes. Due to TEMPO's limited solubility in aqueous solutions, derivatives like 4-hydroxy-TEMPO (TEMPOL) have been developed.

Other aqueous organic chemistries that have been demonstrated include those based on phenazines, ferrocenes, and viologens. In each case, functional groups were added to modify the redox potential and increase the solubility and stability of the compounds for a specific operating pH. In general, the cell potentials are limited by the water stability window of the electrolyte, and therefore rarely exceed 1.2-1.5V.

2.6.3. Nonaqueous Organometallic Redox Flow Chemistry

Nonaqueous redox flow batteries (RFBs) have been developed to achieve higher battery voltages by surpassing the limited potential window of water. Organometallic complexes play a crucial role as active materials in these nonaqueous RFBs, with a wide range of complexes explored based on their metal centers (e. g., V, Mn, Fe) or ligands (such as bipyridine and acetylacetonate). Specific systems utilizing redox-active ligands to create complexes functioning as active materials on both sides of the RFB have shown promise. Ionic liquids containing metal ions have also been synthesized and proposed as redox-active materials, including an all-copper RFB system incorporating copper-containing ionic liquids. Similarly, nonaqueous hybrid RFBs have emerged, featuring lithium metal anodes and organometallic complexes on the cathode sides. For example, a membrane-less ferrocene-based hybrid RFB with lithium metal anodes demonstrated significant advancements.

2.6.4. Nonaqueous Organic Redox Flow Chemistry

Transitioning from metal to organic redox-active materials in nonaqueous redox flow chemistry has been noted for its benefits, such as enhanced redox potential window and overall improved performance. However, challenges persist, including high cost, low conductivity, and solubility issues. Technical obstacles like limited power capability due to low ion mobility in nonaqueous solvents and membrane-related problems contribute to cross-contamination and irreversible capacity decay in nonaqueous redox flow batteries. Further research focusing on cost-effectiveness and better enhanced conductivity, while leveraging the unique advantages of nonaqueous systems, holds promise for significant future advancements. Due to the constraint associated with non-

aqueous chemistries, my research and thus this thesis will be exclusively focused on aqueous based RFBs.

2.7. Chemical Properties of redox flow battery electrolytes

The efficient operation of RFBs depends on the properties of electrolyte as the energy carrier. The key desirable characteristics are:

2.7.1. Wide Potential Window

The key to achieving high cell voltages is to increase the difference between the redox potentials of active materials. For aqueous flow batteries however, it is important to design within the electrochemical stability range of water, which thermodynamically requires reactant redox potentials to fall between 0 to 1.23V vs. standard hydrogen electrode (SHE).[13] Negolytes are species with low redox potentials (electron-rich compounds) such as anthraquinones, meanwhile, species with lower electron densities are usually employed as posolytes such as benzoquinones.[14] To achieve a large potential difference and overall high battery voltage, electron-withdrawing groups (EWGs) such as NO_2 , SO_3^- , and PO_3^{2-} are coupled with posolyte materials, while electron-donating groups (EDGs) such as NH_2 and OH are coupled with negolyte materials. EWGs can increase the electron affinity of molecules and hence enhance the redox potential. Conversely, EDGs can decrease the redox potential. Another way to modify the redox potential of redox-active materials is by adjusting the pH value.[14] According to the Nernst equation, the redox potential can decrease linearly with an increase in pH value in proton-coupled electrochemical reactions, where protons or hydroxyl ions are released or consumed.[15]

A Pourbaix diagram as depicted in Fig. 2.2 illustrates the stability of different chemical species at specific pH and potential levels. It also delineates a region known as the “water stability window” situated between two dotted lines. These lines are consistent across all aqueous Pourbaix diagrams and mark the potentials at which the hydrogen evolution reaction (HER) and oxygen evolution reaction (OER) occur.

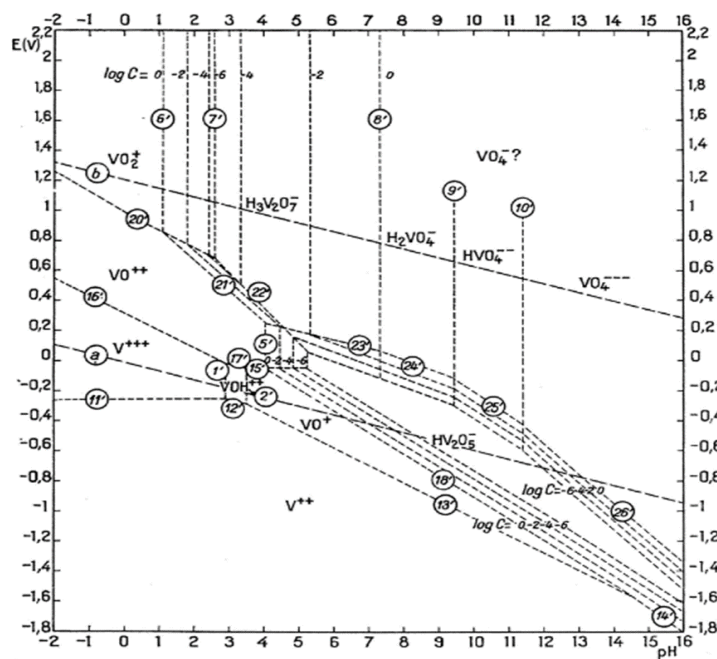


Figure 2. 2 Pourbaix diagram of Vanadium at different pHs.¹⁹

2.7.2. High Solubility

The solubility of both the oxidized and reduced form of electrolyte reactants is a critical factor in determining energy density. A higher effective concentration, calculated by multiplying solubility by the number of electrons transferred in redox reactions, results in greater energy density. Hydrophilic functional groups such as hydroxyl, carboxylate, amino, and sulfonic acid groups have been employed to improve the water solubility.[16] This process transforms nonpolar organic molecules into polar solutes, making them dissolvable in polar water solvents. The solubility of organic species can also be influenced by the spatial arrangement of substituents on their molecular structure. For instance, incorporating long alkyl chains with hydrophilic functional groups away from the quinone core has been found to increase solubility while not affecting the reduction potential. In addition, incorporating electron-donating or electron-withdrawing groups in close proximity to the quinone core can have an impact on both solubility and reduction potential[11].

2.7.3. High Ionic Conductivity

Active species must migrate from the bulk electrolyte to the electrode-electrolyte interface during the charge/discharge process. Simultaneously, counter ions must traverse the membrane to maintain charges on both sides. Although the ionomer membrane is typically the most resistive component in a flow battery due to its low ionic conductivity, the electrolytes can also contribute to this ohmic loss when used in conjunction with nanoporous electrodes. In general, flow battery electrolytes typically contain a high concentration ($> 1\text{M}$) of supporting electrolyte to maximize the ionic conductivity at all SOCs. For neutral electrolytes, this supporting electrolyte is most often KCl, whereas sulfuric acid is used for low pH electrolytes and KOH is used for high pH electrolytes.

2.7.4. Fast reaction kinetics

As with most electrochemical technologies, redox flow batteries benefit from fast reaction kinetics to increase their overall voltage efficiency. In addition, accelerated reaction rates can also minimize undesirable side reactions, such as recombination or the evolution of gases like oxygen and hydrogen. Many organic and metalorganic flow battery reactants, such as ferrocyanide or anthraquinone derivatives, have reversible or near reversible kinetics due to their simple reaction mechanisms. Hence, many kinetic studies of flow batteries have focused on the more sluggish redox reactions involving elemental reactants such as vanadium.

2.7.5. Low viscosity

Maintaining a constant flow of electrolyte is vital for storing energy in external electrolyte reservoirs. To enhance device operational efficiency and minimize energy consumption, a low viscosity is preferred. Higher viscosity demands more effort from the pumping system, leading to diminished Energy Efficiency and increased pressure drops. As with other chemical properties, the viscosity can be highly dependent on the SOC of each electrolyte.

2.7.6. Robust Chemical Stability

Ensuring the long-term stability of the electrolyte under operational conditions is crucial for designing an effective energy storage device. The generation of new species with reduced solubility or activity during the charge/discharge process can lead to potential efficiency reduction. Elevated concentrations, while offering high energy density, can lead to capacity degradation, through the formation of non-soluble species, such as the $\text{V}_2(\text{SO}_4)_3$ in the electrolyte of Vanadium

Redox Flow Batteries (VRFBs). Certain organic structures may form reactive intermediate species, such as radicals, which may interact with reactants and lead to irreversible decomposition, while others may decompose spontaneously via disproportionation or other irreversible reactions. In many cases, these degradation mechanisms may be exacerbated by high operating temperatures.

2.7.7. Synthetic cost

Although not a chemical property of the electrolyte, the cost of the reactants is one of the most important considerations for the commercialization of this grid storage technology. Aqueous electrolytes incur minimal costs due to the solvent but are constrained by the potential window. Organic solvents, while overcoming this limitation, introduce higher solvent costs.

2.7.8. Safety

Another critical aspect of flow battery electrolytes is their safety to society and the environment throughout their operational, manufacturing, and disposal phases. One of the notable advantages of RFBs is their ability to exchange electrolytes directly from the tanks which facilitates the upkeep of systems. However, the process of electrolyte replacement results in the generation of residues, and their associated environmental impact. A key focus in battery research should be on reducing the presence of polluting metals and limiting the content of organic solvents, aligning with the broader trend toward more environmentally friendly energy storage solutions.

2.8. Degradation mechanisms

2.8.1. Precipitation

One of the primary mechanisms contributing to capacity fade in aqueous RFBs is the precipitation of redox-active species within the electrolyte solution. This precipitation can occur due to various factors, including oversaturation of solute concentrations, changes in temperature, and alterations in electrolyte composition. The formation of precipitates leads to a reduced concentration of active species, thereby limiting their availability for charge transfer reactions during battery cycling and an associated reduction in capacity.

For instance, In VRFBs, capacity fade associated with precipitation is primarily observed in the negative electrolyte, typically containing vanadium ions in the form of V^{2+} and V^{3+} species. Precipitation of insoluble vanadium compounds such as $V_2(SO_4)_3$ can occur under certain operating conditions, particularly at high concentrations and elevated temperatures. This precipitation leads to reduced vanadium utilization and diminished battery performance over time.^{1,2} In addition, precipitation of iron and chromium compounds, such as $Fe(OH)_3$ and $Cr(OH)_3$, may occur due to the formation of hydroxide species under alkaline conditions. Hence, changes in pH due to oxygen or hydrogen evolution side reactions can also lead precipitation and loss capacity over time. In larger systems, these precipitates can accumulate on electrode surfaces and block flow channels entirely, leading to complete cell failure.³

2.8.2. Chemical decomposition

Although flow battery reactants composed purely of transition metals or other elements may precipitate, they still retain their original elements and may be reprocessed back to their original state. Organic molecules however, are susceptible to chemical decomposition involving irreversible bond cleavage or formation. Decomposition processes may involve nucleophilic addition/substitution reactions, disproportionation, dimerization, polymerization, and tautomerization of redox-active organic molecules. These reactions result in the formation of redox inactive species, ultimately leading to capacity fade.

Nucleophilic addition or substitution is a common mechanism of chemical decomposition in aqueous RFB reactants. This process involves a nucleophilic species (such as water, hydroxyl/hydroperoxide anions, or reduced redox-active species) interacting with an electron-deficient redox-active species, typically the oxidized form of the organic redox couple. The nucleophile can either displace a leaving substituent attached to the molecule irreversibly or bond to an unsubstituted position, leading to either the loss of conjugation (resulting in complete loss of redox activity) or a significant decrease in reactant reduction potential and/or solubility.[17] For example, in quinone-based electrolytes, the reduction potential is vital. Quinones possessing both a reduction potential exceeding 0.9 V are highly prone to Michael addition and/or gemdiol formation on a thermodynamic basis. This is linked to higher electron deficiency on the electrophilic carbon adjacent to the carbonyl group in the quinone ring, making them Lewis acids resulting to their reactions with water.[18] Modifying the quinone structure by introducing electron-withdrawing substituents may be a good strategy to mitigate this.

Chemical studies have established that nucleophilic reactions occur in other nonquinone-related high-potential substrates such as nitroxide radicals and organometallic complexes based on ferrocene (Fc) or ferrocyanide, with reduction potentials of 0.8V and $\sim 0.4\text{--}0.6$ V respectively. TEMPO has the ability to undergo a reversible one-electron transfer between the radical and corresponding oxoammonium cation at approximately 0.6 V vs. SHE. The use of 4-OH TEMPO as an AORFB electrolyte showed the possibility of TEMPO derivatives for energy storage, but there was a severe capacity fade, especially at high electrolyte concentrations. Research conducted later revealed that the oxidized form of 4-OH-TEMPO reacts with OH^- ions present in the solution, resulting in the acidification of the electrolyte.[19]

Some low-potential redox couples are also susceptible to decomposition by nucleophilic attack, which may limit their preferred operating conditions. Viologen derivatives are one such example and have been studied as negolytes for AORFBs due to their ability to undergo two reversible redox reactions at low potentials. For instance, Methyl viologen (MV) has low reduction potentials for the first and second electrons, but its ammonium functional groups in the fully oxidized (MV^{2+}) or singly reduced ($\text{MV}^{\bullet+}$) states can be vulnerable to OH^- attack. Meanwhile, the doubly reduced MV^0 species is not water-soluble and can be prone to protonation under acidic conditions.[20] Esters, ethers, and amides are some other functional groups that are susceptible to nucleophilic attacks which may result to the collapse of the oxidized form of their redox-active molecules, hence, loss in redox activity.[21] Experimentally, the addition of electron-donating groups to organic molecules that are susceptible to hydrolysis by OH^- is anticipated to decrease their reactivity.[22]

Chemical decomposition can also be triggered by disproportionation of certain reactants. This occurs when two species with the same oxidation state react and produce two different products with different oxidation states, one being reduced and the other oxidized.[23] If one of these products is redox-inactive or has low solubility and precipitates, capacity fade would occur in the battery. An apparent capacity fade can also be observed if one of the products has a more extreme redox potential than the original couple or has slower kinetics. For example, the oxidized form of 4-OH-TEMPO⁺ can react with OH^- ions in solution, leading to electrolyte acidification. As the pH decreases, 4-OH-TEMPO⁺ reacts with H^+ ions and undergoes disproportionation to produce 1,4-dihydroxy-2,2,6,6-tetramethylpiperidine, which is redox-inactive, and 4-OH-TEMPO⁺.

Another possible decomposition route for organic species is the formation of dimers or even oligomers. For instance, 1,4-dihydroxy-2,2,6,6-tetramethylpiperidine has been observed to form dimers with TEMPO, resulting in a loss of redox activity.[24] Similarly, it was observed that capacity fade in methyl viologen electrolytes is chiefly due to the tendency of the reduced form of MV, the radical cation, to form dimers, which can then undergo disproportionation to produce MV^{2+} and insoluble MV^0 which can precipitate and become redox inactive.[25]

Tautomers are isomers of a molecule that differ in the position of a hydrogen atom and a double bond. They have different chemical properties, such as different acidity/basicity, dipole moments, and reactivity.[26] Since tautomers have different electronic configurations, they can exhibit different redox potentials, which can lead to capacity fade or reduced energy density in electrochemical devices. Tautomers can be stabilized by the presence of specific functional groups or solvents, and their equilibrium ratios can be affected by temperature, pressure, and pH. Phenols are typically found in the enolic form because the energy decrease associated with rearrangement to the tautomeric keto-structure is offset by a large decrease in resonance energy.[27] However, in certain compounds such as naphthoquinones, polyhydric phenols, and hydroxyl derivatives of polycyclic aromatic hydrocarbons, the tautomeric ketonic structures become especially energetically favorable.[28] For instance, Tong et al.(2019) reported a naphthoquinone dimer, namely, bislawsone, which exhibited enhanced cycling stability. However, this dimer irreversibly experiences enol-ketone tautomerization in the quinonehydroquinone state developing into 2, 3-dihydrobislawsone (4), which is redox-inactive and easily precipitates out of the solution.[49] Methods to stabilize the enol generally involve the introduction of electron withdrawing substituents in the α position or unsaturated groups of conjugated structures.[29] In summary, understanding the primary degradation mechanisms of aqueous organic redox flow battery electrolytes is necessary to extending battery lifetime and creating longer lasting electrolytes.

2.9. Characterization of electrolyte degradation

This section describes some of the theory behind the key techniques used in this thesis for studying the electrolytes under investigation.

2.9.1. Cell Cycling

The primary way of characterizing electrolyte degradation is via full or symmetric cell cycling. Both the coulombic efficiency and capacity of the cell will be the first measurements indicating the health of the capacity limiting electrolyte. As mentioned above, coulombic efficiency is indicative of crossover of reactant species and/or presence of side reactions at the electrodes, and may only be occurring at and indicative of a problem with the non-capacity-limiting electrolyte. On the other hand, unless apparent capacity fade mechanisms are present, the cycling capacity is a direct measurement of the dissolved concentration and health of the redox active reactants in the limiting electrolyte. In potentiostatic cycling (also known as constant voltage or CV cycling), charge or discharge is performed with a constant voltage instruction. In galvanostatic-potentiostatic cycling (Constant current-constant voltage), charge or discharge is performed with a constant current until the limit voltage is reached, followed by a constant voltage phase until the current has decreased below a stated value, usually a 20th or a 50th of the total cell capacity. In the latter method, the constant voltage step enables accessing total available capacity in the electrolyte.[30] Pauses at various SOC between the cycles, also called current interruptions, can provide information on the influence of SOC on the degradations of aqueous organic electrolytes.[31] It is important to note that capacity fade could be hidden in the electrochemical

cycling test if it was not conducted under 100% SOC. For example, if the cell is cycling at 50% SOC, even if the total available capacity decays during cycling, the apparent discharge capacity may stay stable for a while, giving a false impression of the cycling stability.[32] However, 100% SOC represents a very challenging operating condition that is not commonly used in the commercially available batteries.

2.9.2. Cyclic Voltammetry

Cyclic Voltammetry (CV) is a widely used electrochemical technique that assesses the current response to a cyclic linear voltage sweep. Typically performed with a three-electrode configuration (comprising working, counter, and reference electrodes), the potential of the working electrode is repeatedly scanned over a given range. The resulting current response is graphed against the applied voltage sweep, generating a voltammogram fig 2.3.

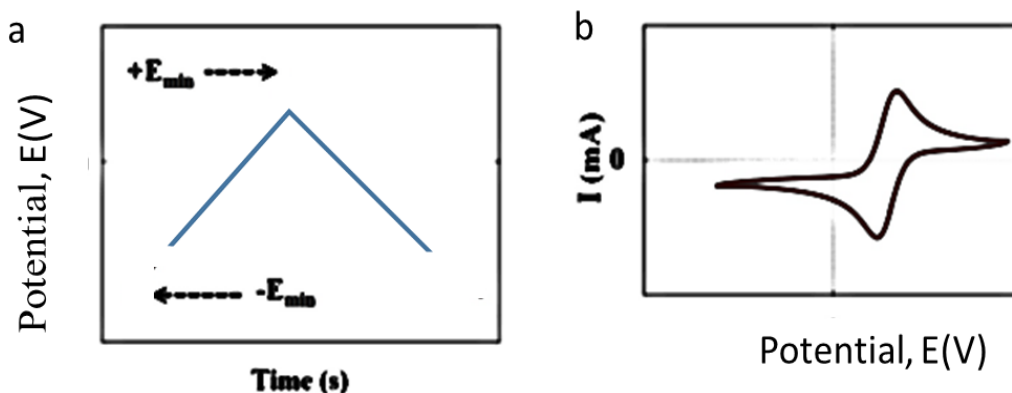


Figure 2. 3 a) cyclic voltammetry analysis demonstrating the controlled variation of working electrode voltage between two vertex potentials over time. b) Resulting current measurements plotted against the controlled voltage.

This method is commonly applied in the preliminary investigation of novel electrochemical systems to determine the redox potential of any possible reactions. Cyclic voltammetry (CV) is commonly employed for the analysis of electrodes, comparison of treatments (such as catalysts and additive particles), and evaluation of various electrode preparation processes. It is also utilized to assess the feasibility of new electrolyte chemistries and extensively applied in the performance evaluation of porous electrodes for capacitive deionization. While CV is often associated with kinetics studies, it has a broader scope of applications; for instance, Small et al. (2019) used CV to identify chemical species in a membrane crossover study.[33] Standard benchmark electrodes like glassy carbon, Pt, and graphite are frequently used in CV, with novel electrode structures and materials often compared against these benchmarks. A crucial parameter in CV analysis is the voltage scan rate (ν), measured in volts per second (V/s). The relationship between peak current and peak potential separation in response to the scan rate can offer insights into the reversibility of a process. Reversible and quasi-reversible processes exhibit peak currents that scale with the square root of the scan rate, as described by the Randles-Sevcik equation. The equation for peak current (i_p) at 25°C is given by:

$$i_p = 2.69 \times 10^5 n^3 A C D^{\frac{1}{2}} \nu^{\frac{1}{2}}$$

In this equation, 'ip' stands for peak current density, 'n' represents the number of electrons transferred in the limiting charge transfer step, 'A' denotes the electrode area, 'C' is the concentration of the reacting species, and 'D' is the diffusivity.

Categorizing a process as reversible or quasi-reversible provides insights into electrochemical efficiency and allows for the determination of the diffusion coefficient using the Randles-Sevcik equation. Alternatively, if the diffusion coefficient and surface area of the electrode are known, then the Randles-Sevcik equation can be used to measure the concentration of the redox active species in the electrolyte. Hence, it is often a preliminary ex situ measurement for monitoring the redox activity of a cycled electrolyte. Despite its widespread use, CV has notable limitations due to the complex interplay of various experimental factors (e. g., electrochemical surface area, voltage loss and capacitive currents), requiring meticulous analysis or supplementary experiments for quantitative and reproducible results. When conducting ex-situ experiments, it is crucial to consider the differences and limitations associated with using electrodes of varying morphologies compared to those intended for in-situ use, particularly concerning surface area and 3D morphology. Replicating realistic cell conditions in an ex-situ environment poses a significant challenge in obtaining meaningful CV results.

2.9.3. Rotating disc electrode (RDE) voltammetry

Rotating disk electrode (RDE) voltammetry is a commonly utilized method for examining the behavior of reaction mechanisms and mass transport characteristics. In RDE, the working electrode rotates within the electrolyte, creating a laminar flow above its surface, resulting in the development of a steady-state current as fresh electrolyte continuously reaches the working electrode. The peak current is constrained by the mass transport of reactants to and products away from the electrode. An RDE setup is inherently ex-situ and typically employs high purity and perfectly flat electrode materials which are not representative of highly porous RFB electrodes. While glassy carbon is commonly used as the base electrode material in RDE studies, its electrochemical behavior may not accurately reflect the behavior of a 3D electrode surface. The typical outcome of an RDE experiment is a linear sweep voltammogram, indicating a steady state limiting current rather than a peak current observed in CV (Fig 2.4).

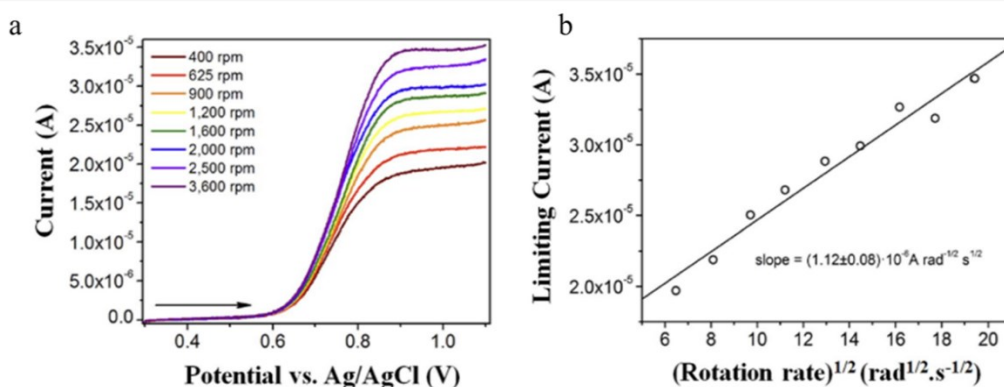


Figure 2. 4 a) Linear voltammograms obtained at different Rotating Disk Electrode (RDE) rotation rates. b) Levich plot illustrating the linear relationship between the limiting current and the square root of the rotation rate.

When the Levich plot shows linearity over a wide range of rotation rates (e. g., 50 - 10,000 rpm), it indicates a rapid transfer of n electrons with a high rate constant. The Levich equation is expressed as:

$$I_L = (0.620) n F A D^{\frac{2}{3}} \omega^{\frac{1}{2}} \nu^{-\frac{1}{6}} C$$

By knowing two variables in the Levich equation, we can find the third property. For instance, if we have n and ν , we can derive D from the slope. Typically, this method combines RDE experiments with stationary CV for complementary outcomes. In some cases, systems may exhibit slow kinetics and limitations in mass transport within an RDE setup. In such scenarios, a modification to the Levich equation, known as the Koutecky-Levich equation, is necessary. In its common form, the reciprocal of the measured current includes both a reciprocal kinetic current and a component dominated by mass transport:

$$\frac{1}{i} = \frac{1}{iK} + \left(\frac{1}{0.620 n F A D^{\frac{2}{3}} \nu^{-\frac{1}{6}} C} \right) \omega^{-\frac{1}{2}}$$

During Koutecky-Levich analysis, linear sweeps are performed for an RDE at different rotation speeds (ω). The reciprocal steady-state currents at specific overpotentials are plotted against $\omega^{-1/2}$ (Fig. 2.5) This technique allows the determination of the kinetic current (iK) and resulting kinetic rate constant from the y-intercept of the Koutecky-Levich plot. Moreover, based on the slope of the graph, we can confirm or identify the values of n or D .

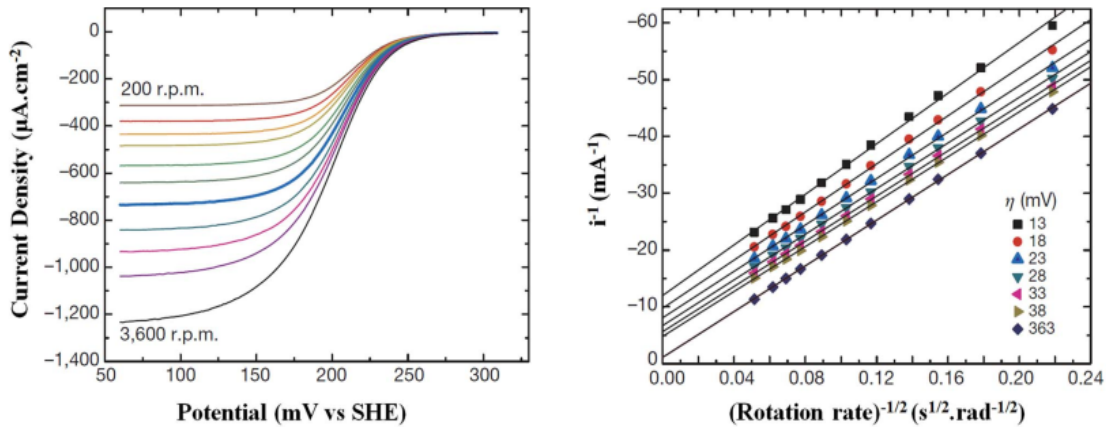


Figure 2. 5 a) Linear Voltammogram. b) Koutecky-Levich Plot showcasing the reciprocal kinetic current at different electrode overpotentials.

One challenge in RDE analysis is that the kinetic details obtained are greatly influenced by how the electrode is prepared and its form. The kinetic rate constant can vary significantly due to the electrode's original structure and behavior, as well as any modifications made for RDE analysis. Efforts to address this issue include preparing RDE electrodes with RFB electrode material, which requires pulverization and mixing with a binder, altering material characteristics. Regardless of the electrode type, it must withstand high rotational speeds (e. g., up to 3000 rpm). In a Koutecky-Levich evaluation of any transport-related property (such as the number of electrons, diffusivity, or viscosity), it is crucial that all other factors remain constant with rotation rate and overpotential, and that they are uniform across the entire RDE surface. Any variation in these parameters can lead to inaccurate calculations and significant over- or underestimation of a property.

2.9.4. Ultraviolet and visible light (UV-Vis) spectroscopy

This technique falls under absorption spectroscopy, operating within the ultraviolet-visible spectral region. UV-Vis spectroscopy relies on a light source emitting in the visible and near-ultraviolet ranges, coupled with a spectrometer. Its underlying principle lies in the absorption of energy by non-bonding electrons when exposed to ultraviolet (10-380 nm) or visible (380-780 nm) light. Such absorption excites these electrons to higher anti-bonding molecular orbitals, with the absorbed wavelength correlating to the excitable electron's energy level, where longer wavelengths indicate more easily-excited electrons.[34]

The UV-Vis method offers a straightforward and reliable quantitative approach for concentration determination. Additionally, UV-Vis spectroscopy, when coupled with a permeability cell, proves useful in measuring crossover phenomena. This method targets concentration gradient-induced crossover, wherein an electroactive species-enriched solution is circulated on one side of a membrane, while the other side lacks electroactive species.

The setup for UV-Vis spectroscopy is depicted in Fig. 2.7. UV-Vis spectroscopy proves useful in quantitatively determining concentrations in solutions or electrolytes, with vividly colored samples such as transition metal ions and highly conjugated organic compounds.

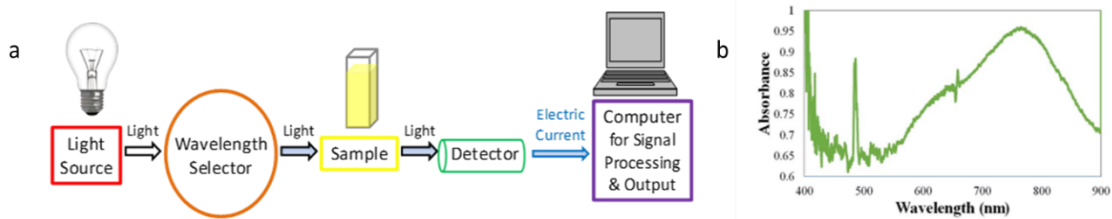


Figure 2. 6 a) A schematic UV-Vis spectrometer set-up. b) A typical absorbance spectrum.

To determine the concentration of a specific species in solution, the intensity of transmitted light through the solution relative to a clear medium is measured, as indicated by:

$$I = I_0 e^{-xNI}$$

Where I is the measured light intensity of the solute-bearing solution, I_0 is the baseline intensity of a solution without the solute, l is the path length, x is the cross-sectional area, and N is the number density of the absorbing molecules. Absorbance A is defined as:

$$A = -\text{Log} \left(\frac{I}{I_0} \right)$$

Beer's law, expressed in terms of molar concentration (c) and molar absorptivity (a_m), is employed to calculate absorbance (A^*), as depicted in the equation:

$$A^* = a_m cl$$

In cases when multiple absorbing solutes are present in a solution, the total absorbance is commonly regarded as a linear combination of the individual absorbances of each solute. This linear relationship holds true under the assumption that the absorbance of each solute is additive and independent of the others.

For a two-compound system with isosbestic points, where the absorbance remains constant at certain wavelengths regardless of the relative concentrations of the compounds, it simplifies the analysis. Isosbestic points provide a reference point for determining the concentrations of the individual compounds in the mixture. However, in a three-compound system without isosbestic points, distinguishing between the contributions of each compound becomes more challenging. This complexity arises because the absorbance at any given wavelength is influenced by all three compounds, making it difficult to deconvolute their individual effects. Consequently, analyzing mixtures with numerous degradation compounds using UV-Vis spectroscopy usually requires advanced analytical techniques to unravel the overlapping absorbance spectra effectively.[35] Moreover, a crucial requirement for concentration determination using this method is a linear relationship between absorption and concentration. However, this condition may not be met for all solutions and RFB electrolytes, thus necessitating calibrations for different compositions.

CHAPTER 3: LITERATURE REVIEW

Pioneering studies in flow batteries began in the 1970s at NASA leading to the development of the iron-chromium flow battery.[36] Since then, many new flow battery chemistries have been proposed and demonstrated in both academic and commercial research. The following section outlines some of the key developments in flow battery electrolyte research.

3.1. Aqueous electrolytes of interest

3.1.1. Inorganic

Vanadium redox couples are one of the most commonly used reactants found in commercial flow battery systems today. VRFBs offer abundant and easily prepared electrolyte solutions, adjustable capacity, and minimal environmental impact. They're highly recyclable, minimize cross-contamination, and boast long-lasting stability with unlimited electrolyte cycle life.

Skyllas-Kazacos et al. conducted a series of experiments to assess various supporting electrolytes, such as HCl, H₂SO₄, and HClO₄, for VRFB applications. They discovered that sulfuric acid offers the best balance of vanadium-ion solubility and redox-couple reversibility. Despite the possibility of oxygen evolution during overcharge reactions in sulfuric acid H₂SO₄, has been chosen as the preferred supporting electrolyte for both the V(II)/V(III) and V(IV)/V(V) redox couples. The capacity of a VRFB relies on the concentrations of vanadium ions, which are affected by the solubility of each redox couple ion (V(II), V(III), V(IV)). The solubility of these ions is influenced by factors like temperature, sulfuric acid concentration, and SOC.[37]

The concentration of vanadium in VRFB electrolytes is crucial for determining their energy density, influenced by the solubility and temperature stability of vanadium ions in different oxidation states and the supporting electrolyte. To prevent vanadium precipitation, which could cause blockages, it's important to maintain a maximum vanadium concentration within the operational temperature range. Skyllas-Kazacos and colleagues summarized the solubility of vanadium species in sulfuric acid at various temperatures and acid concentrations to set these limits[38]. Among the species, V(V) is the least stable and prone to precipitating into V₂O₅ crystals when the VRFB cell is fully charged, leading to extensive research. The group has actively researched methods to improve the thermal stability of V(V) at different concentrations, precipitation behavior at various temperatures and solution compositions, and precipitation inhibitors for supersaturated vanadyl electrolytes. They have also studied electrolyte optimization in terms of concentration, temperature, precipitation behavior, density, and viscosity[39]. Vijayakumar et al.(2011) showed that the V(V) species exists as a hydrated penta-coordinated vanadate ion VO₂(H₂O)³⁺, stable at low temperatures but deprotonates at higher temperatures to form the neutral VO(OH)₃ species, which then condenses to form V₂O₅ precipitate. [40]

In addition to temperature, the concentration of sulfuric acid is crucial for stabilizing the V(V) solution. Increasing the total sulfate/bisulfate concentration has been shown to improve the stability of the V(V) solution. For example, at 40°C, a 3M V(V) solution has an apparent V(V) concentration of only 1.6M in 5M sulfate/bisulfate, while it is 2.8M in 6M sulfate/bisulfate. The enhanced stability at higher sulfuric acid concentrations is due to the higher concentration of H⁺ ions. However, higher sulfuric acid concentration has limitations as it decreases the solubility of V(II), V(III), and V(IV) leading to precipitation as vanadium sulfate salts due to the common ion effect, unlike V(V) which undergoes thermal precipitation. Zhao et al. (2018) studied the solubility

and parameters of V(III) species in the anolyte under various H₂SO₄ concentrations and temperatures, showing that lower temperatures and prolonged exposure decrease V(III) solubility. [41] Xiao et al. (2016) investigated the physical properties of different vanadium species at sub-zero temperatures, demonstrating the reversibility of low-temperature precipitates upon warming except for V(V), which requires electrochemical means for redissolution. These findings highlight the importance of balancing temperature, vanadium concentration, and sulfuric acid concentration for optimal VRFB performance. Several studies have identified the preferred electrolyte composition for an operating temperature range of 10°C to 40°C as 1.6M to 2M vanadium and 4M to 5M total sulfate. [42]

3.1.2. Metal ligand complexes

Various ligands have also been investigated to stabilize certain metal oxidation states, such as Ethylenediaminetetraacetic acid EDTA,[43] phenanthroline,[44] triethanolamine,[45] and diethylenetriaminepentaacetic acid DTPA,[46] among others.

Modiba et al. (2013) conducted research on ligand complexes for the Ce (III/IV) redox couple, including EDTA, Ethylenediamine-N, N'-disuccinic acid (EDDS), Nitrilotriacetic acid (NTA), and DTPA, with the objective of enhancing the reversibility and electron transfer rate of the reaction. They also examined the influence of DTPA ligands on the electrokinetics of Ce(III/IV), Cr(II/III), and V(IV/V) for flow battery electrodes[47]. Ibanez et al. integrated multiple redox couples like Fe (II/III), Co (II/III), Cr (III/IV), and Ru (II/III), with various ligands such as EDTA, DTPA, phenanthroline, tetraethyl acetate, bipyridine, ethylene diamine, and diethylene triamine, for applications in flow batteries and photoelectrochemical cells.[48] Chen et al. complexed the Fe(II/III) redox couple with o-phenanthroline type ligands to positively shift the redox potential, albeit facing limited solubility in acidic media.[49] Wen et al. investigated the complexation of Fe (II/III) with triethanolamine for negative electrode utilization in an iron-bromine RFB, achieving solubility in alkaline media and an open circuit voltage of 1.9V.[45] Murthy et al. (1989) explored ligand complexes like EDTA, DTPA, and nitrilotriacetic acid for the Fe (II/III) couple, noting a negative shift in potential.[46]

Ferri/ferrocyanide, has often been employed in flow battery electrolytes due to the reversibility of its redox reaction around 450mV vs. SHE, good solubility in water, and low cost. Additionally, its high stability against chemical degradation makes it a reliable choice for redox flow battery applications. Although aqueous solutions of ferrocyanide stored in darkness or ambient indoor lighting conditions remain chemically stable, it has been shown that exposing neutral or alkaline pH solutions of ferrocyanide to light with wavelengths below approximately 500 nm leads to the chemical degradation of the anion into pentacyanide/iron hydroxides[50]. In acidic environments, ferri-/ferrocyanide has the potential to release free cyanide into the solution, resulting in the formation of hydrogen cyanide (HCN).[51] Early investigations on zinc-ferrocyanide hybrid RFBs by Adams et al. (1978) revealed that ferri-/ferrocyanide demonstrates chemical stability in solutions up to 7 N NaOH at temperatures reaching 50 °C. However, at temperatures exceeding this threshold, ferricyanide starts to decompose into electrochemically inactive iron pentacyanide, eventually transitioning into insoluble iron hydroxides, though they also acknowledged the presence of pentacyanide impurities in their initial material. Moreover, they highlighted the potential for pentacyanides in solution to be converted back to ferrocyanide through the addition of free cyanide.[52] Goulet and Aziz (2018) have reported the reduction of ferricyanide to ferrocyanide upon interaction with carbon paper electrodes with a reaction rate dependent on pH.[53]

Cazot et al. (2019) observed notably reduced rates of capacity degradation in ferri-/ferrocyanide capacity-balanced compositionally symmetric cells at elevated pH levels. They proposed that variations in membrane resistance during cell cycling could lead to capacity decline which may be associated with the use of purely galvanostatic cycling.[54] Páez et al. (2020) investigated the chemical instability of ferri-/ferrocyanide in alkaline conditions. They suggested that cell imbalance resulting from the electrochemical OER might significantly contribute to the apparent capacity fade observed.[55] More recently, the Liu group (2023) reported instances of cyanide ligand dissociation and subsequent irreversible hydroxylation. However, they demonstrated this degradation mechanism only under conditions involving the introduction of free cyanide in the solution and exposure to light. Yet, they have revised their interpretation and now attribute a significant portion of the observed capacity fade in capacity-balanced compositionally symmetric "half-cells" to the chemical conversion of ferricyanide to ferrocyanide, counteracted by the oxidation of graphite felt to carbonate (CO_3^{2-}) and ammonia. Once more, the rapid apparent capacity fade was partially linked to irreversible chemical degradation. Furthermore, they proposed that the previously observed undesired reduction of ferricyanide to ferrocyanide in alkaline environments is partially counteracted by a chemical oxidation of the presumed dissociated cyanide (CN^-) to cyanate (OCN^-).[56] However, the validity of this mechanism hinges on the presence of an ample supply of free cyanide in the solution, and if proven correct, the mechanism requires a more intricate elucidation involving hydroxide to thoroughly balance the hypothesized chemical redox reaction and clarify the observed pH sensitivity. Despite these degradation studies, potassium ferro/ferricyanide is generally considered a viable positive electrolyte material in alkaline organic redox flow battery applications.

3.1.3. Organic electrolytes

New redox couples for aqueous RFBs are emerging, utilizing small organic molecules synthesized from affordable raw materials such as anthraquinone and benzoquinone derivatives, priced at \$1 to \$3 per kilogram. These molecules are modified with additional substituents and ring structures to enhance solubility, stability, and electrode potential.[57] This modification aims to enhance solubility, improve chemical stability, reduce crossover, or achieve a specific electrode potential.[58]

While various molecular configurations are possible for organic redox couples, their vulnerability to degradation reactions still remains a bottleneck. Anthraquinone derivatives are considered a promising category of materials as negolyte of the battery. Anthraquinone disulfonic acid (AQDS) and anthraquinone monosulfonic acid are known for their stability in acidic environments and have been widely utilized in flow battery research.[59] Recent research conducted by Carney et al. has highlighted that AQDS and its reduced form generate a reversible 'quinhydrone' dimer, which increases viscosity, reduces utilization, but does not lead to permanent capacity loss.[60] Dihydroxyanthraquinone (DHAQ) and its derivatives have been investigated as negolytes in basic media. However, it has been shown that 2,6-DHAQ undergoes disproportionation when stored in the charged (reduced) state, resulting in the formation of an anthrone intermediate that may subsequently dimerize and lead to a loss in capacity. Goulet et al proposed a strategy to address capacity fade by avoiding higher charge states or introducing oxygen to chemically oxidize the anthrone intermediate.[61]

Benzoquinone derivatives utilized as posolytes are susceptible to nucleophilic addition reactions in aqueous settings. The molecule's higher positive electrode potential correlates with an increased propensity to interact with nucleophiles.[62] In acidic and neutral solutions, water serves as the

nucleophile, while in basic solutions, the hydroxide ion takes on this role. Electron-withdrawing groups, while advantageous for enhancing both the reversible electrode potential towards more positive values and solubility, exacerbate the electron deficiency in the ring, rendering the molecule more prone to nucleophilic attack. For example, the reaction of 1,2-dihydroxybenzene-3,5-disulfonic acid in its quinone form with water results in the formation of 1,2,4,6-tetrahydroxybenzene-3,5-disulfonic acid, resembling a Michael reaction (1,4-addition) of water to the quinone[63](Fig 3.1a and b). One strategy to mitigate this reactivity is exemplified by 1,4-dihydroxy-2,6-dimethylbenzoquinone-3-sulfonic acid (DHDMBBS), where electron-donating groups beneficially modify the local electron density distributions.[61] Despite the increased stability conferred by an electron-donating methyl group, the molecule's electrode potential is diminished.[64] In basic media, benzoquinones undergo rapid Michael addition due to the strong nucleophilic nature of the hydroxide ion. Addition of methyl groups is not advantageous as the hydroxide ion deprotonates them to form a quinone methide intermediate, which irreversibly decomposes to yield other products (Fig 3.1c). By enhancing the electron density on the aromatic ring, as exemplified in DHDMBBS, these compounds become vulnerable to electrophilic attacks. In acidic solutions, the H^+ electrophile interacts with such electron-rich arene sulfonic acids, initiating a protodesulfonation reaction (Fig 11d). This process leads to the removal of the sulfonic acid group, crucial for the solubility of the compound, into the solution, resulting in the precipitation of the redox species. Their investigations have indicated that the pace of protodesulfonation can be controlled by adjusting the acidity of the electrolyte.[61] Hence, a delicate balance must be maintained to prevent the occurrence of both the Michael addition reaction and the protodesulfonation reaction. AQDS and anthraquinone monosulfonic acid serve as examples of compounds that exhibit significant resistance to Michael addition in acidic or basic environments, as well as protodesulfonation in highly acidic conditions.

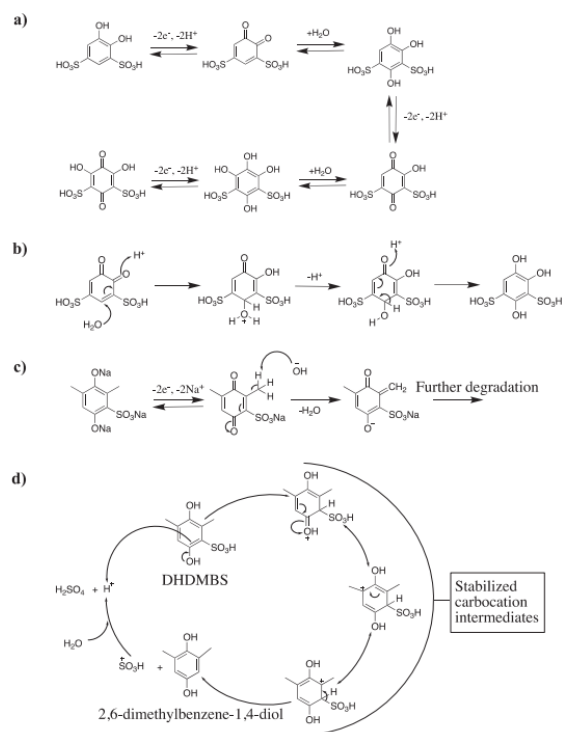


Figure 3.1 a) Schematic of the Michael reaction on BQDS during charging. b) Mechanism of Michael reaction on BQDS showing nucleophilic addition of water. c) Quinone methide formation: reaction of methyl groups with the basic media. d) Mechanism of protonation.⁶⁶⁻⁶⁷

3.2. Electrolyte Characterization

Several studies have utilized diverse techniques in the characterization of aqueous redox battery molecules and in assessing molecule degradation. Some of these are outlined below.

3.2.1. Cyclic voltametric study

CV is a fundamental electrochemical technique utilized for investigating redox processes of electrolytes. In RFBs, CV plays a crucial role in identifying redox couples and determining the redox potentials of active redox species.[65] Additionally, it serves as a valuable tool for assessing degradation by comparing CV curves of fresh electrolytes with those of used ones. Key indicators of potential degradation include the disappearance or reduction of original redox peaks and the appearance of new peaks. Changes in peak current and potential are essential for evaluating molecule degradation.[66]

Pinheiro et al. (2021) utilized CV measurements to evaluate the stability of electrolytes in sulfonated tryptanthrin-based RFBs. The cyclic voltammogram profiles of sulfonated tryptanthrin (TRYP-SO₃H) and 4,5-dihydroxy-1,3-benzenedisulfonic acid disodium salt monohydrate (BQDS) revealed degradation of the active materials. In the cycled TRYP-SO₃H, new anodic and cathodic peaks emerged, along with a higher current density in the redox peaks of the fresh electrolyte compared to the cycled one, indicating potential loss of the active material. Furthermore, CV measurements of BQDS unveiled a new peak associated with degradation due to a Michael addition reaction.[67]

Fahad Alkhayri et al. (2021) investigated the stability of bispyridinylidene anolytes and TEMPO catholytes for non-aqueous redox flow batteries (NARFBs) using CV. crossover of both anolyte

and catholyte through the anion exchange membrane was identified from the CV curve. Additionally, the CV confirmed the decomposition of the catholyte, as evidenced by the presence of new peaks at 0.0 V and 0.7 V, indicating the presence of new species.[68] Fig. 3.2 illustrates a typical CV plot for electrolyte degradation studies in RFBs.

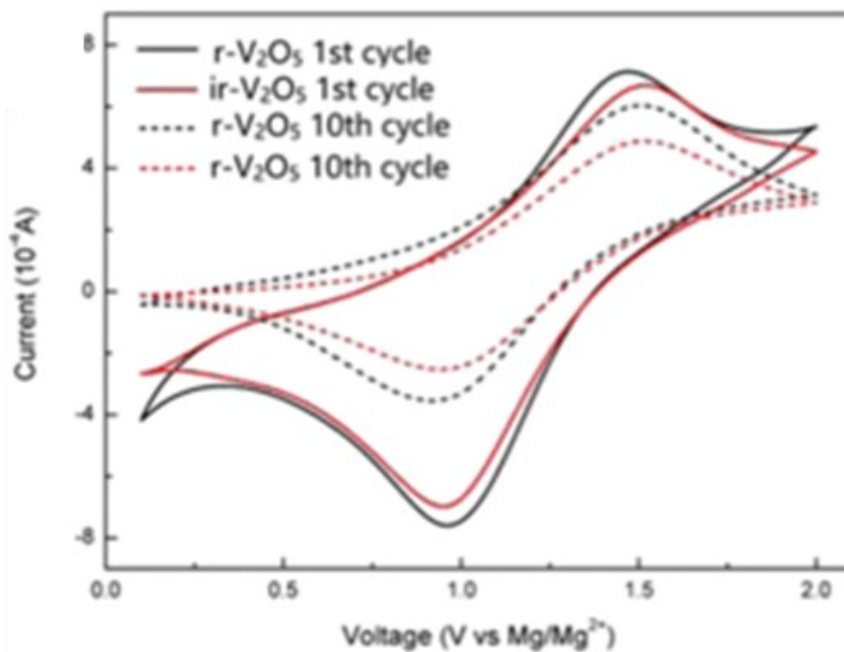


Figure 3. 2 a) A typical CV showing degradation of electrolyte overtime⁷²

3.2.2. Ultraviolet-visible (UV-Vis) spectroscopy/spectrophotometry

Ultraviolet-visible (UV-Vis) spectroscopy is a technique that reveals the characteristics of an electrolyte by measuring the intensity of light absorbed or transmitted in the ultraviolet and visible regions of the electromagnetic spectrum. Absorbance and transmittance, influenced by the composition and concentration of the sample, enable the analysis and quantification of molecules.[69] In this approach, a decrease in peak intensity or the appearance of new peaks indicates potential decomposition of the redox-active materials (Fig. 3.3).

Liu et al. (2021) utilized UV-Vis spectroscopy to evaluate the stability of ethyl viologen radical (EV^+) with and without α -cyclodextrin (α -CD) as a bystander in aqueous organic RFBs. The UV-Vis results of EV^+ without α -CD showed decomposition over a nine-day observation period. Conversely, the UV-Vis results of the cation with α -CD as a bystander demonstrated enhanced stability, with minimal degradation observed.[70]

Kwon, et al. (2018) investigated 5,10-dihydro-5,10-dimethyl phenazine (DMPZ) as a positive redox-active material in RFBs. Using UV-Vis spectroscopy, they examined the stability of any intermediate radical cations during the redox process of DMPZ. The UV-Vis spectra of $DMPZ^+$ remained unchanged during a 24-hour monitoring period, confirming the robust stability of the intermediate radical cation.[71]

Attanayake, et al. (2021) also employed UV-Vis spectroscopy to assess the stability of organic radical cations as positive electrolytes in an organic RFBs. Their investigation revealed that positive redox-active materials with lower oxidation potentials exhibited superior stability compared to those with higher oxidation potentials. Phenothiazine tetrafluoroborate derivatives with higher oxidation potentials demonstrated lower stability.[72]. The figure below is a typical example of a UV-Vis spectra comparing different electrolyte samples.

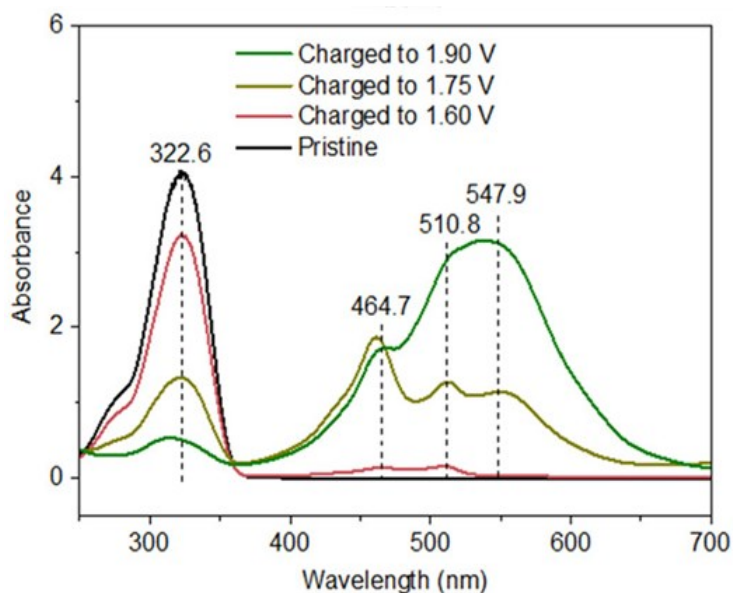


Figure 3.3 Ultraviolet-visible (UV-Vis) absorption spectra of 1.0 mmol/L [(NPr)₂PV]·4Cl anolyte at different charge states.⁷⁷

3.2.3. Mass spectrometry

Mass spectrometry (MS) is an analytical technique that assesses the mass-to-charge ratio (m/z) to quantify and identify molecules. Various forms of MS, including Liquid Chromatography-Mass Spectrometry (LC-MS), Matrix-assisted laser desorption/ionization-time of flight (MALDI-TOF), Inductively coupled plasma mass spectrometry (ICP-MS), Direct Analysis in Real Time Mass Spectrometry (DART-MS), Secondary ion mass spectrometry (SIMS), and others, can be effectively employed to investigate organic electroactive molecules. Xu et al. (2021) utilized Gas Chromatography-Mass Spectrometry (GC-MS) to explore decomposition phenomena in 2,5-di-tert-butyl-1-methoxy-4-[20-methoxyethoxy] and 3-nitrotoluene (3-NT) as catholyte and anolyte, respectively. Analysis of mass spectra revealed the appearance of new peaks, confirming the degradation of 3-NT into 3,30-dimethylazobenzene during battery cycling.[73] Furthermore, Bo et al. (2021) employed LC-MS to investigate the stability of electrolytes in neutral aqueous RFBs based on 3-carbamoyl-2,2,5,5-tetramethylpyrroline-1-oxyl (CPL). The mass spectrum of the cycled CPL electrolyte displayed an additional peak at a mass-to-charge ratio of 151.89, corresponding to a positively charged diene structure. This occurrence was linked to CPL undergoing a ring-opening side reaction on the nitroxide radicals due to attacks by water molecules.[74]

3.2.4. Nuclear magnetic resonance (NMR) spectroscopy

NMR spectroscopy enables the detailed analysis of the molecular structure of organic compounds by examining the interactions between nuclear spins and radiofrequency electromagnetic radiation in a high-intensity magnetic field.[75] Wang Caixing et al. (2021) applied NMR spectroscopy to study the stability of 2,6-diaminoanthraquinone, specifically N,N'-(9,10-anthraquinone-2,6-diyl)-di-β-alanine (DAEAQ). Analysis of the cycled DAEAQ anolyte using NMR revealed the appearance of new spectral peaks, indicating the irreversible degradation of the molecule, a significant factor contributing to capacity loss in this battery system. Control experiments, supported by Hydrogen Nuclear Magnetic Resonance (H-NMR) spectroscopy, confirmed the presence of degradation by-products through the detection of new peaks when the DAEAQ anolyte was stored at 80°C for 7 days.[76] H-NMR analysis confirmed the degradation of 3,3'-dimethylaminemethylene-4,4'-biphenol (DABP) catholyte in a silicotungstic acid (SWO)/DABP flow battery, as reported by Liu Wanqiu et al. (2021). The decomposition was attributed to side reactions between DABP and solvent molecules, supported by the identification of new peaks in the NMR spectrum.[77]

3.2.5. Fourier-transform infrared (FTIR) spectroscopy

Fourier-transform infrared (FTIR) spectroscopy is a fundamental analytical tool in the field of electrochemical engineering for the identification of organic molecules. It operates by producing an infrared absorption spectrum that reveals the chemical bonds and functional groups present within the molecule.[78] Changes in peak patterns, such as the disappearance or appearance of peaks, indicate the formation of new functional groups, signaling potential degradation or decomposition of redox-active materials, as depicted in Fig. 3.4. Duan et al. (2016) demonstrated the effectiveness of FTIR in evaluating electrolyte concentration and state of charge in the 2-phenyl-4,4,5,5-tetramethylimidazoline-1-oxyl-3-oxide (PTIO) based symmetric flow battery. Through FTIR analysis, the study differentiated between PTIO species (PTIO, PTIO⁺, and PTIO⁻) by monitoring their concentrations throughout the charge/discharge cycle, enabling the detection of any variations in the active molecule.[79] Additionally, Liang et al. (2022) verified the stability of ester linkages between redox-active groups and backbones by observing consistent signals at 1650 and 1550 cm⁻¹ before and after cycling, with the integrity of these linkages confirmed by an ATR-FTIR signal at 1730 cm⁻¹. [80] These results highlight the effectiveness of FTIR spectroscopy as an essential technique for decomposition investigations in RFBs.

3.3. Different SOC evaluation techniques

The estimation of state of SOC in flow batteries electrolytes has garnered considerable attention in scientific literature. various methodologies investigated for SOC estimation, will be presented in this section.

3.3.1. Coulomb counting

A practical, cost-effective, and technology-independent method for tracking the SOC is the ampere-hour or coulomb counting approach. This method involves integrating the current, i , flowing through the battery over time to calculate the total charge, ΔQ , transferred between the two half-cells. The SOC can be determined using this method by:

$$\text{SOC}^B(t) = \text{SOC}^B_0 + \text{CE} \frac{\Delta Q}{Q_B}$$

it is assumed that the initial SOC, represented as SOC^{B_0} , the total capacity of the battery (QB), and the coulombic efficiency of the redox reaction are determinable at any specific moment. Therefore, it is crucial to precisely determine these parameters using alternative methods either before or during battery operation. Rudolph et al reported this approach to be prone to accumulating errors over time stemming from slight inaccuracies in current measurement, unidentified background currents, side reactions, battery degradation (leading to variations in QB), and erratic changes in coulombic efficiency.[81] Due to its lack of reliability for prolonged monitoring, sole dependence on coulomb counting is not recommended. Nevertheless, its precision and ease of use for short-term assessments make it useful for both ex-situ and in-situ calibration of alternative techniques.

3.3.2. Open circuit voltage (OCV)

The validity of the equation above is contingent upon both electrolytes reaching equilibrium in their state-of-charge (SOC), represented as:

$$SOCB = SOCE_{pos} = SOCE_{neg}$$

Yet, deviations in the SOC of the positive or negative electrolyte caused by side reactions and crossover may introduce unforeseen imbalances between the electrolytes during battery operation. Although frequent recalibration can alleviate SOC estimation errors at the full-cell level, SOC drift at the half-cell level remains undetectable unless a standard reference electrode can be used. This method allows for the determination of individual electrolyte state-of-charge (SOC^E) and facilitates the identification of electrolyte imbalances. However, for this technique to be effective, the stability of the standard reference electrode potential is essential. Ressel et al. (2024) introduced a direct online calibration approach to establish the reference potential, E^{0ref} , during flow battery. By integrating the Nernst equation with the coulomb counting method, the researchers illustrated that nonlinear regression of experimentally derived OCV capacity data to a theoretical equation provides estimations for electrolyte capacity ($Q_{th=m}^{-1}$), reference potential (E^{0ref}), and initial electrolyte state-of-charge (SOC^{E_0}).[82]

$$\Delta E = E^{0ref} + \frac{RT}{z_e F} \ln \left(\frac{SOC^{E_0} + m\Delta Q}{1 - SOC^{E_0} - m\Delta Q} \right)$$

Reference electrodes in flow battery systems are prone to significant potential drift over extended periods, necessitating frequent recalibrations. Yang et al. (2019) introduced a remedy by creating a specialized open-circuit cell where the 2.6 M H_2SO_4 reference electrolyte encompassing the hydrogen reference electrode is consistently replenished.[83] While this method effectively mitigates potential drift, its feasibility for industrial use is impeded by the substantial amount of acid needed. Another approach to mitigate reference drift involves employing compositionally symmetric open-circuit cells, where a segment of the flow battery electrolyte itself, maintained at a fixed state-of-charge, acts as the reference electrolyte. This technique reduces potential drift and enables on-site generation of the reference electrolyte during battery operation.[84] Additionally, real-time recalibration can be executed by substituting the reference half-cell with fresh reference electrolyte, offering enhanced resolution and efficiency in the recalibration process. Nonetheless, considering reference electrolyte exchange as a recalibration procedure necessitates additional hardware, leading to increased cost and complexity. Investigations by Ngamsai et al. (2015) [85] and Stolze et al. (2019) [86] have documented the effectiveness of these strategies in detecting

electrolyte imbalances in VRFBs and monitoring state-of-charge in organic flow batteries, respectively.

3.3.3. Spectroscopy and photometry

Various spectroscopic and photometric techniques have been demonstrated for precise ex situ and/or in situ SOC measurements in diverse RFB electrolytes. In the context of aqueous vanadium-based electrolytes, absorption spectroscopy at specific UV-Vis wavelengths has been identified as a reliable method for the negative electrolyte. However, initial attempts to apply this method to the positive vanadium electrolyte were hindered by observed non-linear absorbance behavior. Geiser et al. (2019) introduced SOC calibration methods based on titration and open-circuit voltage for UV-Vis absorbance measurements. While these methods were suggested for in situ SOC measurement of concentrated vanadium polysolutes and negolytes, there was lack of empirical data from operational VRFBs and error assessments.[87]

In contrast, Kyung-Hee et al. (2020) presented an in situ SOC measurement technique for concentrated vanadium electrolytes, utilizing the difference in UV-Vis absorbance between the negolyte and polysolute measured with a specialized 0.1 mm thick quartz cuvette. Although this technique enabled the determination of the negolyte's state-of-charge (SOC^E), challenges arose for the polysolute due to inherent non-linearity in the UV-Vis spectra.[88] Addressing the difficulties with positive vanadium electrolytes in UV-Vis absorbance measurements, Liu et al. (2012) suggested measuring full UV-Vis transmittance spectra to ascertain the SOC^E of both positive and negative vanadium electrolytes. By creating a comprehensive database of full transmittance spectra at known SOC^E , vanadium concentrations, and H_2SO_4 concentration, and employing correlation analysis, these researchers predicted SOC^E , total vanadium species concentration, and H_2SO_4 concentration for both electrolytes with an absolute error margin of around 2% in ex situ and in situ scenarios.[89]

Buckley and colleagues (2014) expressed reservations regarding the susceptibility of this method to calibration errors and its computational complexity.[90] Instead, they conducted ex situ analyses on the solution chemistry of positive vanadium electrolytes, providing evidence for the existence of a strongly absorbing 1:1 mixed valence complex $V_2O_3^{3+}$ and formulated equations to predict the excess absorbance of such electrolytes using a $V_2O_3^{3+}$ equilibrium model. Building upon these discoveries, the team developed a methodology to forecast SOC calibration curves for absorbance spectra of VRFB polysolutes across a wide range of total concentrations and wavelengths. As a result, they successfully determined polysolute SOC values with absolute errors of less than 3% by measuring UV-Vis absorbance at two distinct wavelengths, albeit requiring prior knowledge of the total vanadium species concentration. The authors proposed that unlike other spectroscopic techniques, this concentration could be determined independently from measurements at more than two wavelengths. While the majority of research on UV-Vis spectroscopy for SOC monitoring has concentrated on aqueous VRFBs, the method is also adaptable to various other flow battery electrolytes, including organic flow batteries. For example, Gokoglan et al. (2019) observed a simplified UV-Vis absorption spectrum for vanadium(IV) bis-hydroxyiminodiacetate species compared to its aqueous counterpart, utilizing it for SOC measurements.[91] Aziz and collaborators (2018) showed that 9,10-anthraquinone-2,7-disulfonic acid forms a quinhydrone dimer leading to deviation from the anticipated equilibrium voltage for a two-electron redox reaction.[92] Furthermore, Agulio-Aguayo et al. (2018) introduced an alternative UV-Vis absorption technique for measuring SOC in iron-based redox flow batteries (RFBs). The formation of a strongly absorbing Fe(II)-1,10-phenanthroline complex enables precise detection of

Fe^{2+} concentration, while the use of hydroxylamine for the reduction of Fe^{3+} to Fe^{2+} allows for total iron concentration measurement. This method is purported to be independent of pH, temperature, and total analyte concentration, although it is limited to ex situ SOC measurement of iron-based RFB electrolytes.[93]

Rudolph et al. (2013) initially reported on Infrared (IR) absorption measurements of a VRFB electrolyte.[81] The sensor was calibrated using coulomb counting during galvanostatic VRFB operation. The authors highlighted a precision error below 1% for their SOC measurement; however, this value pertained to repeatability rather than accuracy concerning true SOC values. In a subsequent study, the same research team applied this method for in situ examination of VRFB electrolyte imbalances and for forecasting electrolyte equilibrium potential. A deviation of 4 mV from the measured value was observed in the SOC range from 2% to 98%, corresponding to an absolute SOC difference of approximately 4% between the OCV and the IR approach.

Duan et al. (2017) utilized FTIR spectroscopy to investigate the SOC of a symmetric organic-based RFB utilizing 2-phenyl-4,4,5,5-tetramethylimidazoline-1-oxyl-3-oxide (PTIO).[94] Although the authors suggested that the total PTIO/PTIO⁺ couple concentration could be inferred from FTIR, SOC calculation assumed a constant and pre-established total concentration.

Spectroscopic methods offer numerous benefits for SOC monitoring, including versatility across various electrolyte types, high accuracy in SOC prediction and half-cell resolution. However, the spectroscopic response of the electrolyte may be influenced by factors such as complexation and dimerization, necessitating a thorough comprehension of the underlying solution chemistry at different analyte concentrations. Furthermore, spectroscopic methods typically require extensive calibration across all potential electrolyte compositions and temperatures to generate meaningful results, primarily due to the significantly non-linear relationship between molar extinction coefficients and species concentration.

CHAPTER 4: PRELIMINARY ELECTROLYTE CHARACTERIZATION

Electrolyte properties are fundamental to flow battery performance and operating conditions. Novel electrolytes, such as the organic ones that have been developed in recent years, are typically screened to assess their key properties before they are cycled in flow batteries. Some of the most important properties of flow battery electrolytes are the pH and redox potential relationship, the solubility, the kinetic rate constant on carbon electrodes, the diffusion coefficient, etc. This chapter presents such results for two different electrolytes and is divided by technique/property.

4.1. Experimental Methods

4.1.1. Reagents

1,2- Dihydroxyanthraquinone (1,2-DHAQ, 97%) and Vanadium (IV) sulphate oxide hydrate (VOSO_4 , 99.9%) were obtained from thermo scientific. Potassium Ferrocyanide ($\text{K}_4\text{Fe}(\text{CN})_6$) and Potassium Ferrocyanide Trihydrate ($\text{K}_4\text{Fe}(\text{CN})_6 \cdot 3\text{H}_2\text{O}$) were obtained from fisher chemical. Potassium hydroxide (KOH) and Sulphuric acid were purchased from Sinopharm Chemical Reagent Co. Ltd. All chemicals were used as received without further purification.

4.1.2 Electrochemical measurements

Characterizations were performed using CV, Pourbaix, k^0 and D0 analyses. The electrochemical experiments were conducted on an electrochemical working station (Bio-logic, SAS) at 25°C using a conventional three-electrode electrochemical cell, where a graphite carbon rod was utilized as the counter electrode, unless otherwise stated, Ag/AgCl in 1 M KCl served as the reference electrode, and a glassy carbon (GC, 0.1963 cm²) disk electrode used as the working electrode, respectively. All potentials are reported relative to the Ag/AgCl electrode. Before measurements, the GC disk electrode was polished with 0.03 μm Alumina micro-polish and cleaned with deionized water. The Alizarin (1,2-DHAQ) and Ferri/Ferrocyanide (FeCN) were dissolved in a 1 M KOH solution while the VOSO_4 was dissolved in 1M H_2SO_4 , all served as the electrolytes. Rotating-disk electrode (RDE) experiments were performed using a modified glassy carbon rotating disk electrode (RDE, 5 mm diameter) mounted onto a Cole Parmer rotator (Pine Research Instrumentation). The Pourbaix diagram (E^0 versus pH) was constructed using 10 mM 1,2-DHAQ aqueous solutions in pH buffers using the following reagents: $\text{K}_2\text{HPO}_4/\text{K}_3\text{PO}_4$ (pH 10-12), and KOH (pH > 12). The pH of each solution was adjusted with KOH solutions (0.001-1 M) and measured with an Oakton pH meter.

4.2. Results

4.2.1. CVs for Redox Potential

Fig. 4.1 illustrates the CV of the 1,2-DHAQ redox couple recorded at a scan rate of 100 mV/s. CV being an essential electrochemical technique, was used to investigate the redox behavior of this electroactive species. By varying the potential linearly with time and recording the resulting current, valuable information about the redox processes, kinetics, and mechanisms of the studied compounds can be deduced.

In the CV of 1,2-DHAQ, the anodic peak (E_{pa}) corresponds to the oxidation process where the molecule loses electrons, and the cathodic peak (E_{pc}) corresponds to the reduction process where the molecule gains electrons. These peaks are clearly distinguishable in the voltammogram, indicating a well-defined redox couple.

When standard conditions are used for a reversible redox couple, the redox potential for the reaction, $E_{1/2}$, can be estimated as the average of the anodic peak potential (E_{pa}) and the cathodic peak potential (E_{pc}):

$$E_{1/2} = \frac{E_{pa} + E_{pc}}{2}$$

From the CV, of 1,2-DHAQ, $E_{1/2}$ is found to be approximately -0.864 V. This negative value indicates that the reduction process of 1,2-DHAQ occurs at a relatively low potential, suggesting that 1,2-DHAQ would be used as a negolyte in an aqueous battery.

In addition, the difference between the anodic and cathodic peak potentials (ΔE) is another critical parameter. It is defined as:

$$\Delta E = \frac{E_{pa} - E_{pc}}{n}$$

The ΔE for 1,2-DHAQ is approximately 58mV, indicating a quasi reversible 2-electron transfer process, only 28mV greater than a reversible system. This ΔE value typically indicates an efficient redox process with good electron transfer and minimal activation energy for the redox reaction. This is a desirable characteristic for materials used in redox flow batteries (RFBs), crucial for maintaining battery performance over extended cycles.

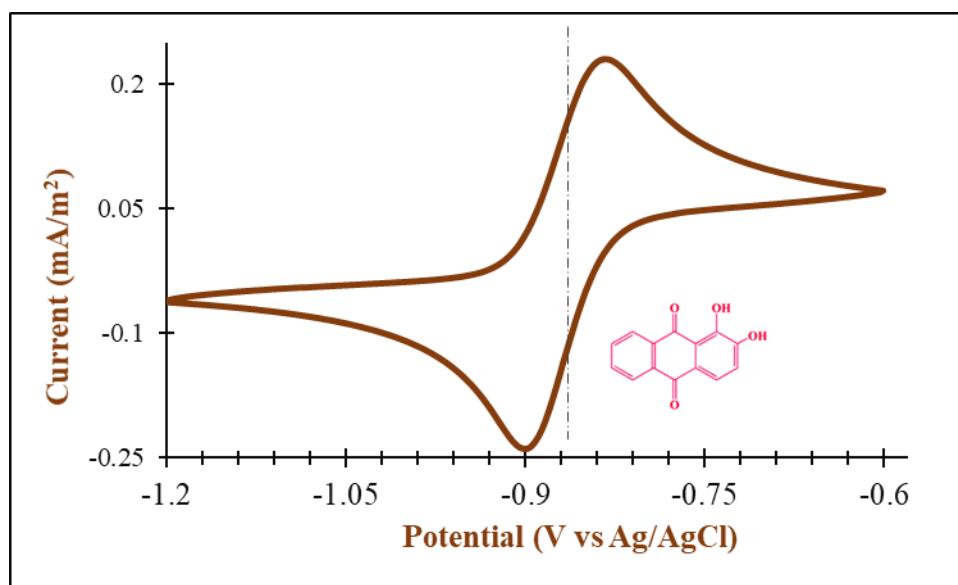


Figure 4. 1 CV of 10mM 1,2-DHAQ measured at a glassy carbon electrode in 1M KOH; scan rate 100 mV s⁻¹; room temperature.

The CV of the FeCN redox couple as shown in Fig. 4.2, demonstrates distinct anodic and cathodic peaks. These peaks correspond to the oxidation of Fe²⁺ to Fe³⁺ and the reduction of Fe³⁺ back to Fe²⁺, respectively. The presence of these well-defined peaks indicates a clear and reversible redox couple.

The $E_{1/2}$ for the FeCN redox couple, calculated as the average of the anodic and cathodic peak potentials (E_{pa} and E_{pc}), is approximately 0.253V vs AgCl.

The measured ΔE is approximately 85 mV for FeCN. This ΔE value suggests relatively good reversibility of the redox process, though it is slightly higher than that observed for 1,2-DHAQ, indicating a somewhat higher activation energy for the electron transfer process. The moderate ΔE value for FeCN points to efficient but slightly less rapid electron transfer kinetics compared to highly reversible systems.

The fast kinetics and high redox potential of FeCN, as evidenced by its CV profile, make it a viable candidate as a polysolite for redox aqueous flow batteries (RFBs).

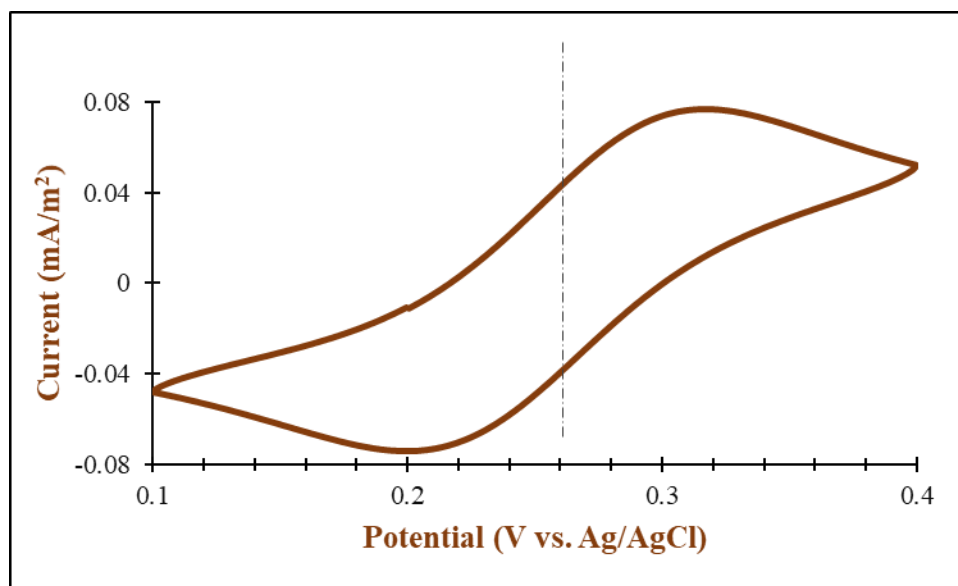


Figure 4. 2 : CV of 5mM FeCN in 1M KOH measured at a glassy carbon electrode; scan rate 100 mV s⁻¹; room temperature.

4.2.2. Pourbaix Diagrams

The CV curves of 10 mM 1,2-DHAQ on a glassy carbon electrode at different pH values are shown in Fig. 4.3a, from which a Pourbaix diagram ($E_{1/2}$ vs pH, Fig. 4.3b) are plotted. Previously, Lin et al. (2015) reported a slope of Pourbaix diagram for 2,6-DHAQ, calculated to be -61 mV pH⁻¹, corresponding to 2-proton/2-electron process in the pH range 10-12, while the slope changes to 0 mV when the pH is above 12 [95]. In other words, the redox potential is pH-independent above pH 12. However, different from that of 2,6-DHAQ, the Pourbaix diagram ($E_{1/2}$ vs pH) of 1,2-DHAQ can be fitted to two dashed lines indicating slopes of -37 mV (pH 10.3-12.2) and approximately -4 mV (pH above 13). This means that the redox potential of 1,2-DHAQ is almost pH-independent above pH 13. This is because the hydroxy groups formed during the reduction of the molecule are fully deprotonated at this pH and therefore the reduction is no longer proton coupled.

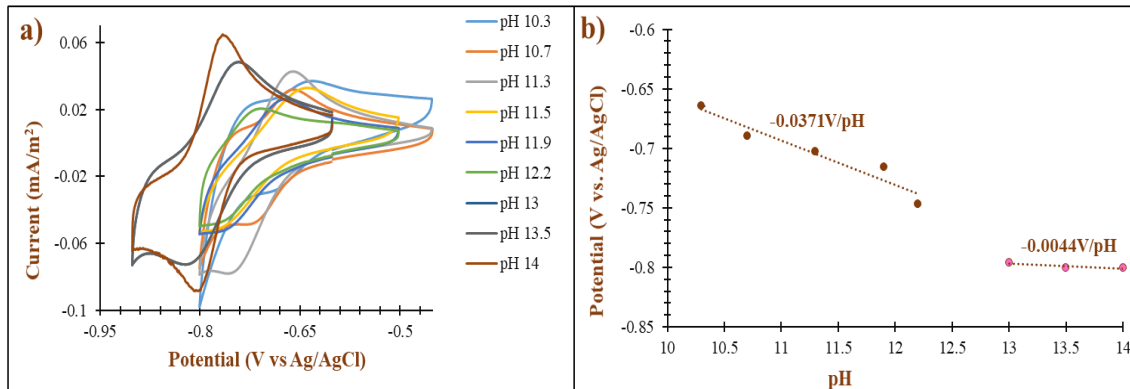


Figure 4. 3 a) Combined CVs of 5mM 1,2-DHAQ in pH buffers measured at a glassy carbon electrode; scan rate 100 mV s^{-1} ; room temperature; b) Pourbaix diagram (E^0 vs pH)

Different from 1,2-DHAQ, Ferrocyanide, $\text{Fe}(\text{CN})_6^{4-}$, consisting of a central iron (Fe) ion coordinated with six cyanide (CN^-) ligands, forming a stable complex with the formula $\text{Fe}(\text{CN})_6^{3-}$ when oxidized lacks hydrogen ions (H^+) or hydroxyl ions (OH^-) within its structure. These ions typically participate in acid-base reactions that can affect redox potential. Without these reactive groups i.e., H^+ and OH^- , FeCN remains relatively inert to pH changes (Fig. 4.4a and b).

Consequently, the anodic and cathodic peaks, corresponding to the oxidation and reduction of the $\text{Fe}^{2+}/\text{Fe}^{3+}$ couple, show minimal shifts in potential across the pH range. This stability is highlighted by the overlapping curves, indicating that the current response remains nearly constant regardless of the pH.

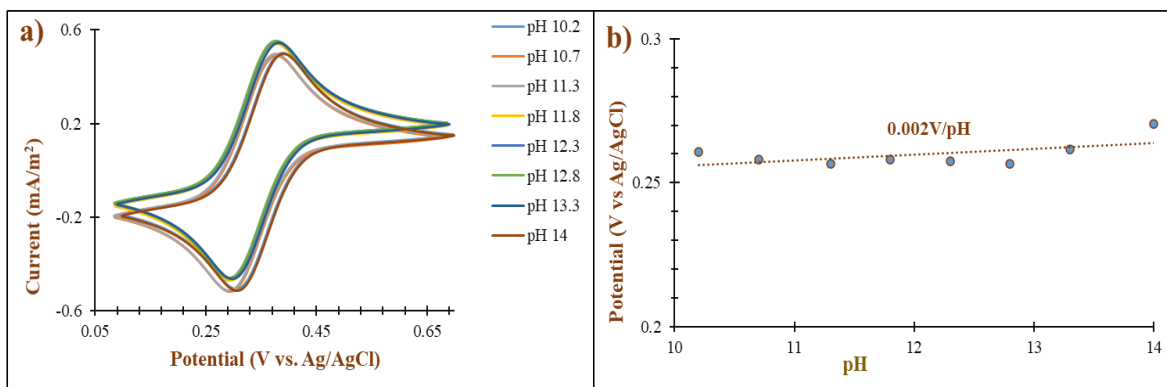
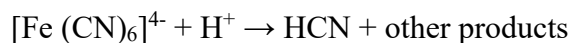


Figure 4. 4 a) Combined CVs of 50mM FeCN in pH buffers measured at a glassy carbon electrode; scan rate 100 mV s^{-1} ; room temperature; b) Pourbaix diagram (E^0 vs pH)

FeCN is usually analyzed in alkaline conditions this is because in acidic conditions, there is a risk of forming hydrocyanic acid (HCN), which is highly toxic and volatile. This can occur via the following reaction:



Therefore, the alkaline media help to prevent the release of HCN because the high pH ensures that CN^- ions remain in their ionic form rather than being converted to HCN gas.

4.2.3. Kinetics

Rotating Disk Electrode (RDE) voltammetry was used to study the kinetics of redox reactions. Fig. 4.5a presents the RDE voltammograms of the 1,2-DHAQ redox couple recorded at various rotation rates. These curves show how the current varies with the electrode rotation, indicating the influence of diffusion and kinetic control on the overall current response. At higher rotation rates, the current increases due to enhanced mass transport to the electrode surface. Fig. 4.5b displays the Koutecký-Levich (K-L) plots derived from these voltammograms. The K-L plots are constructed by plotting the reciprocal of the current density ($1/i$) against the reciprocal of the square root of the rotation rate ($1/\sqrt{\omega}$). The linearity and parallelism of these plots at different overpotentials suggest consistent kinetic behavior and confirm that the reaction is primarily controlled by both diffusion and kinetics.

The K-L equation is given by:

$$\frac{1}{i} = \frac{1}{id} + \frac{1}{ik}$$

where i is the observed current density, id is the diffusion-limited current density, and ik is the kinetic current density.

Fig. 4.5c shows the plot of overpotential (η) versus $\log iK$. This plot is analyzed using the Butler-Volmer equation:

$$\eta K = \frac{2.3RT}{\alpha nF} \log ik - \frac{2.3RT}{\alpha nF} \log i^0 = b \cdot \log ik + a$$

where $b = \frac{2.3RT}{\alpha nF}$ is the Tafel slope ($V\text{dec}^{-1}$) and $a = -\frac{2.3RT}{\alpha nF} \log i^0$ is the Tafel intercept (Am^{-2}).

The charge transfer coefficient (α) is derived from the slope of this plot, and in this case, it is determined to be 0.23. The x-intercept of the plot gives $\log i^0$, where i^0 is the exchange current density.

The relationship between i^0 and the rate constant (k^0) is:

$$i^0 = FAc k^0$$

where A and c are the active area of the RDE electrode and the concentration of 1,2-DHAQ, respectively. This gives a rate constant (k^0) of $1.05 \times 10^{-3} \text{ cm s}^{-1}$. Above $\log(ik) = 2.8$, the overpotential seems to deviate from linearity which influences the k^0 value derived. Meanwhile, due to low redox potential of 1,2-DHAQ, the reduced form is highly sensitive to oxidation by atmospheric oxygen. Hence, this experiment was conducted in the discharged form (oxidized state) i.e., 0% SOC, in which case only the reduction reaction is possible.

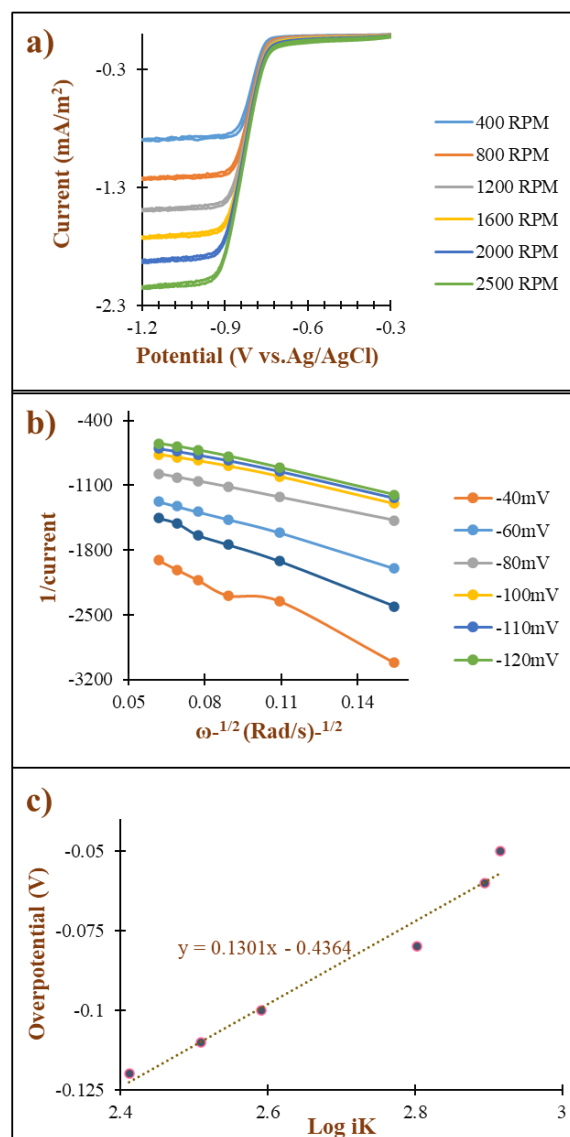


Figure 4. 5 a) RDE voltammetry curves of 1,2-DHAQ (10 mM) in 1 M KOH solution on a glassy carbon electrode at 6 rotation rates ranging from 400 to 2500 rpm. (b) Koutecky-Levich plots derived from RDE data at 7 different 1,2-DHAQ reduction overpotentials.

Fig.4.6a shows the RDE voltammograms for the FeCN redox couple at different rotation rates. Similar to the 1,2-DHAQ system, these voltammograms reflect how the rotation rate influences the current response, with higher rotation rates enhancing mass transport and current response. Fig. 4.6b presents the Koutecky-Levich plots for the FeCN redox couple. These plots demonstrate linearity and parallelism at different overpotentials, confirming a consistent kinetic behavior and allowing for accurate determination of ik from the intercepts. The plot of overpotential versus $\log ik$ for FeCN is illustrated in Fig. 4.6c. By applying the Butler-Volmer equation, the α is found to be 0.7, and the k^0 is determined to be $1.2 \times 10^{-3} \text{ cm s}^{-1}$ for both reactions owing to almost similar tafel slope and intercept (Fig.4.6c and d).

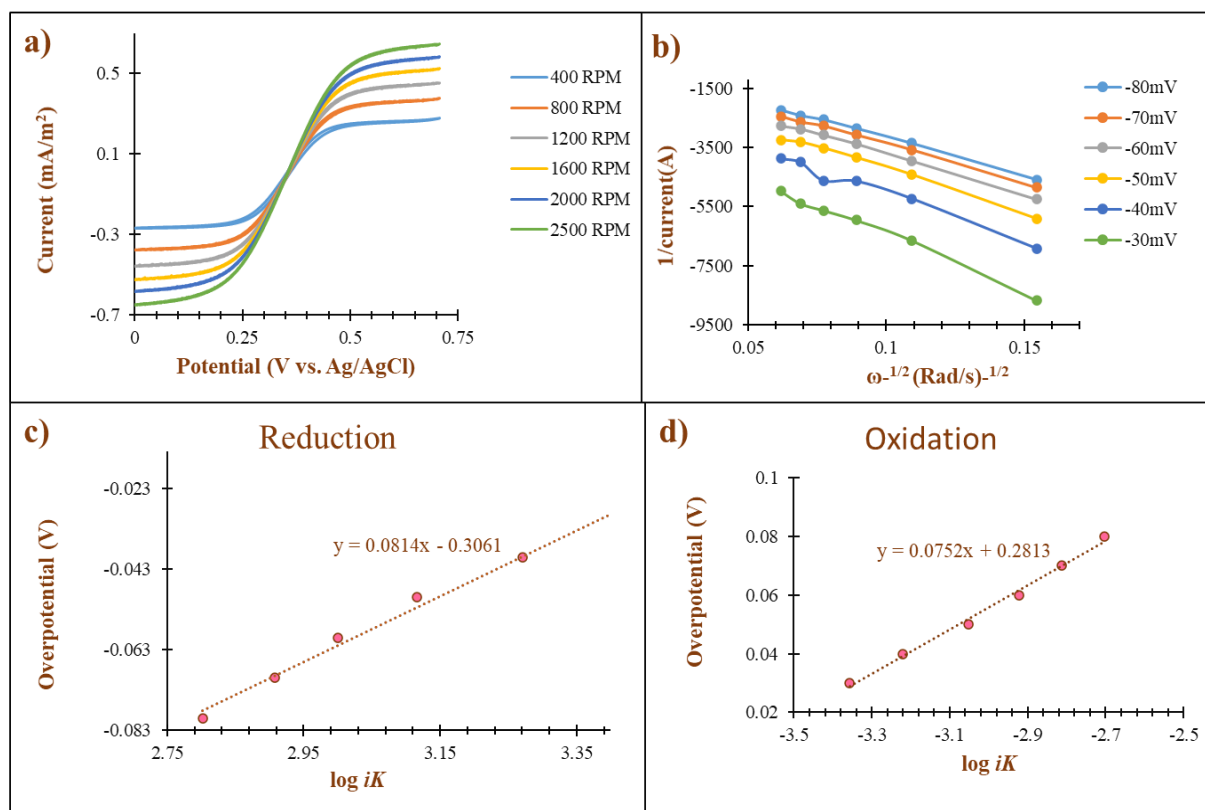


Figure 4. 6 a) RDE voltammetry curves of FeCN (10 mM) in 1 M KOH solution on a glassy carbon electrode at 6 rotation rates ranging from 400 to 2500 rpm. (b) Koutecky-Levich plots derived from RDE data at 7 different FeCN reduction overpotentials. (c and d) Fitted curve of Butler-Volmer equation for FeCN using the kinetic current density (i_k) obtained from the zero-intercept of Koutecky-Levich plots in (b) at six different reduction overpotentials

4.2.4. Diffusion coefficient

Fig. 4.7a illustrates the CVs for the diffusion analysis in 1,2-DHAQ. As the scan rate increases, distinct peaks corresponding to the redox reactions of 1,2-DHAQ are observed. The reduction peak current densities (i_p) show a proportional increase with the square root of the scan rate ($v^{1/2}$), indicating a diffusion-controlled process, as confirmed by the linear relationship depicted in Fig. 4.7b.

The Randles-Sevcik equation was employed to calculate the diffusion coefficient (D^0) of 1,2-DHAQ and using the measured values from the cyclic voltammograms, the diffusion coefficient for 1,2-DHAQ was determined to be $1.78 \times 10^{-6} \text{ cm}^2 \text{ s}^{-1}$. This value is consistent with the expected diffusion behavior of small organic molecules in aqueous solutions and further corroborates the diffusion-controlled nature of the electrochemical process observed. [96]

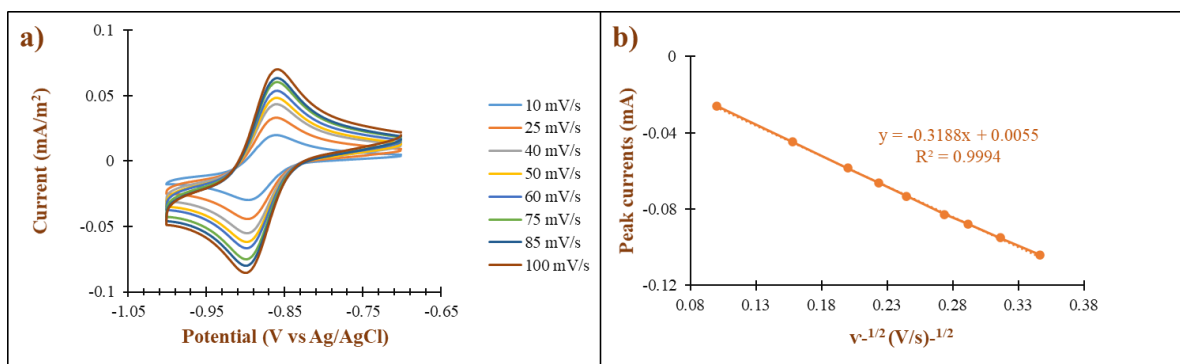


Figure 4. 7 a) CVs of 1,2-DHAQ (10 mM) in 1 M KOH solution on a glassy carbon electrode at different scan rates; b) Plot of the reduction peak current density versus square root of the scan rates for 1,2-DHAQ.

The diffusion coefficient was also evaluated for FeCN redox couples as displayed in Fig.4.8. The cyclic voltammograms exhibit well-defined redox peaks corresponding to the $\text{Fe}^{2+}/\text{Fe}^{3+}$ and $\text{Fe}^{3+}/\text{Fe}^{2+}$ transitions. As with the previous example, the linear dependence indicated in Fig.4.8b is characteristic of diffusion-controlled electrochemical reactions, where the peak current is governed by the rate of mass transport of the redox species to the electrode surface. The FeCN redox couple is a widely studied system due to its well-defined electrochemical behavior. The obtained diffusion coefficient of $1.17 \times 10^{-6} \text{ cm}^2 \text{ s}^{-1}$ is indicative of the mobility of the ferricyanide/ferrocyanide ions in aqueous solution, which is essential for designing and optimizing electrochemical devices that utilize this redox couple.

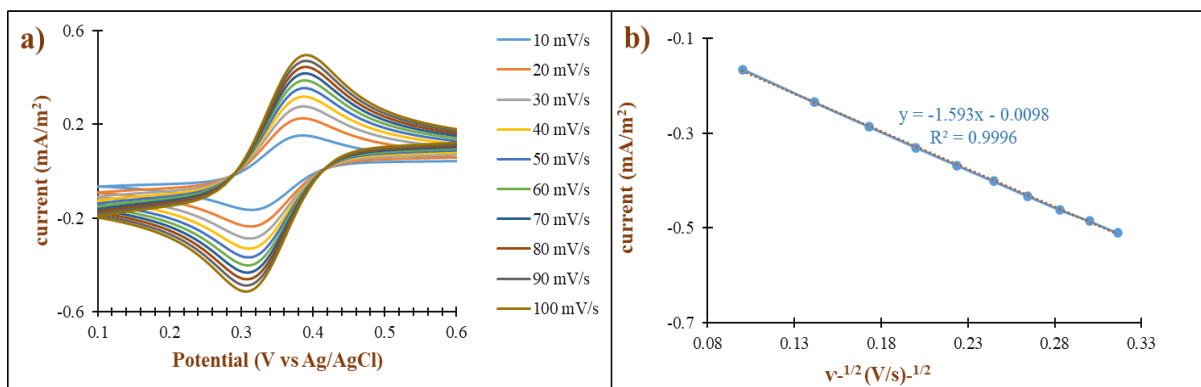


Figure 4. 8 a) CVs of FeCN (50 mM) in 1 M KOH solution on a glassy carbon electrode at different scan rates; b) Plot of the reduction peak current density versus square root of the scan rates for FeCN.

4.3. Discussion

The electrochemical characteristics of the 1,2-DHAQ (1,2-dihydroxyanthraquinone) redox couple and the FeCN (ferrocyanide/ferricyanide) redox couple were systematically investigated using cyclic voltammetry (CV), rotating disk electrode (RDE) voltammetry, and Pourbaix diagrams. These techniques provide comprehensive insights into their redox mechanisms, kinetic properties, and potential utility in redox flow batteries (RFBs).

The cyclic voltammetry (CV) profiles of both 1,2-DHAQ and FeCN exhibited distinct anodic and cathodic peaks, indicating well-defined redox reactions. Specifically, for 1,2-DHAQ, the anodic peak (E_{pa}) corresponds to the oxidation of the molecule, while the cathodic peak (E_{pc}) corresponds to its reduction. The separation between these peaks, denoted as ΔE , was

approximately 56 mV, suggesting a relatively efficient quasi-reversible redox process which would imply minimal kinetic overpotential during battery operation, essential for minimizing energy losses during charge-discharge cycles. FeCN displayed a ΔE of around 100 mV, also indicating relatively good electron transfer kinetics.

The standard redox potential (E^0) is a critical parameter derived from CV data. For 1,2-DHAQ, E^0 was calculated as the average of anodic and cathodic peak potentials, resulting in approximately -0.864 V_{vs Ag/AgCl}. This negative E^0 value indicates 1,2-DHAQ's strong propensity for reduction, making it beneficial for RFB applications. The thermodynamic favorability of the reduction reaction, quantified by Gibbs free energy change ($\Delta G = -nFE^0$), supports this characteristic.

FeCN's E^0 was approximately 0.253_{vs Ag/AgCl}, representing the equilibrium potential where the Fe²⁺/Fe³⁺ redox pair balances. FeCN's higher E^0 value compared to 1,2-DHAQ suggests a stronger tendency for oxidation. The Nernst equation further elucidates this equilibrium by relating redox potential to the ratio of oxidized and reduced species, providing a thermodynamic perspective on electron transfer processes.

The redox behavior of 1,2-DHAQ can be further elucidated by considering its molecular structure and proton-coupled electron transfer (PCET) mechanisms. The two quinone functional groups in 1,2-DHAQ that are redox active become protonated hydroxyl groups when the molecule is reduced. However, at high pH, these hydroxyl groups are fully deprotonated, resulting in a redox potential that becomes nearly independent of pH. This behavior is explained by the decoupling of proton transfer from electron transfer, a phenomenon that stabilizes the redox potential across a range of high pH values.

In contrast, FeCN consists of a central iron (Fe) ion coordinated with six cyanide (CN⁻) ligands, forming a stable complex with the formula Fe(CN)₆³⁻ when oxidized. FeCN lacks hydrogen ions (H⁺) or hydroxyl ions (OH⁻) within its structure, which typically participate in acid-base reactions affecting redox potential. This pH-independent nature of FeCN's redox potential enhances its reliability and efficiency in varying electrolyte conditions. The minimal shifts in potential for the anodic and cathodic peaks across the pH make FeCN a straightforward electrolyte to use.

Furthermore, both redox couples were further characterized using RDE voltammetry, a technique used to study the kinetics of redox reactions by examining the current response changes with rotation rate. Higher rotation rates enhance mass transport to the electrode surface, resulting in increased current.

For 1,2-DHAQ, the Koutecky-Levich (K-L) plots, which plot the reciprocal of the current density ($1/i$) against the reciprocal of the square root of the rotation rate ($1/\sqrt{\omega}$), were linear and parallel at different overpotentials. This linearity confirms that the redox process is governed by a combination of diffusion and kinetic control. The K-L equation helps in separating the contributions of mass transport and kinetic effects on the overall current.

Similarly, the K-L plots for FeCN showed consistent kinetic behavior, confirming the reliable performance of FeCN in electrochemical applications. The diffusion-limited current density (i_d) and kinetic current density (i_k) for FeCN can be derived from the slope and intercept of the K-L plots, providing insights into the efficiency of mass transport and the intrinsic reaction kinetics.

The charge transfer coefficient (α) and the rate constant (k^0) are crucial parameters for understanding the kinetics of redox reactions. For 1,2-DHAQ, α was found to be 0.23, reflecting

the asymmetry of the energy barrier for electron transfer during the redox reaction. The rate constant (k^0) was calculated to be 1.05×10^{-3} cm/s, indicating relatively fast electron transfer, which is beneficial for maintaining high power densities in RFB systems.

For FeCN, α was found to be 0.7, and k_0 was calculated to be 1.2×10^{-3} cm/s, indicating slightly faster electron transfer kinetics than 1,2-DHAQ. In general, these rate constants confirm that both reactants have sufficiently fast kinetics to be used with simple carbon electrodes without the need for expensive electrocatalysts.

Lastly, the diffusion coefficient (D^0) is a key parameter in understanding the mass transport properties of electroactive species in solution. It quantifies the rate at which molecules or ions move through a solvent due to concentration gradients and plays a significant role in determining the kinetics of electrochemical reactions.

The diffusion coefficients of the 1,2-DHAQ and FeCN redox couples were evaluated using the Randles-Sevcik equation, which relates the peak current in cyclic voltammetry to the diffusion coefficient. The equation highlights the dependency of the peak current on the diffusion coefficient, making it a valuable tool for quantifying D^0 from experimental cyclic voltammetry data.

For 1,2-DHAQ, the diffusion coefficient (D^0) was found to be 1.78×10^{-6} cm²/s. This value is consistent with the behavior expected for small organic molecules in aqueous solutions, indicating moderate mobility.

For FeCN, the diffusion coefficient (D^0) was determined to be 2.17×10^{-6} cm²/s. The kinetics seems faster for 1,2-DHAQ using the RDE technique compared to CV technique. This explains the fundamental differences between these two electrochemical techniques. In CV, the peak current is directly related to the diffusion of the electroactive species to the electrode surface as illustrated by the Randles-Sevcik equation. The linear dependence of the peak current (i_P) on the square root of the scan rate ($v^{1/2}$) indicates a diffusion-controlled process. At a higher scan rate, the time for diffusion to the electrode surface decreases, potentially leading to non-ideal conditions where the reaction kinetics might appear slower due to limiting the rate at which reactants are delivered to the electrode surface, especially for fast reactions. In addition, the peak separation may also be influenced by the roughness of the electrode surface. In general, peak separation in cyclic voltammetry is only used to gain a qualitative estimate of reaction kinetics. In contrast, the RDE technique involves rotation of the electrode, which induces convective transport in addition to diffusion. This results in a steady and controlled flow of reactants to the electrode surface, significantly enhancing mass transport compared to the purely diffusive process in CV. The convective mass transport reduces concentration polarization, ensuring a constant supply of reactants, which is crucial for maintaining high reaction rates. The increasing rotation creates a laminar flow that reduces the thickness of the diffusion layer, thereby increasing the mass transport rate enabling the reactants reaching the electrode surface more quickly and facilitating faster reaction kinetics. In addition, the viscosity of 1,2-DHAQ is considered in the RDE equation, augmenting the potential influence on kinetics.

CHAPTER 5: CHARACTERIZATION OF ELECTROLYTE DEGRADATION

Although all of the previous properties can be monitored and tracked during flow battery operation, either by sampling the electrolyte and performing ex situ experiments, or by placing measurement devices ‘in line’ with the electrolyte flow for in situ measurements, not all of them are useful for qualifying the health of the electrolyte. For example, measurements of kinetic rate constants are more relevant to the interaction with specific electrode materials and are intrinsic to the reactant and electrode combination. Typically, cycled electrolytes are less pure than initial electrolytes, thereby making such fundamental measurements impossible or uninformative. In general, chemical analysis of cycled electrolytes is usually performed to assess their degradation due to cycling. As mentioned in chapter 2, this degradation can be due to precipitation, decomposition, and crossover.

Concentration measurements are the most direct way of establishing such degradation mechanisms and are therefore the most common in the literature. In addition, other indirect measurements may be performed to indicate the presence of side reactions or the formation of decomposition products, such as mass spectroscopy and pH measurements. In this chapter, we focus entirely on the direct concentration measurements as qualifiers of electrolyte degradation. Among the various options available, CVs and UV-Vis were primarily used. Although the degradation of other electrolytes was also monitored, this chapter focuses on the 1,2-DHAQ electrolyte.

5.1 Experimental methods

Cell cycling was performed by PhD student Meysam Maleki using a flow cell, with Nafion membranes prepared by soaking in 1M KOH concentrations. The 0.1M 1,2-DHAQ electrolytes were mixed into 1, 1.2 and 2M KOH supporting electrolytes. The cell was assembled using two approximately 2 x 2 cm sheets of carbon cloth with 454 μ m thickness with an interdigitated graphite plate as a flow field and current collector in each half-cell. A gasket was used to seal the carbon papers into the cell, which compressed the electrodes to approximately 70 % of the original thickness. The two half-cells were separated by a 2 x 2 cm section of Nafion 117 membrane and bolted together between the two metallic endplates. The assembled cell was then transferred into a N₂-filled glovebox for testing. A peristaltic pump was used to circulate electrolyte between the cell and the reservoirs (with each containing different proportions of electrolytes, the CLS and the NCLS) at (150 ml/min). All solution preparations and cycling were carried out in an N₂-filled Mbraun UNIlab glovebox to minimize exposure to ambient oxygen. During one set of experiments, the cell was cycled symmetrically with different proportions of 0.1M 1,2-DHAQ in 2M KOH while the second set involves a full cell cycling experiments of 0.1M 1,2-DHAQ in 1.2M KOH, cycled with 0.1M FeCN as the posolyte. After cycling the cell was discharged to 0 % SOC. Aliquots of the discharged electrolyte were then collected for post-mortem analysis. The post mortem analyses (CV and UV-Vis) was conducted three times for each sample and their averages with their standard deviations was used as the final value.

5.2 Results

5.2.1 Crossover data

Before assuming that a change in reactant concentration is due to electrolyte decomposition, it is a good idea to check whether other phenomena such as reactant crossover may be to blame. Although flow battery membranes are supposed to allow only supporting ions to pass through them, there is always a small amount of reactants that pass through to the counter electrolyte. When this crossover occurs, it leads to a loss in reactant concentration and irreversible capacity loss for

RFBs with different electrolyte species (not vanadium RFBs). The simple crossover experiment in this section is meant to determine an ‘upper bound’ on the crossover of 1,2-DHAQ in a flowing battery. To do this, a flow battery cell is assembled as usual with the same components described for all other cycling tests. Instead of cycling however, the 1,2-DHAQ electrolyte is simply pumped through the negolyte side of the battery with a blank 1.2MKOH electrolyte flowing on the other side of the Nafion117 membrane. The flow rate was the same as other cycling experiments (150 ml/min). Aliquots were taken out of the positive side of the battery system at specific times and with assistance of UV-vis, the concentration of crossed over 1,2-DHAQ was measured.

To validate these concentration measurements, a UV-Vis calibration was performed using known concentrations of 1,2-DHAQ in 1.2M KOH. These are shown in Fig. 5.1a which shows the absorbance spectra of the electrolyte at various concentrations of 1,2-DHAQ in 1.2M KOH, with an inset showing the linear calibration curve. The absorbance peaks at specific wavelengths indicate the presence of 1,2-DHAQ and its concentration in the solution. The calibration curve demonstrates a strong linear relationship between concentration and absorbance, validating the UV-Vis method for concentration determination a standard curve was obtained to determine the 1,2-DHAQ content, as shown in Fig. 5.1b.

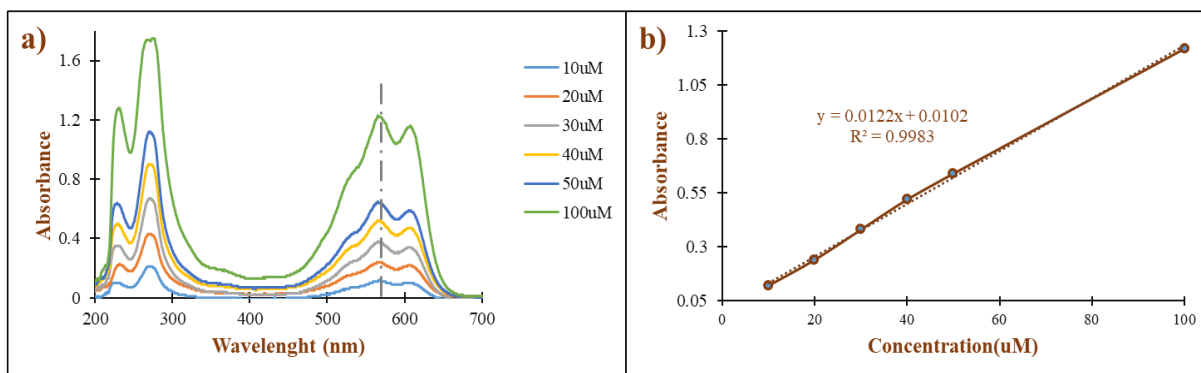


Figure 5. 1a) UV-Vis calibration spectra at different concentrations of 1,2-DHAQ in 1.2M KOH, b) A standard calibration curve determining the absorbance of 1,2-DHAQ at different concentrations,

As indicated in Fig. 5.2a and b, the increasing permeability of 1,2-DHAQ through the membrane in the receiving KOH electrolyte is rather low, on the order of micro molar, for as long as 144 hours. This may be due to the employing the thick Nafion117 membrane which is beneficial to prevent the penetration of ions of two half-cells and also due to the large size of the 1,2-DHAQ.

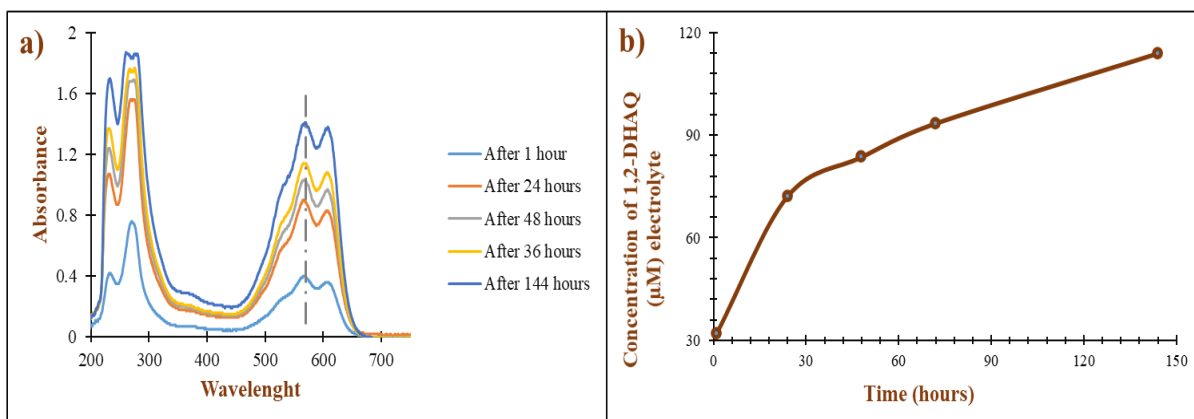


Figure 5.2 : a) UV-Vis absorption spectra of 1,2-DHAQ in 1.2M KOH over time, b) Concentration of 1,2-DHAQ electrolyte obtained by the flow through redox battery over time

5.2.2. Symmetric cycling with of 1,2-DHAQ in 2 M KOH concentration.

A 0.1M 1,2-DHAQ electrolyte was prepared in roughly 2M KOH concentration to investigate the effect of pH on the stability of the electrolyte. The 50% SOC electrolyte used for the symmetric cell cycling was prepared by charging a portion of initially-uncharged 1,2 DHAQ electrolyte in a full cell and against 0.1M ferrocyanide until the theoretical capacity was attained. This was followed by mixing this charged electrolyte in equal proportions with uncharged electrolyte. Potentiostatic cycling of all cells was performed in a nitrogen-filled glove box. The potential limits were set to ± 400 mV to access over 99% of the CLS capacity. In the two-electrode symmetric cells, one reservoir was filled with an excess of 50% SOC electrolyte to make the other side of the cell capacity limiting. this excess was increased (roughly double the volume) to ensure that oxidation of the NCLS electrolyte by low levels of oxygen in the glove box would not lead to both sides becoming capacity limiting and fading at the rate of oxidation. In addition, small aliquots of 50% SOC electrolyte were occasionally added to the NCLS to confirm that the NCLS had not become limiting. From the Fig.5.3a, the result for continuous cycling indicates an instantaneous capacity fade of about 4% at the end of the 7 days cycling.

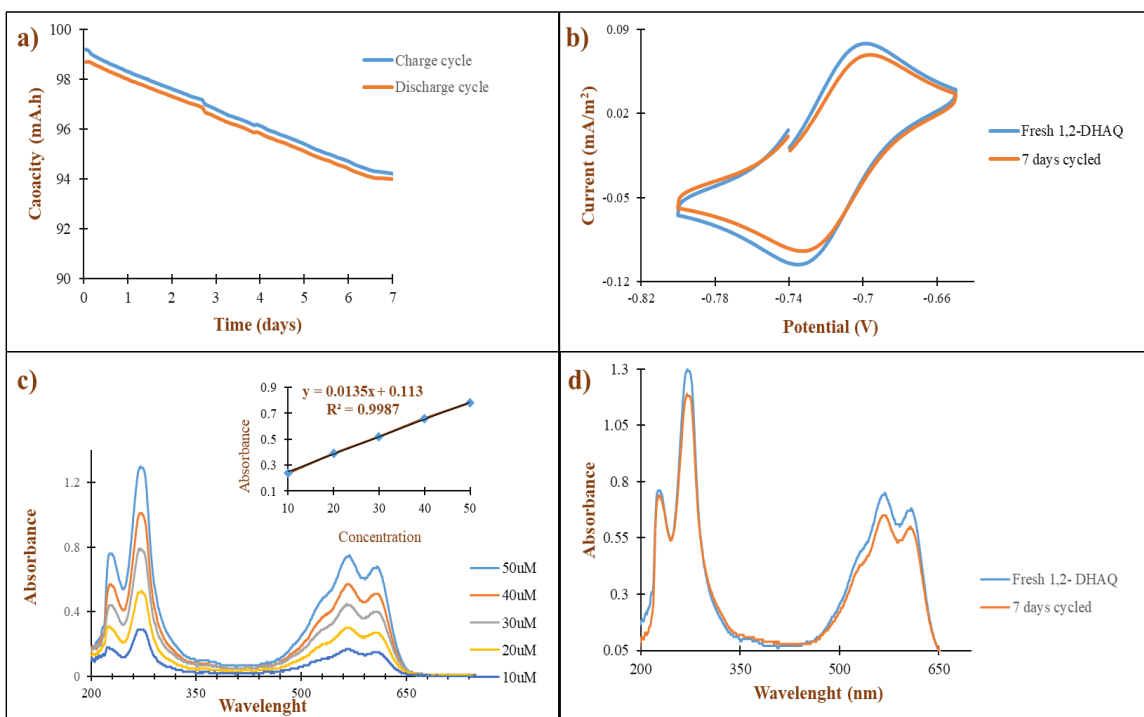


Figure 5. 3: Symmetric cell cycling of 0.1M 1,2-DHAQ in 2M KOH at cut off voltage of +/- 400mV with a limiting current density of 5mA/cm². a) Cycling performance. b) CV degradation profiles. c) UV-Vis calibration curve at different concentration with absorbance wavelength of 567.767nm, d) UV-Vis degradation profile

The cycled CLS negolyte was further diluted with 2M supporting KOH electrolyte for cyclic voltammetry and UV-Vis characterization. Fig. 5.3b compares the cyclic voltammetry of fresh and cycled electrolytes using a glassy carbon working electrode. The electrolytes showed the expected redox features for fresh 1,2-DHAQ at -0.698 V and -0.735 V vs. Ag/AgCl for oxidation and reduction reactions respectively. The cycled electrolyte collected after 7 days of cycling indicates about 12.2% +/- 0.4 concentration deviation from the fresh 1,2-DHAQ electrolyte. No new peak is observed in the cycled electrolytes hence chemical decomposition into another redox active compound is not suspected.

The UV-Vis spectra comparing fresh and cycled 0.1 mM 1,2-DHAQ electrolytes after 7 days of cycling are shown in Fig. 5.3d. The absorption feature of interest is visible at 567.727 nm, in agreement with previous reports[97], The change in relative peak intensity between the fresh and 7 days cycled 1,2-DHAQ electrolyte resulted to a 20.2% +/- 0.1 decrease in concentration.

5.2.3. Full cell cycling with 1.2 M KOH concentration.

Contrary to the symmetric cell cycling procedure as described above, full cell cycling experiment involves evaluating the performance of a complete redox flow battery system under operational conditions. It consists of two half-cells separated by an ion-conducting membrane, with each half-cell containing an electrode and an electrolyte solution: one with the positive redox couple (posolyte) and one with the negative redox couple (negolyte).

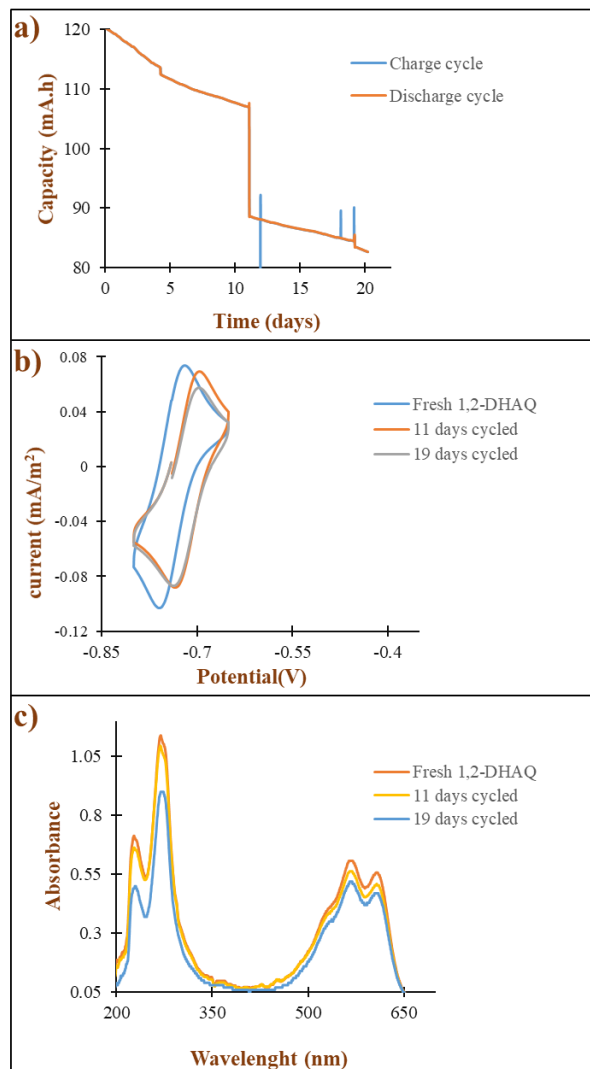


Figure 5. 4: Full cell normal cycling of 0.1M 1,2-DHAQ in 1.2M KOH a) Cycling performance. b) CV degradation profiles, c) UV-Vis degradation profile

I employed 0.1M 1,2-DHAQ as negolytes dissolved in 1.2M KOH and 0.1M ferricyanide dissolved in 1.2M KOH as the posolyte. The full cell potentiostatic cycling as displayed in Fig.5.4a, was also performed in a nitrogen-filled glove box. The cycling started by using a potential limit of 1.4V and 0.5V for the charging and discharging at a current density of 40mA/cm² as well as cut off currents of 2.5mA/cm² and 1.75mA/cm² for charge and discharge respectively, until a near theoretical capacity for a 2 electron-1,2- DHAQ CLS electrolyte was obtained. Here the positive electrolyte (0.1M ferricyanide in 1M KOH) served as the NCLS, aliquot was occasionally added to NCLS to confirm that the NCLS had not become limiting. The battery was cycled for about 4.15 days then the charging and discharging potentials was changed to 1.35V and 0.9V respectively, this was allowed to run for about 11 days after which the first aliquot was taken for postmortem analyses, the capacity fade at this point corresponds to about 12%. After the first aliquot collection, the charging and discharging potentials was returned to 1.4V and 0.9V and allowed to run for 8 more days after which regeneration of capacity was made by changing the discharge potential to 0.4V with current density of 10mA/cm² and cut off discharge current 0f

0.15mA/cm². After the capacity regeneration, the charge and discharge potentials were returned to 1.4V and 0.9V and another aliquot was taken for postmortem analyses at 19.2 days with capacity fade corresponding to about 17% capacity fade

The CV plot as displayed in Fig. 5.4b, shows the current vs. potential for fresh, and cycled 1,2-DHAQ electrolytes. The fresh sample exhibits clear redox peaks, indicating the expected electrochemical activity of 1,2-DHAQ. The 11 days and 19.2 days cycled electrolytes shows some deviations from fresh electrolytes, corresponding to 10.3% +/- 0.5 and 20.1% +/- 0.3 concentration deviations respectively based on the oxidation peak, indicating reduced electrochemical activity, likely due to reduced active material concentration.

The UV-Vis plot in Fig. 5.4c compares the absorbance spectra of fresh, and cycled 1,2-DHAQ electrolytes. The fresh electrolyte shows distinct absorbance peaks, characteristic of 1,2-DHAQ at wavelength of 567.727nm. The 11 and 19 days cycled electrolytes shows some deviations from fresh electrolytes, corresponding to 9.4% +/- 0.2 and 18.2% +/- 0.6 concentration deviations respectively.

In addition to the above full cell experiment, another full cell was cycled with more aggressive conditions to investigate their effect on capacity. Fig. 5.5a describes the cell containing 7 mL of 0.1 M 1,2-DHAQ in 1.2 M KOH and 0.06 M ferrocyanide + 0.03 M ferricyanide in 1.2 M KOH from approximately 25 days of cycling. Voltages of 1.35 and 0.9 V were applied as charge and discharge voltage at current density of 25 mA/ cm². The current cut-offs were 2.5 and 1.75 mA cm⁻² for charge and discharge, respectively. A discharge at 0.2 V caused a large capacity fade possibly due to the oxidation of redox-active 1,2-DHAQ resulting to 32 % capacity fade from 110.59 C before deep discharge at 0.2 V to 80.16 C. The CV curves in Fig. 5.5b indicate that the 0.2V discharged electrolyte has changed considerably from the fresh electrolyte. The original redox peak for DHAQ is no longer present, and a new much smaller redox peak is visible around -0.6V vs Ag/AgCl. In addition, an almost zero absorbance at 567.767nm wavelength was observed on the 0.2V discharged electrolyte with new absorbance peaks at other wavelengths, suggesting a conversion of the 1,2-DHAQ into a new species with a difference absorbance profile.

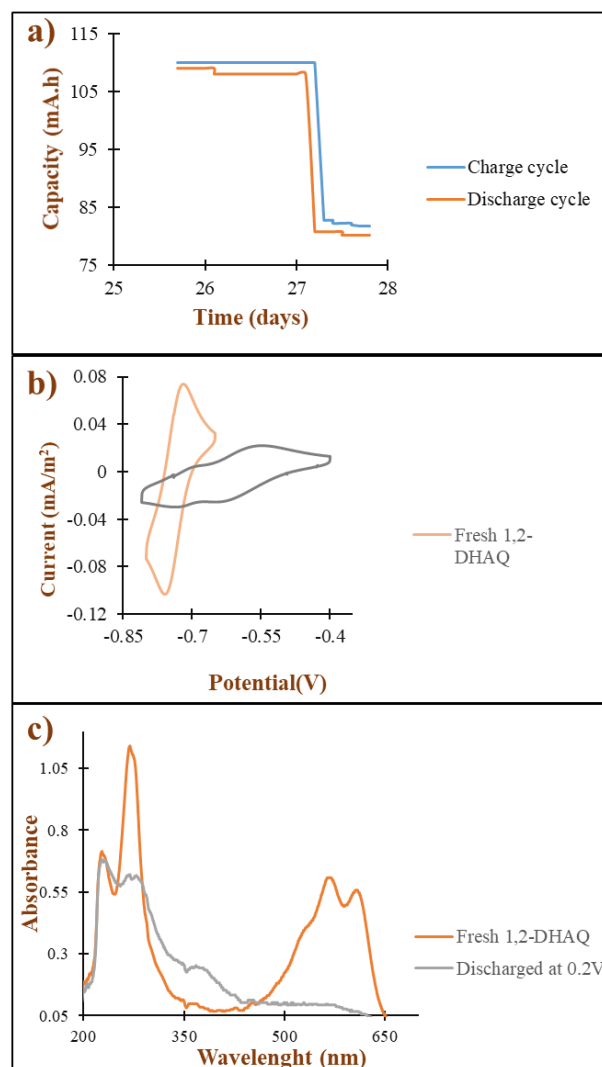


Figure 5. 5: Full cell aggressive cycling of 0.1M 1,2-DHAQ in 1.2M KOH a) Cycling performance. b) CV degradation profiles, c) UV-Vis degradation profile

5.3. Discussion

The extent of 1,2-DHAQ crossover through the Nafion 117 membrane was quantified using UV-Vis spectroscopy over 144 hours. The observed minimal crossover of 1,2-DHAQ through the Nafion 117 membrane can be attributed to several factors such as the membrane thickness and density. Nafion 117 being a thick membrane ($\sim 183 \mu\text{m}$) provides a substantial physical barrier to the diffusion of large molecules such as 1,2-DHAQ. The thickness increases the path length for diffusion, thereby reducing the rate of crossover. In addition, the dense structure of Nafion 117 restricts the movement of larger molecules. This density is due to its highly cross-linked polymer matrix, which creates a tight network that larger molecules find difficult to navigate. The size and polarity of 1,2-DHAQ also plays an important role in minimizing its cross over. 1,2-DHAQ is a relatively large organic molecule with significant steric hindrance. Larger molecules experience greater resistance when diffusing through the membrane's polymer matrix, leading to reduced crossover rates. Nafion membranes soaked in 1M KOH are composed of negatively charged sulfonate groups with bound potassium ions, which impart a high degree of ionic conductivity and

selectivity. The interaction between these fixed anionic groups and the 1,2-DHAQ molecules further hinders their passage through the membrane. Specifically, the sulfonate groups in Nafion can create electrostatic repulsion against the negatively charged or polar regions of 1,2-DHAQ, impeding their movement.

In general, the observed % capacity fade during the cycling experiment represents the overall performance degradation of the redox flow battery under operational conditions. However, post-mortem analyses using CV indicated higher percentages of concentration loss in most cases. Although these discrepancies may be due to experimental error, extracting concentration from CVs is notoriously difficult due to variability in electrode surface area and possible deposition of material. It shows the peak currents and potentials corresponding to oxidation and reduction processes, but it may not measure capacity directly. Higher accuracy was expected for UV-Vis, however, the amount of concentration loss was again higher than the capacity fade observed. Beyond experimental error, the most likely reason for such discrepancies would be the crossover of water from one side of the batteries to the other. If water crosses to the analyzed side of the cell, it would dilute the concentration of the 1,2-DHAQ without affecting the overall capacity of the electrolyte. Hence, a combination degradation and water crossover could lead to small amounts of capacity fade with higher amounts of concentration loss.

CHAPTER 6: STATE OF CHARGE MEASUREMENTS

In this study, a method to measure the SOC of electrolytes is explored for different systems such as the reversible, quasi reversible and the irreversible systems. OCV in combination with CV was implemented and used to predict the SOC of electrolyte solutions. The relationship between the redox potential and the OCV is demonstrated to be useful for determining SOC can therefore be used to detect electrolyte imbalance. The proposed method is simple and less time-consuming, compared with other conventional direct and indirect methods. Finally, the use of a pseudo reference electrode for this method is also explored as a further improvement for simplified SOC determination. The use of a pseudo reference electrode is particularly advantageous in systems where a traditional reference electrode might introduce additional complexities or interferences. By characterizing a range of electrochemical systems and incorporating a pseudo reference electrode, the practical application of this model is explored.

6.1. Experimental

6.1.1. Materials

All reagents were of analytical reagent grade unless otherwise stated. The description of reagents 1,2-Dihydroxyanthraquinone (1,2-DHAQ, 97%), Potassium Ferrocyanide ($K_4Fe(CN)_6$) and Potassium Ferrocyanide Trihydrate ($K_4Fe(CN)_6 \cdot 3H_2O$) and potassium hydroxide, are same as in experimental section of section 2. Vanadium (IV) sulphate oxide hydrate (VO_2SO_4 , 99.9%) is obtained from thermo scientific. potassium hydroxide (KOH) and Sulphuric acid were purchased from Sinopharm Chemical Reagent Co. Ltd.

6.1.2. Preparation of samples

A three-electrode electrochemical cell was used. A glass carbon electrode was used as a working electrode. Graphite carbon rod and Ag/AgCl were used as the counter and reference electrode respectively. Electrolytes with well defined SOC were prepared by mixing ratios of fully oxidized and fully reduced electrolytes. These solutions were then transferred to the electrochemical cell. The OCV of the electrolytes was first measured for about a minute and the steady state value was used in calculations. Subsequently, cyclic voltammograms were measured at $\pm 0.5mV$ around that OCV value at a scan rate of $100mV/sec$. These measurements were repeated for each electrolyte SOC prepared. For the highly oxygen sensitive 1,2-DHAQ, analyses were conducted in a glove box to prevent oxygen from changing the SOC during the measurements. Prior to conducting test, the 0.1M fresh/commercial and oxidized form of 1,2-DHAQ was charged in a redox flow battery with 0.1M Ferrocyanide, both dissolved in 1M KOH until full charged. Then the charged 1,2-DHAQ was mixed with uncharged 1,2-DHAQ to achieve the intended SOC. The same procedure was used for evaluating the pseudo reference electrode, which was a platinum electrode in place of the Ag/AgCl. All analyses were repeated three times for each of the different redox couples and the average from the OCVs and CVs were used for the graphs.

6.2. Results

6.2.1. Theoretical Prediction

The SOC of an electrolyte is directly related to the mole fraction between the reduced and oxidized species in the electrolyte. The relationship between this mole fraction and the equilibrium potential of an electrode is given by the Nernst equation. This equation can be rewritten in the following form which is used in this set of experiments:

$$(E - E_{1/2}) = \frac{RT}{nF} \ln \left(\frac{1}{X_{red}} - 1 \right)$$

Where X_{red} is the mole fraction of the reduced species. Experimentally, the mole fraction X is controlled whereas the equilibrium potential E is measured by the OCV and the $E_{1/2}$ is measured by cyclic voltammetry.

Using the formula above, an example theoretical curve is plotted below for a 1-electron reaction at standard conditions (Fig. 6.1):

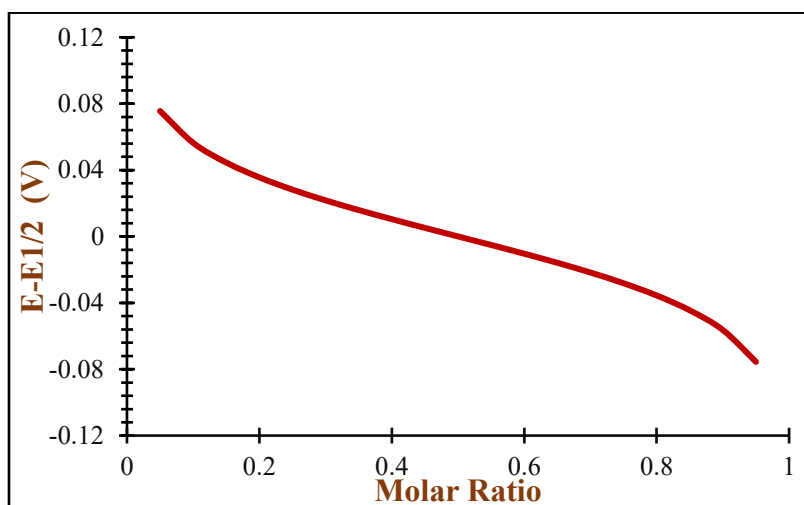


Figure 6.1 Theoretical relationship between equilibrium potential and mole fraction of reduced and oxidized species for a 1-electron reaction.

The theoretical model presented above is applicable to a completely reversible electrochemical system. Such a system would exhibit perfectly reversible redox reactions, with no significant kinetic or mass transport limitations, ensuring that the thermodynamic predictions of the Nernst equation are precisely met. In most cases however, practical flow battery electrolytes do not exhibit fully reversible kinetics and therefore I focus on these examples to determine whether the above method may be suitable for these more common electrolytes with slower quasi-reversible kinetics. In addition, I investigate irreversible systems, where significant deviations from theory are present due to sluggish and asymmetric kinetic.

6.2.2 Quasi-reversible systems

A reversible redox system is characterized by its ability to undergo oxidation and reduction reactions with high efficiency and minimal energy loss. These systems feature rapid electron transfer kinetics, resulting in quick equilibrium and diffusion-controlled reactions. They exhibit very small overpotentials to drive chemical reactions. In cyclic voltammetry, reversible redox systems show symmetrical and reproducible oxidation and reduction peaks, with peak separations close to theoretical values of around 59 and 30mV at room temperature (for a one and two-electron transfer processes respectively). In addition, it is generally required for both the oxidized and reduced species in these systems to be chemically stable to allow for multiple redox cycles without significant degradation. A 'quasi-reversible' redox system describes a system where the oxidation and reduction reactions occur at a moderate rate, with $k^0 \geq 10^{-2}$ cm/s for the rapid and reversible processes, 10^{-5} cm/s $\leq k^0 < 10^{-2}$ cm/s for quasi-reversible processes and $k^0 \leq 10^{-5}$ for the sluggish and irreversible reactions[98].

Unlike fully reversible systems where electron transfer is rapid and equilibrium is quickly established, quasi-reversible systems exhibit larger peak separations ($\Delta E_p > 59\text{mV}$ for 1-electron transfer process) in cyclic voltammetry due to the kinetic limitations of electron transfer. Both 1,2-DHAQ and FeCN fall into this category, as well as many of the newly developed flow battery reactants in the literature

Fig. 6.2 a-c shows that for a quasi-reversible system like 1,2-DHAQ, the measured values for $E_{1/2}$ are all within the standard deviation from the theoretically predicted value from the Nernst equation for a 2-electron reaction.

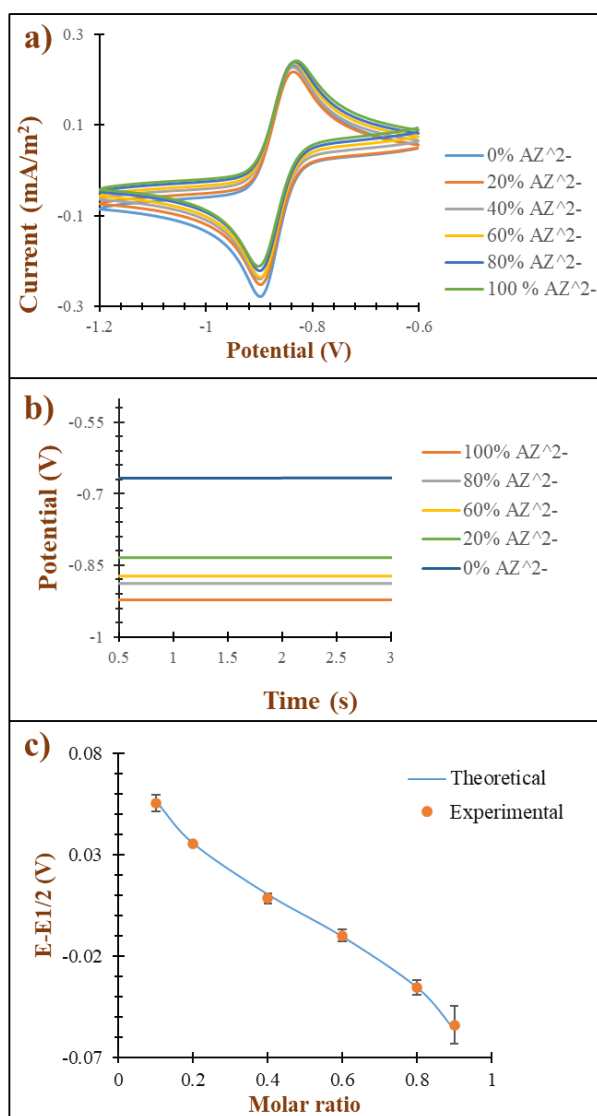


Figure 6. 2: 1,2- DHAQ a) Combined CVs at different SOC levels. b) Combined OCVs at different SOC levels. c) Comparison of experimental ' $E-E_{1/2}$ ' vs mole fraction of reduced 1,2-DHAQ with theoretical curve.

In addition, Table 6.1 shows that the average experimental values are within standard deviation from the theoretically predicted values.

Table 6. 1: Deviation of 1,2-DHAQ from theory

Molar ratio	Theoretical (E-E1/2)	Experimental (E-E1/2)	Standard deviation	Difference
0.1	0.056	0.055	0.004	0.001
0.2	0.036	0.035	0.001	0.001
0.4	0.01	0.008	0.002	0.002
0.6	-0.01	-0.011	0.003	0.001
0.8	-0.036	-0.0355	0.004	-0.0005
0.9	-0.056	-0.054	0.009	-0.002

Due to the logarithmic nature of the Nernst equation, it may be expected that the accuracy of this model may diminish at extreme SOC's i.e. at high and low mole ratio of reduced 1,2-DHAQ due to large variations in potential with minor changes in concentration. However, in the case of 1,2-DHAQ, such behaviour was not observed, making this technique still effective at extreme mole ratios.

The same technique was repeated on the commonly used FeCN electrolyte. At 0% SOC i.e. 0% Fe²⁺ and 100% Fe³⁺ ions of FeCN, an anodic and cathodic peak potential of around 0.325 and 0.225V were observed respectively. The anodic and cathodic peak potentials gradually changed at different SOC's. The FeCN cyclic voltammograms illustrate a quasi-reversible 1-electron transfer reaction with a ΔEP of around 100mV, 41 mV greater than the 59 mV expected for a reversible system. This is again an indication of a quasi-reversible electrochemical behaviour. Fig.6.3a-b shows the combined CV and OCV plots at different SOC's.

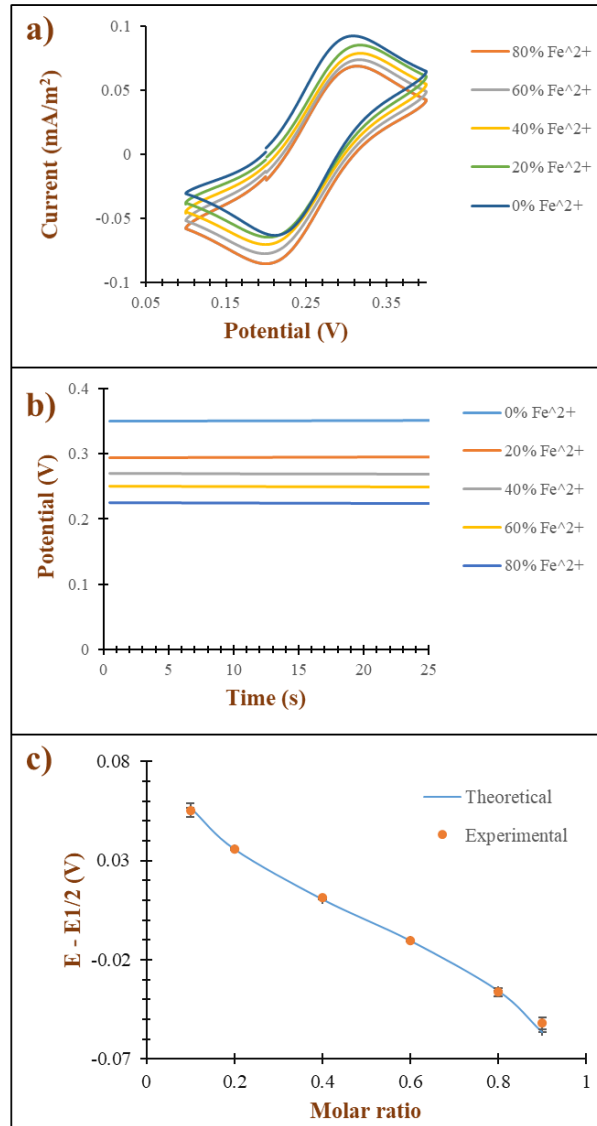


Figure 6. 3: FeCN a) Combined CVs at different SOC. b) Combined OCVs at different SOC. c) Comparison of experimental 'E - E_{1/2}' vs mole fraction of reduced 1,2-DHAQ with theoretical curve

Table 6.3 shows the dependence of the SOC on the OCV and CV analysis, displaying a good correlation of the experimental analyzed molar ratio of Fe²⁺ with that of the theoretical expectations, hence the success of this technique in a quasi-reversible system.

Table 6. 2: Deviation of FeCN electrolyte from theory

Molar ratio	Theoretical (E-E _{1/2})	Experimental (E-E _{1/2})	Standard deviation	Difference
0.1	0.056	0.055	0.0035	0.001
0.2	0.036	0.036	0.00032	0
0.4	0.01	0.01	0.00031	0
0.6	-0.01	-0.01	0.00019	0
0.8	-0.036	-0.035	0.0021	-0.001
0.9	-0.056	-0.052	0.0031	-0.004

6.2.4 Irreversible system

Studies on vanadium as redox flow battery electrolytes have shown that this compound has promising commercial application as flow battery electrolyte, therefore this SOC technique was employed on it and investigated [3]. It has also been shown that the V^{4+}/V^{5+} reaction is irreversible and highly asymmetric as well. Hence, I use this electrolyte as our model irreversible system in this study. An irreversible redox system describes a situation where oxidation and reduction reactions occur with significantly hindered electron transfer kinetics, resulting in a lack of equilibrium between the oxidized and reduced forms of the redox couple. This sluggish electron transfer manifests in asymmetrical cyclic voltammetry peaks, where the reduction peak is typically broader and less defined compared to the oxidation peak and vice versa. They also exhibit very large peak separations, ΔEP . Irreversible systems require higher overpotentials to drive redox reactions due to their slow kinetics, and they exhibit non-Nernstian behavior where changes in concentration do not proportionally affect the electrochemical potential.

As can immediately be seen from Fig. 6.4a, the CVs of the V^{4+}/V^{5+} electrolyte do not have symmetric oxidation and reduction peaks. In addition, the peaks are very far apart, making a measurement of the halfwave potential $E_{1/2}$ quite difficult or dubious. The peak ratios of the anodic and the cathodic peaks for all electrolytes are greater than 1, indicating that the cathodic reaction is more favourable than the anodic reaction. At 0% SOC of V^{4+} an anodic and cathodic peak potential of around 1.323 and 0.438 V was observed respectively. The anodic and cathodic peak potentials changed at different SOC. The V^{4+}/V^{5+} cyclic voltammograms illustrate an irreversible system with a ΔEP of about 1000mV. Fig. 6.4a and b shows the combined OCV and CV plots at different SOC.

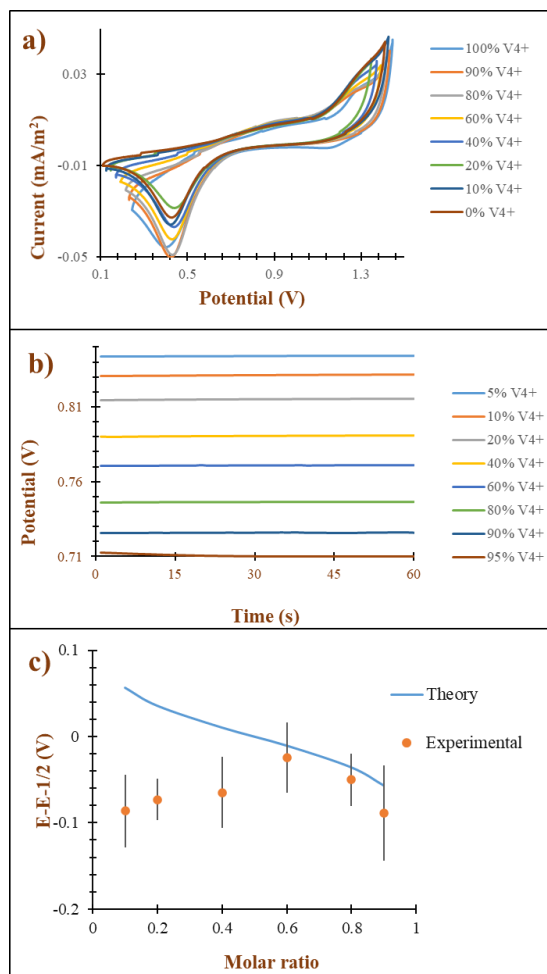


Figure 6. 4: Vanadium a) Combined CVs at different SOC. b) Combined OCVs at different SOC. c) Comparison of experimental 'E-E_{1/2}' vs mole fraction of V₄₊ with theoretical curve

Table 6.4 shows the dependence of the SOC on redox potential monitored from the OCV and CV, as seen from the table, there is rather a huge deviation from theoretical expectation. The huge percentage deviation from theory indicates that this technique may not be applicable in an irreversible system. In addition, the plot of E-E_{1/2} vs. molar ratio displayed a non-nerstian relationship as displayed in Fig 6.4c

Table 6. 3: Deviation of vanadium electrolyte from theory

Molar ratio	Theoretical (E-E _{1/2})	Experimental (E-E _{1/2})	Standard deviation	Difference
0.1	0.056	-0.09	0.042	0.146
0.2	0.036	-0.073	0.024	0.109
0.4	0.01	-0.065	0.042	0.075
0.6	-0.01	-0.024	0.041	0.014
0.8	-0.036	-0.05	0.03	0.014
0.9	-0.056	-0.087	0.055	0.031

6.2.5. A Pseudo-Reference Electrode

To monitor flow battery SOC during operation, it is ideal to have instruments in line with the flow of the electrolytes. To this end, this study investigates the use of a pseudo reference electrode to

replace standard reference electrodes such as the Ag/AgCl used in the rest of this work. Without the need for a carefully controlled electrolyte environment, a simple inert metallic electrode can be placed directly in contact with the electrolyte to be studied while avoiding contamination issues. This method was validated using the FeCN redox couple. Herein, the glassy carbon was used as the working electrode, platinum as reference electrode while the graphite carbon rod was used as the counter electrode. The same technique as the above was repeated and table 6.5 shows the percentage deviation from standard.

Interestingly, the experimental derived “ $E-E_{1/2}$ ” values corrected with the theoretical values with only minimal deviation further validating this technique with a non-standard reference electrode.

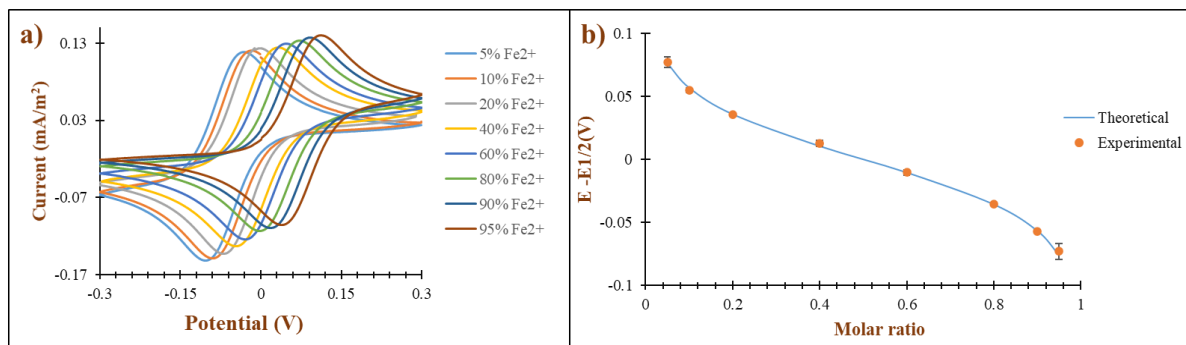


Figure 6. 5: FeCN with a pseudo reference electrode a) Combined CVs at different SOC's, c) Comparison of experimental 'E-E_{1/2}' vs mole fraction of reduced FeCN with theoretical curve

Table 6. 4: Deviation of FeCN with the use of a pseudo reference electrode from theory

Molar ratio	Theoretical (E-E _{1/2})	Experimental (E-E _{1/2})	Standard deviation	Difference
0.05	0.076	0.078	0.004	-0.002
0.1	0.056	0.055	0.002	0.001
0.2	0.0356	0.0357	0.001	-0.0001
0.4	0.01	0.011	0.002	-0.001
0.6	-0.01	-0.01	0.002	0
0.8	-0.0356	-0.0357	0	0.0001
0.9	-0.056	-0.057	0	0.001
0.95	-0.076	-0.073	0.006	-0.003

6.3. Discussion

The SOC of an electrolyte is directly related to the mole fraction of the reduced and oxidized species in the solution. The equilibrium potential of an electrode can be described by the Nernst equation, which, in the context of this study, is adapted to measure SOC.

For the 1,2 DHAQ and FeCN redox couples, the CVs illustrate a quasi-reversible 2 and 1-electron transfer reaction with ΔE_p values greater than 30mV and 59 mV respectively. Despite being quasi reversible systems, the SOC measurement technique combining OCV and CV remains effective. The quasi-reversible nature of the redox couples means that while the electron transfer is not as rapid as in fully reversible systems, the relationship between redox potential and SOC can still be approximated by the Nernst equation.

Irreversible redox systems are characterized by significantly hindered electron transfer kinetics, resulting in a lack of equilibrium between the oxidized and reduced forms of the redox couple.

These systems exhibit broad, asymmetrical CV peaks and large peak separations, indicative of slow kinetics and non-Nernstian behavior. The V^{4+}/V^{5+} redox couple, commonly used in VRFB, serves as a model for irreversible systems in this study. The fundamental challenge with irreversible systems is that the slow electron transfer processes do not allow the redox reactions to reach equilibrium, making the Nernst equation inapplicable. Experimentally, reduction and oxidation peaks may be highly asymmetric or missing altogether during cyclic voltammetry, thereby making the method intractable. For irreversible systems such as vanadium, it would therefore be necessary to develop another method of measuring the ratio between the oxidized and reduced species. The CVs of the V^{4+}/V^{5+} redox couple demonstrate these challenges, with highly asymmetric peaks and large ΔE_p values that make accurate measurement of $E_{1/2}$ difficult. The slow kinetics and non-Nernstian behavior prevent the establishment of a predictable relationship between OCV and SOC, undermining the effectiveness of the proposed technique.

The use of pseudo-reference electrodes offers a practical and effective alternative to traditional reference electrodes such as the Ag/AgCl electrode. A pseudo-reference electrode typically simplifies the experimental setup and mitigates contamination risks associated with standard reference electrodes because traditional reference electrodes require a carefully controlled electrolyte environment to maintain a stable potential.

In contrast, a pseudo-reference electrode can be placed directly in the electrolyte stream, making it well-suited for in-line monitoring applications in flow batteries. This direct placement eliminates the need for junctions or barriers to prevent mixing, thereby reducing the complexity and potential sources of error in the experimental setup. The pseudo-reference electrode's effectiveness hinges on its ability to maintain a stable and reproducible potential relative to the electrolyte. This stability is crucial for accurate SOC measurements, which depend on the precise determination of the OCV and the electrochemical potential during CV experiments. The SOC measurement method was validated with a pseudo-reference by using the FeCN electrolyte and found to be equally accurate to the case with a standard Ag/AgCl reference. This may not be the case with other electrolytes however, and a similar validation step would need to be completed with any new electrolyte being studied, to ensure that the pseudo-reference is compatible with the electrolyte.

CHAPTER 7: CONCLUSIONS AND FUTURE WORK

7.1 Summary of results

The electrochemical behaviour of aqueous redox flow battery electrolytes consisting of 1,2-DHAQ and FeCN were investigated using CV and RDE. Their suitability for RFB systems were determined by analysing their reversibility, pH stability, the kinetics and diffusion coefficient. In addition, the cycling stability of 1,2-DHAQ under two distinct conditions including the symmetry and full cell conditions was also investigated by CV and UV-Vis for postmortem analyses. Furthermore, an OCV- SOC analyses technique was explored on different redox systems along with its application using a pseudo reference electrode. The results of this study to characterize aqueous redox battery electrolytes and to evaluate cycled 1,2-DHAQ electrolytes as well as exploring the OCV-SOC technique in different redox systems have shown that:

- From CV profiles both systems displayed a quasi-reversible behaviour with ΔE of around 58mV and 100mV for 1,2-DHAQ (2-electron transfer process) and FeCN (1-electron transfer process) respectively. In addition, $E_{1/2}$ for 1,2-DHAQ (-0.864V) and FeCN (0.349V) made them suitable for a negolyte and posolyte in RFB applications respectively.

- Pourbaix analysis revealed that 1,2-DHAQ is influenced by PCET mechanisms, due to hydroxyl groups that participate in redox reactions at lower pHs than 13 whereas, FeCN consisting of a central iron ion coordinated with six cyanide ligands, exhibits pH-independent redox behavior due to the absence of proton-coupled reactions.

- Kinetics and diffusion analyses on 1,2-DHAQ and FeCN indicate 1,2-DHAQ to possess α of 0.23 and k^0 of 1.05×10^{-3} cm/s, while FeCN possessed α was 0.7 and k^0 was 1.2×10^{-3} cm/s. While the diffusion coefficients of 1,2-DHAQ and FeCN evaluated using the Randles-Sevcik equation showed 1.78×10^{-6} cm²/s and 2.17×10^{-6} cm²/s, respectively.

- Crossover of active materials across the membrane which can significantly affects the efficiency and longevity of AORFBs can be minimized through the use of Nafion 117 membrane and was quantified using UV-Vis spectroscopy to display only about 110 μ M crossover of 1,2-DHAQ electrolyte on the receiving 1.2M KOH electrolyte after 144 hours.

- Symmetric cell cycling of 1,2-DHAQ lead to a drop of 4% in capacity after 7 days. Concentration measurements by CV indicated a concentration change of 12% with no additional peaks while the UV-Vis analysis corresponds to a 20% decrease in concentration.

Meanwhile, for the full cell cycling, a capacity fade corresponding to about 17% corresponded to 20% concentration drop measured by CV and 18% concentration drop measured via UV-Vis.

Aggressive full cell cycling conditions resulted to a 32% capacity fade and a considerably deformation of redox peak in comparison with the fresh electrolyte. In addition, an almost zero absorbance peak at the wavelength of interest (567.767nm) was observed from UV-Vis,

- The combined CV-OCV SOC measurement method works accurately for quasi-reversible systems like 1,2-DHAQ and FeCN but failed in irreversible systems, such as the V^{4+}/V^{5+} redox couple. It was demonstrated that the method could also be implemented with a pseudo-reference electrode.

7.2 Overall conclusion

The preliminary characterization of electrolytes is a necessary step in the development of new flow battery chemistries. The results observed for 1,2-DHAQ and FeCN are in line with the requirements of flow battery applications which explains the persistence of these reactants in the flow battery literature. The redox potentials, the kinetic rate constants and diffusion coefficients are all sufficient to allow for reasonably efficient flow battery operation. Although no novel electrolytes were studied in this work, the procedures laid out here would be utilized to benchmark the performance of any new electrolytes under development.

Regarding the state of health of electrolytes however, more work needs to be done to refine the methods used to track electrolyte degradation. Discrepancies between observed capacity fade and concentration loss, measured by UV-Vis spectroscopy and CV, suggest that these methods would benefit from more replication and systematic adjustment of experimental parameters. Although it is plausible that these discrepancies may be attributed to water crossover, it would be beneficial to investigate this possibility systematically to quantify its effect for future electrolyte stability testing. In addition, complex systems such as flow batteries may require a third or fourth experimental concentration measurement technique to really confirm the amount of reactants lost over time.

In chapter 6, the determination of the SOC in redox flow batteries was correlated with the mole fraction of redox-active species and the electrode's equilibrium potential, typically described by the Nernst equation. In systems like 1,2-DHAQ and FeCN, which exhibit quasi-reversible redox kinetics, CV and OCV measurements provided insight into SOC. Despite the possible deviations from ideal Nernstian behavior, the combined use of CV and OCV can still offer a reliable approximation for SOC. In contrast, irreversible redox systems, such as the V^{4+}/V^{5+} couple, pose significant challenges for SOC measurement due to their inherently sluggish electron transfer kinetics and lack of equilibrium between oxidized and reduced states. These systems are marked by broad and asymmetric CV peaks, which complicate the direct application of the Nernst equation.

Pseudo-reference electrodes offer a pragmatic approach to overcoming some limitations of traditional reference electrodes, particularly in dynamic environments such as flow batteries. Unlike traditional reference electrodes that require stable and controlled environments to prevent contamination and maintain potential stability, pseudo-reference electrodes can be directly integrated into the electrolyte stream, simplifying the experimental setup. This direct integration helps mitigate issues related to contamination and potential drift, though it necessitates rigorous calibration to ensure accurate SOC measurements.

7.3 Future recommendations

Future work can be on standardizing CV analyses as this is very crucial for wide range of applications. It is essential to standardize electrode preparation and surface area measurement to minimize variability. Ensuring a clean and consistent electrode surface will help achieve reliable peak currents and potentials as well as investigating the deposition of degradation products on the electrode surface and its impact on CV results. This investigation can involve pre- and post-experimental surface characterization using techniques such as scanning electron microscopy (SEM) or X-ray photoelectron spectroscopy (XPS).

In addition, an area of focus can be on the rigorous preparation of electrolyte samples with precisely known amounts of degradation. This step is crucial for verifying the reproducibility of degradation measurements using each chosen analytical method. To achieve this, there should be implementation of controlled degradation protocols, ensuring consistent degradation across multiple samples. These protocols could involve accelerated aging tests, where the electrolytes are subjected to elevated temperatures, cycling stresses, or chemical oxidants to induce predictable and measurable degradation.

Furthermore, addressing discrepancies between observed capacity fade and concentration loss using UV-Vis may require a multifaceted approach. A detailed study on water crossover and its impact on electrolyte concentration and overall battery performance can be investigated. This could involve using isotopic tracing techniques to monitor water movement across the membrane.

Also, replication of established methodologies and the incorporation of additional degradation analysis techniques can further enhance the understanding and quantification of capacity fade in redox flow batteries. Techniques such as Nuclear Magnetic Resonance (NMR), Fourier Transform Infrared Spectroscopy (FTIR), and High-Performance Liquid Chromatography (HPLC) provide detailed insights into the chemical changes and degradation pathways of the electrolyte components.

Meanwhile, enhancing the performance of 1,2-DHAQ through the strategic addition of functional groups represents a promising approach to improving its redox potential, stability, and solubility. By introducing electron-donating or electron-withdrawing substituents, the redox potential can be finely tuned to achieve more optimal electrochemical characteristics, thereby increasing the energy efficiency of the redox flow battery. Furthermore, the incorporation of functional groups that enhance stability can mitigate degradation pathways, leading to longer cycle life and greater overall durability of the electrolyte. Hydrophilic functional groups, in particular, can significantly improve the solubility of 1,2-DHAQ in aqueous solutions, enabling higher concentration electrolytes and potentially increasing the energy density of the system.

Lastly, utilizing nanostructured or more modified electrode surfaces may enhance electron transfer kinetics of irreversible systems by increasing the active surface area and improving mass transport. These electrodes can reduce the overpotentials required for redox reactions, as well as lowering the activation energy in turn improving the reversibility of redox reactions and making SOC analysis more accurate.

By addressing these future research directions, the understanding and optimization of redox flow battery performance can be significantly enhanced, leading to more reliable and efficient energy storage systems.

REFERENCES

- [1] L. F. Arenas, C. Ponce De León, and F. C. Walsh, “Engineering aspects of the design, construction and performance of modular redox flow batteries for energy storage,” *J. Energy Storage*, vol. 11, pp. 119–153, Jun. 2017, doi: 10.1016/j.est.2017.02.007.
- [2] L. Zhang, R. Feng, W. Wang, and G. Yu, “Emerging chemistries and molecular designs for flow batteries,” *Nat. Rev. Chem.*, vol. 6, no. 8, pp. 524–543, Aug. 2022, doi: 10.1038/s41570-022-00394-6.
- [3] C. Zhang *et al.*, “Progress and prospects of next-generation redox flow batteries,” *Energy Storage Mater.*, vol. 15, pp. 324–350, Nov. 2018, doi: 10.1016/j.ensm.2018.06.008.
- [4] M. M. Petrov *et al.*, “Redox flow batteries: role in modern electric power industry and comparative characteristics of the main types,” *Russ. Chem. Rev.*, vol. 90, no. 6, pp. 677–702, Jun. 2021, doi: 10.1070/RCR4987.
- [5] X. Shi *et al.*, “Polymer Electrolyte Membranes for Vanadium Redox Flow Batteries: Fundamentals and Applications,” *Prog. Energy Combust. Sci.*, vol. 85, p. 100926, Jul. 2021, doi: 10.1016/j.pecs.2021.100926.
- [6] B. Fang, S. Iwasa, Y. Wei, T. Arai, and M. Kumagai, “A study of the Ce(III)/Ce(IV) redox couple for redox flow battery application,” *Electrochimica Acta*, vol. 47, no. 24, pp. 3971–3976, Sep. 2002, doi: 10.1016/S0013-4686(02)00370-5.
- [7] M. Rychcik and M. Skyllas-Kazacos, “Characteristics of a new all-vanadium redox flow battery,” *J. Power Sources*, vol. 22, no. 1, pp. 59–67, Jan. 1988, doi: 10.1016/0378-7753(88)80005-3.
- [8] G. L. Soloveichik, “Flow Batteries: Current Status and Trends,” *Chem. Rev.*, vol. 115, no. 20, pp. 11533–11558, Oct. 2015, doi: 10.1021/cr500720t.
- [9] R. M. Darling, K. G. Gallagher, J. A. Kowalski, S. Ha, and F. R. Brushett, “Pathways to low-cost electrochemical energy storage: a comparison of aqueous and nonaqueous flow batteries,” *Energy Env. Sci*, vol. 7, no. 11, pp. 3459–3477, Sep. 2014, doi: 10.1039/C4EE02158D.
- [10] M.-A. Goulet and M. J. Aziz, “Flow Battery Molecular Reactant Stability Determined by Symmetric Cell Cycling Methods,” *J. Electrochem. Soc.*, vol. 165, no. 7, pp. A1466–A1477, 2018, doi: 10.1149/2.0891807jes.
- [11] K. Lin *et al.*, “Alkaline quinone flow battery,” *Science*, vol. 349, no. 6255, pp. 1529–1532, Sep. 2015, doi: 10.1126/science.aab3033.
- [12] B. Hu, C. DeBruler, Z. Rhodes, and T. L. Liu, “Long-Cycling Aqueous Organic Redox Flow Battery (AORFB) toward Sustainable and Safe Energy Storage,” *J. Am. Chem. Soc.*, vol. 139, no. 3, pp. 1207–1214, Jan. 2017, doi: 10.1021/jacs.6b10984.
- [13] T. Lv and L. Suo, “Water-in-salt widens the electrochemical stability window: Thermodynamic and kinetic factors,” *Curr. Opin. Electrochem.*, vol. 29, p. 100818, Oct. 2021, doi: 10.1016/j.coelec.2021.100818.
- [14] D. P. Tabor, R. Gómez-Bombarelli, L. Tong, R. G. Gordon, M. J. Aziz, and A. Aspuru-Guzik, “Mapping the frontiers of quinone stability in aqueous media: implications for organic aqueous redox flow batteries,” *J. Mater. Chem. A*, vol. 7, no. 20, pp. 12833–12841, 2019, doi: 10.1039/C9TA03219C.
- [15] W. D. McCulloch, M. Yu, and Y. Wu, “pH-Tuning a Solar Redox Flow Battery for Integrated Energy Conversion and Storage,” *ACS Energy Lett.*, vol. 1, no. 3, pp. 578–582, Sep. 2016, doi: 10.1021/acseenergylett.6b00296.
- [16] D. G. Kwabi *et al.*, “Alkaline Quinone Flow Battery with Long Lifetime at pH 12,” *Joule*, vol. 2, no. 9, pp. 1894–1906, Sep. 2018, doi: 10.1016/j.joule.2018.07.005.

- [17] Y. Liu *et al.*, “Degradation of electrochemical active compounds in aqueous organic redox flow batteries,” *Curr. Opin. Electrochem.*, vol. 32, p. 100895, Apr. 2022, doi: 10.1016/j.coelec.2021.100895.
- [18] D. P. Tabor, R. Gómez-Bombarelli, L. Tong, R. G. Gordon, M. J. Aziz, and A. Aspuru-Guzik, “Mapping the frontiers of quinone stability in aqueous media: implications for organic aqueous redox flow batteries,” *J. Mater. Chem. A*, vol. 7, no. 20, pp. 12833–12841, 2019, doi: 10.1039/C9TA03219C.
- [19] N. Kumpan, T. Poonsawat, L. Chaicharoenwimolkul, S. Pornsuwan, and E. Somsook, “Ferrocenated nanocatalysts derived from the decomposition of ferrocenium in basic solution and their aerobic activities for the rapid decolorization of methylene blue and the facile oxidation of phenylboronic acid,” *RSC Adv.*, vol. 7, no. 10, pp. 5759–5763, Jan. 2017, doi: 10.1039/C6RA25515A.
- [20] C. L. Bird and A. T. Kuhn, “Electrochemistry of the viologens,” *Chem. Soc. Rev.*, vol. 10, no. 1, pp. 49–82, Jan. 1981, doi: 10.1039/CS9811000049.
- [21] C. O’Connor, “Acidic and basic amide hydrolysis,” *Q. Rev. Chem. Soc.*, vol. 24, no. 4, pp. 553–564, Jan. 1970, doi: 10.1039/QR9702400553.
- [22] K. Lin *et al.*, “A redox-flow battery with an alloxazine-based organic electrolyte,” *Nat. Energy*, 2016, doi: 10.1038/nenergy.2016.102.
- [23] R. Feng *et al.*, “Reversible ketone hydrogenation and dehydrogenation for aqueous organic redox flow batteries,” *Science*, vol. 372, no. 6544, pp. 836–840, May 2021, doi: 10.1126/science.abd9795.
- [24] A. Orita, M. G. Verde, M. Sakai, and Y. S. Meng, “The impact of pH on side reactions for aqueous redox flow batteries based on nitroxyl radical compounds,” *J. Power Sources*, vol. 321, pp. 126–134, Jul. 2016, doi: 10.1016/j.jpowsour.2016.04.136.
- [25] Z. Zhao, C. Zhang, and X. Li, “Opportunities and challenges of organic flow battery for electrochemical energy storage technology,” *J. Energy Chem.*, vol. 67, pp. 621–639, Apr. 2022, doi: 10.1016/j.jechem.2021.10.037.
- [26] A. Ramar, F.-M. Wang, R. Foeng, and R. Hsing, “Organic redox flow battery: Are organic redox materials suited to aqueous solvents or organic solvents?,” *J. Power Sources*, vol. 558, p. 232611, Feb. 2023, doi: 10.1016/j.jpowsour.2022.232611.
- [27] K. Deuchert and S. Hünig, “Multistage Organic Redox Systems—A General Structural Principle,” *Angew. Chem. Int. Ed. Engl.*, vol. 17, no. 12, pp. 875–886, Dec. 1978, doi: 10.1002/anie.197808753.
- [28] G. C. Sedenho *et al.*, “Effect of Molecular Structure of Quinones and Carbon Electrode Surfaces on the Interfacial Electron Transfer Process,” *ACS Appl. Energy Mater.*, vol. 3, no. 2, pp. 1933–1943, Feb. 2020, doi: 10.1021/acsaem.9b02357.
- [29] L. Tong *et al.*, “Molecular Engineering of an Alkaline Naphthoquinone Flow Battery,” *ACS Energy Lett.*, vol. 4, no. 8, pp. 1880–1887, Aug. 2019, doi: 10.1021/acsenerylett.9b01321.
- [30] Q. Chen, M. R. Gerhardt, and M. J. Aziz, “Dissection of the Voltage Losses of an Acidic Quinone Redox Flow Battery,” *J. Electrochem. Soc.*, vol. 164, no. 6, pp. A1126–A1132, 2017, doi: 10.1149/2.0721706jes.
- [31] M.-A. Goulet and M. J. Aziz, “Flow Battery Molecular Reactant Stability Determined by Symmetric Cell Cycling Methods,” *J. Electrochem. Soc.*, vol. 165, no. 7, p. A1466, May 2018, doi: 10.1149/2.0891807jes.

- [32] Y. Yao, J. Lei, Y. Shi, F. Ai, and Y.-C. Lu, "Assessment methods and performance metrics for redox flow batteries," *Nat. Energy*, vol. 6, no. 6, Art. no. 6, Jun. 2021, doi: 10.1038/s41560-020-00772-8.
- [33] L. J. Small, H. D. Pratt, and T. M. Anderson, "Crossover in Membranes for Aqueous Soluble Organic Redox Flow Batteries," *J. Electrochem. Soc.*, vol. 166, no. 12, pp. A2536–A2542, 2019, doi: 10.1149/2.0681912jes.
- [34] F. S. Rocha, A. J. Gomes, C. N. Lunardi, S. Kaliaguine, and G. S. Patience, "Experimental methods in chemical engineering: Ultraviolet visible spectroscopy—UV-Vis," *Can. J. Chem. Eng.*, vol. 96, no. 12, pp. 2512–2517, Dec. 2018, doi: 10.1002/cjce.23344.
- [35] G. Verma and D. M. Mishra, "DEVELOPMENT AND OPTIMIZATION OF UV-VIS SPECTROSCOPY- A REVIEW," *World J. Pharm. Res.*, vol. 7, no. 11.
- [36] M. K. Ravikumar, S. Rathod, N. Jaiswal, S. Patil, and A. Shukla, "The renaissance in redox flow batteries," *J. Solid State Electrochem.*, vol. 21, no. 9, pp. 2467–2488, Sep. 2017, doi: 10.1007/s10008-016-3472-4.
- [37] M. Skyllas-Kazacos, L. Cao, M. Kazacos, N. Kausar, and A. Mousa, "Vanadium Electrolyte Studies for the Vanadium Redox Battery—A Review," *ChemSusChem*, vol. 9, no. 13, pp. 1521–1543, Jul. 2016, doi: 10.1002/cssc.201600102.
- [38] M. Skyllas-Kazacos, "Evaluation of Precipitation Inhibitors for Supersaturated Vanadyl Electrolytes for the Vanadium Redox Battery," *Electrochem. Solid-State Lett.*, vol. 2, no. 3, p. 121, 1999, doi: 10.1149/1.1390754.
- [39] M. Skyllas-Kazacos, C. Menictas, and M. Kazacos, "Thermal Stability of Concentrated V(V) Electrolytes in the Vanadium Redox Cell," *J. Electrochem. Soc.*, vol. 143, no. 4, pp. L86–L88, Apr. 1996, doi: 10.1149/1.1836609.
- [40] M. Vijayakumar *et al.*, "Towards understanding the poor thermal stability of V⁵⁺ electrolyte solution in Vanadium Redox Flow Batteries," *J. Power Sources*, vol. 196, no. 7, pp. 3669–3672, Apr. 2011, doi: 10.1016/j.jpowsour.2010.11.126.
- [41] B.-T. Liu *et al.*, "Extraordinary pseudocapacitive energy storage triggered by phase transformation in hierarchical vanadium oxides," *Nat. Commun.*, vol. 9, no. 1, p. 1375, Apr. 2018, doi: 10.1038/s41467-018-03700-3.
- [42] S. Xiao, L. Yu, L. Wu, L. Liu, X. Qiu, and J. Xi, "Broad temperature adaptability of vanadium redox flow battery—Part 1: Electrolyte research," *Electrochimica Acta*, vol. 187, pp. 525–534, Jan. 2016, doi: 10.1016/j.electacta.2015.11.062.
- [43] Y. H. Wen *et al.*, "Studies on Iron „Fe³⁺/Fe²⁺...-Complex/Bromine „Br²/Br⁻... Redox Flow Cell in Sodium Acetate Solution," *J. Electrochem. Soc.*
- [44] M. L. Saha, S. Neogi, and M. Schmittl, "Dynamic heteroleptic metal-phenanthroline complexes: from structure to function," *Dalton Trans*, vol. 43, no. 10, pp. 3815–3834, Jan. 2014, doi: 10.1039/C3DT53570C.
- [45] Y. H. Wen *et al.*, "A study of the Fe(III)/Fe(II)–triethanolamine complex redox couple for redox flow battery application," *Electrochimica Acta*, vol. 51, no. 18, pp. 3769–3775, May 2006, doi: 10.1016/j.electacta.2005.10.040.
- [46] A. S. N. Murthy and T. Srivastava, "Fe(III)/Fe(II) — ligand systems for use as negative half-cells in redox-flow cells," *J. Power Sources*, vol. 27, no. 2, pp. 119–126, Aug. 1989, doi: 10.1016/0378-7753(89)80126-0.
- [47] P. Modiba, M. Matoetoe, and A. M. Crouch, "Kinetics study of transition metal complexes (Ce–DTPA, Cr–DTPA and V–DTPA) for redox flow battery applications," *Electrochimica Acta*, vol. 94, pp. 336–343, Apr. 2013, doi: 10.1016/j.electacta.2013.01.081.

- [48] J. G. Ibanez, C. Choi, and R. S. Becker, “Aqueous Redox Transition Metal Complexes for Electrochemical Applications as a Function of pH,” *J. Electrochem. Soc.*, vol. 134, no. 12, pp. 3083–3089, Dec. 1987, doi: 10.1149/1.2100344.
- [49] Y. W. Chen, D. Cahen, R. Noufi, and J. A. Turner, “Photoelectrochemical test for photovoltaic activity of p-CuInSe₂ films,” *Sol. Cells*, vol. 14, no. 2, pp. 109–121, May 1985, doi: 10.1016/0379-6787(85)90033-X.
- [50] M. Reinhard *et al.*, “Photooxidation and photoaquation of iron hexacyanide in aqueous solution: A picosecond X-ray absorption study,” *Struct. Dyn.*, vol. 1, no. 2, p. 024901, Mar. 2014, doi: 10.1063/1.4871751.
- [51] M. H. Cheah and P. Chernev, “Electrochemical oxidation of ferricyanide,” *Sci. Rep.*, vol. 11, no. 1, p. 23058, Nov. 2021, doi: 10.1038/s41598-021-02355-3.
- [52] G. Adams, R. Hollandsworth, and B. Webber, “Rechargeable alkaline zinc/ferricyanide battery. Final report, 29 September 1978-28 September 1979. [35 mA/cm/sup 2/, 4. 5 kW/m/sup 2/],” LMSC-D-678426, 5282415, Jan. 1979. doi: 10.2172/5282415.
- [53] M.-A. Goulet and M. J. Aziz, “Flow Battery Molecular Reactant Stability Determined by Symmetric Cell Cycling Methods,” *J. Electrochem. Soc.*, vol. 165, no. 7, pp. A1466–A1477, 2018, doi: 10.1149/2.0891807jes.
- [54] M. Cazot, G. Maranzana, J. Dillet, F. Beille, T. Godet-Bar, and S. Didierjean, “Symmetric-cell characterization of the redox flow battery system: Application to the detection of degradations,” *Electrochimica Acta*, vol. 321, p. 134705, Oct. 2019, doi: 10.1016/j.electacta.2019.134705.
- [55] T. Páez, A. Martínez-Cuezva, J. Palma, and E. Ventosa, “Revisiting the cycling stability of ferrocyanide in alkaline media for redox flow batteries,” *J. Power Sources*, vol. 471, p. 228453, Sep. 2020, doi: 10.1016/j.jpowsour.2020.228453.
- [56] M. Hu, A. P. Wang, J. Luo, Q. Wei, and T. L. Liu, “Cycling Performance and Mechanistic Insights of Ferricyanide Electrolytes in Alkaline Redox Flow Batteries,” *Adv. Energy Mater.*, vol. 13, no. 15, p. 2203762, Apr. 2023, doi: 10.1002/aenm.202203762.
- [57] W. Wang and V. Sprenkle, “Redox flow batteries go organic,” *Nat. Chem.*, vol. 8, no. 3, pp. 204–206, Mar. 2016, doi: 10.1038/nchem.2466.
- [58] X. Wei *et al.*, “Materials and Systems for Organic Redox Flow Batteries: Status and Challenges,” *ACS Energy Lett.*, vol. 2, no. 9, pp. 2187–2204, Sep. 2017, doi: 10.1021/acsenergylett.7b00650.
- [59] A. Murali *et al.*, “Understanding and Mitigating Capacity Fade in Aqueous Organic Redox Flow Batteries,” *J. Electrochem. Soc.*, vol. 165, no. 7, pp. A1193–A1203, 2018, doi: 10.1149/2.0161807jes.
- [60] T. J. Carney, S. J. Collins, J. S. Moore, and F. R. Brushett, “Concentration-Dependent Dimerization of Anthraquinone Disulfonic Acid and Its Impact on Charge Storage,” *Chem. Mater.*, vol. 29, no. 11, pp. 4801–4810, Jun. 2017, doi: 10.1021/acs.chemmater.7b00616.
- [61] M.-A. Goulet *et al.*, “Extending the Lifetime of Organic Flow Batteries via Redox State Management,” *J. Am. Chem. Soc.*, vol. 141, no. 20, pp. 8014–8019, May 2019, doi: 10.1021/jacs.8b13295.
- [62] D. P. Tabor, R. Gómez-Bombarelli, L. Tong, R. G. Gordon, M. J. Aziz, and A. Aspuru-Guzik, “Mapping the frontiers of quinone stability in aqueous media: implications for organic aqueous redox flow batteries,” *J. Mater. Chem. A*, vol. 7, no. 20, pp. 12833–12841, 2019, doi: 10.1039/C9TA03219C.

- [63] B. Yang, L. Hooper-Burkhardt, S. Krishnamoorthy, A. Murali, G. K. S. Prakash, and S. R. Narayanan, “High-Performance Aqueous Organic Flow Battery with Quinone-Based Redox Couples at Both Electrodes,” *J. Electrochem. Soc.*, vol. 163, no. 7, pp. A1442–A1449, 2016, doi: 10.1149/2.1371607jes.
- [64] J. Cao, M. Tao, H. Chen, J. Xu, and Z. Chen, “A highly reversible anthraquinone-based anolyte for alkaline aqueous redox flow batteries,” *J. Power Sources*, vol. 386, pp. 40–46, May 2018, doi: 10.1016/j.jpowsour.2018.03.041.
- [65] P. T. Kissinger and W. R. Heineman, “Cyclic voltammetry,” *J. Chem. Educ.*, vol. 60, no. 9, 1983.
- [66] I. L. Escalante-García, J. S. Wainright, L. T. Thompson, and R. F. Savinell, “Performance of a Non-Aqueous Vanadium Acetylacetonate Prototype Redox Flow Battery: Examination of Separators and Capacity Decay,” *J. Electrochem. Soc.*, vol. 162, no. 3, pp. A363–A372, 2015, doi: 10.1149/2.0471503jes.
- [67] D. Pinheiro, M. Pineiro, and J. S. S. De Melo, “Sulfonated tryptanthrin anolyte increases performance in pH neutral aqueous redox flow batteries,” *Commun. Chem.*, vol. 4, no. 1, p. 89, Jun. 2021, doi: 10.1038/s42004-021-00523-0.
- [68] F. Alkhayri and C. A. Dyker, “Evaluation of Two-Electron Bispyridinylidene Anolytes and a TEMPO Catholyte for Non-Aqueous Redox Flow Batteries,” *J. Electrochem. Soc.*, vol. 168, no. 7, p. 070501, Jul. 2021, doi: 10.1149/1945-7111/ac0def.
- [69] F. S. Rocha, A. J. Gomes, C. N. Lunardi, S. Kaliaguine, and G. S. Patience, “Experimental methods in chemical engineering: Ultraviolet visible spectroscopy—UV-Vis,” *Can. J. Chem. Eng.*, vol. 96, no. 12, pp. 2512–2517, Dec. 2018, doi: 10.1002/cjce.23344.
- [70] L. Liu, Y. Yao, Z. Wang, and Y.-C. Lu, “Viologen radical stabilization by molecular spectators for aqueous organic redox flow batteries,” *Nano Energy*, vol. 84, p. 105897, Jun. 2021, doi: 10.1016/j.nanoen.2021.105897.
- [71] G. Kwon *et al.*, “Multi-redox Molecule for High-Energy Redox Flow Batteries,” *Joule*, vol. 2, no. 9, pp. 1771–1782, Sep. 2018, doi: 10.1016/j.joule.2018.05.014.
- [72] N. H. Attanayake *et al.*, “Comparative Study of Organic Radical Cation Stability and Coulombic Efficiency for Nonaqueous Redox Flow Battery Applications,” *J. Phys. Chem. C*, vol. 125, no. 26, pp. 14170–14179, Jul. 2021, doi: 10.1021/acs.jpcc.1c00686.
- [73] D. Xu, C. Zhang, Y. Zhen, and Y. Li, “Liquid Nitrobenzene-Based Anolyte Materials for High-Current and -Energy-Density Nonaqueous Redox Flow Batteries,” *ACS Appl. Mater. Interfaces*, vol. 13, no. 30, pp. 35579–35584, Aug. 2021, doi: 10.1021/acsami.1c05564.
- [74] B. Hu, H. Fan, H. Li, M. Ravivarma, and J. Song, “Five-Membered Ring Nitroxide Radical: A New Class of High-Potential, Stable Catholytes for Neutral Aqueous Organic Redox Flow Batteries,” *Adv. Funct. Mater.*, vol. 31, no. 35, p. 2102734, Aug. 2021, doi: 10.1002/adfm.202102734.
- [75] Y. Ben-Tal *et al.*, “Mechanistic analysis by NMR spectroscopy: A users guide,” *Prog. Nucl. Magn. Reson. Spectrosc.*, vol. 129, pp. 28–106, Apr. 2022, doi: 10.1016/j.pnmrs.2022.01.001.
- [76] C. Wang *et al.*, “N-alkyl-carboxylate-functionalized anthraquinone for long-cycling aqueous redox flow batteries,” *Energy Storage Mater.*, vol. 36, pp. 417–426, Apr. 2021, doi: 10.1016/j.ensm.2021.01.019.
- [77] W. Liu, Z. Zhao, T. Li, S. Li, H. Zhang, and X. Li, “A high potential biphenol derivative cathode: toward a highly stable air-insensitive aqueous organic flow battery,” *Sci. Bull.*, vol. 66, no. 5, pp. 457–463, Mar. 2021, doi: 10.1016/j.scib.2020.08.042.
- [78] “Fourier Transform Infrared Spectroscopy,” vol. 191, 1976.

- [79] W. Duan *et al.*, “A symmetric organic-based nonaqueous redox flow battery and its state of charge diagnostics by FTIR,” *J. Mater. Chem. A*, vol. 4, no. 15, pp. 5448–5456, 2016, doi: 10.1039/C6TA01177B.
- [80] Z. Liang *et al.*, “Metal-free polypeptide redox flow batteries,” *Mater. Adv.*, vol. 3, no. 16, pp. 6558–6565, 2022, doi: 10.1039/D2MA00498D.
- [81] S. Rudolph, U. Schröder, I. M. Bayanov, K. Blenke, and D. Hage, “High resolution state of charge monitoring of vanadium electrolytes with IR optical sensor,” *J. Electroanal. Chem.*, vol. 694, pp. 17–22, Apr. 2013, doi: 10.1016/j.jelechem.2013.01.042.
- [82] N. Janshen, S. Ressel, A. Chica, and T. Struckmann, “A correlated multi-observable assessment for vanadium redox flow battery state of charge estimation — Empirical correlations and temperature dependencies,” *Electrochimica Acta*, vol. 490, p. 144239, Jun. 2024, doi: 10.1016/j.electacta.2024.144239.
- [83] Z. Yang, R. M. Darling, and M. L. Perry, “Electrolyte Compositions in a Vanadium Redox Flow Battery Measured with a Reference Cell,” *J. Electrochem. Soc.*, vol. 166, no. 13, pp. A3045–A3050, 2019, doi: 10.1149/2.1161913jes.
- [84] K. Amini, E. M. Fell, and M. J. Aziz, “The Poor Academic’s DC-Offset for Reversing Polarity in Electrochemical Cells: Application to Redox Flow Cells,” *J. Electrochem. Soc.*, vol. 169, no. 9, p. 090527, Sep. 2022, doi: 10.1149/1945-7111/ac91a8.
- [85] K. Ngamsai and A. Arpornwichanop, “Analysis and measurement of the electrolyte imbalance in a vanadium redox flow battery,” *J. Power Sources*, vol. 282, pp. 534–543, May 2015, doi: 10.1016/j.jpowsour.2015.01.188.
- [86] C. Stolze, M. D. Hager, and U. S. Schubert, “State-of-charge monitoring for redox flow batteries: A symmetric open-circuit cell approach,” *J. Power Sources*, vol. 423, pp. 60–67, May 2019, doi: 10.1016/j.jpowsour.2019.03.002.
- [87] J. Geiser, H. Natter, R. Hempelmann, B. Morgenstern, and K. Hegetschweiler, “Photometrical Determination of the State-of-Charge in Vanadium Redox Flow Batteries Part I: In Combination with Potentiometric Titration,” *Z. Für Phys. Chem.*, vol. 233, no. 12, pp. 1683–1694, Dec. 2019, doi: 10.1515/zpch-2019-1379.
- [88] K.-H. Shin, C.-S. Jin, J.-Y. So, S.-K. Park, D.-H. Kim, and S.-H. Yeon, “Real-time monitoring of the state of charge (SOC) in vanadium redox-flow batteries using UV–Vis spectroscopy in operando mode,” *J. Energy Storage*, vol. 27, p. 101066, Feb. 2020, doi: 10.1016/j.est.2019.101066.
- [89] L. Liu *et al.*, “State of charge monitoring for vanadium redox flow batteries by the transmission spectra of V(IV)/V(V) electrolytes,” *J. Appl. Electrochem.*, vol. 42, no. 12, pp. 1025–1031, Dec. 2012, doi: 10.1007/s10800-012-0477-2.
- [90] D. N. Buckley, X. Gao, R. P. Lynch, N. Quill, and M. J. Leahy, “Towards Optical Monitoring of Vanadium Redox Flow Batteries (VRFBs): An Investigation of the Underlying Spectroscopy,” *J. Electrochem. Soc.*, vol. 161, no. 4, pp. A524–A534, 2014, doi: 10.1149/2.023404jes.
- [91] T. C. Gokoglan, S. K. Pahari, A. Hamel, R. Howland, P. J. Cappillino, and E. Agar, “Operando Spectroelectrochemical Characterization of a Highly Stable Bioinspired Redox Flow Battery Active Material,” *J. Electrochem. Soc.*, vol. 166, no. 10, pp. A1745–A1751, 2019, doi: 10.1149/2.0271910jes.
- [92] D. G. Kwabi, A. A. Wong, and M. J. Aziz, “Rational Evaluation and Cycle Life Improvement of Quinone-Based Aqueous Flow Batteries Guided by In-Line Optical

- Spectrophotometry,” *J. Electrochem. Soc.*, vol. 165, no. 9, pp. A1770–A1776, 2018, doi: 10.1149/2.0791809jes.
- [93] N. Aguiló-Aguayo and T. Bechtold, “Monitoring the State-of-Charge in All-Iron Aqueous Redox Flow Batteries,” *J. Electrochem. Soc.*, vol. 165, no. 13, pp. A3164–A3168, 2018, doi: 10.1149/2.0911813jes.
- [94] W. Duan, R. S. Vemuri, D. Hu, Z. Yang, and X. Wei, “A Protocol for Electrochemical Evaluations and State of Charge Diagnostics of a Symmetric Organic Redox Flow Battery,” *J. Vis. Exp.*, no. 120, p. 55171, Feb. 2017, doi: 10.3791/55171.
- [95] K. Lin *et al.*, “Alkaline quinone flow battery,” *Science*, vol. 349, no. 6255, pp. 1529–1532, Sep. 2015, doi: 10.1126/science.aab3033.
- [96] J.-M. Fontmorin, S. Guiheneuf, T. Godet-Bar, D. Floner, and F. Geneste, “How anthraquinones can enable aqueous organic redox flow batteries to meet the needs of industrialization,” *Curr. Opin. Colloid Interface Sci.*, vol. 61, p. 101624, Oct. 2022, doi: 10.1016/j.cocis.2022.101624.
- [97] B. Lai, Y. Zhou, J. Wang, Z. Yang, and Z. Chen, “Application of excitation and emission matrix fluorescence (EEM) and UV–vis absorption to monitor the characteristics of Alizarin Red S (ARS) during electro-Fenton degradation process,” *Chemosphere*, vol. 93, no. 11, pp. 2805–2813, Nov. 2013, doi: 10.1016/j.chemosphere.2013.09.056.
- [98] A. J. Bard and L. R. Faulkner, *Electrochemical methods: fundamentals and applications*, 2nd ed. New York: Wiley, 2001.